REPORT DOCUMENTATION PAGE

Form Approved
OMB No. 0704-0188

1. AGENCY USE ONLY (Leave blank)	2. REPORT DATE	3. REPORT TYPE AND DATES COVERED
	March 94	final

4. TITLE AND SUBTITLE
Stability & Transition on Swept Wings

5. FUNDING NUMBERS
AFOSR-
91-0262

6. AUTHOR(S)
Thorwald Herbert

AFOSR-TR-95

7. PERFORMING ORGANIZATION NAME(S) AND ADDRESS(ES)
Ohio State U.
Dept of Mechanical Engineering

0784

9. SPONSORING/MONITORING AGENCY NAME(S) AND ADDRESS(ES)
Air Force Office Of Scientific Research
Aerospace & Materials Sciences Directorate
110 Duncan Avenue, Suite B-115
Bolling AFB DC 20332-0001

NA

10. SPONSORING/MONITORING AGENCY REPORT NUMBER
AFOSR-
91-0262

11. SUPPLEMENTARY NOTES

12a. DISTRIBUTION/AVAILABILITY STATEMENT
APPROVED FOR PUBLIC RELEASE
DISTRIBUTION IS UNLIMITED

12b. DISTRIBUTION CODE

13. ABSTRACT (Ma

The thrust of this research program has been the improvement of our capabilities for analyzing stability and transition in compressible boundary-layers as they appear in technologically important flows. Examples of such flows are swept wings of commercial airplanes or the highly cambered blades of gas turbines. We have extended the parabolized stability equations (PSE) for these situations and developed methods for solving these equations in disturbance environments reaching from the low atmospheric levels to the volatile high levels in gas turbines. The extension required both a basic study on the stability analysis of 3D flows and formulating the equations in general curvilinear coordinates. Proper choices have been made to minimize the effect of the parabolization. Major efforts have been spent on characterizing the disturbance environment. More recently, emphasis has been directed toward the control of stability and transition using neural networks.

14. SUBJECT TERMS	15. NUMBER OF PAGES
stability, transition, wings	31
	16. PRICE CODE

17. SECURITY CLASSIFICATION OF REPORT	18. SECURITY CLASSIFICATION OF THIS PAGE	19. SECURITY CLASSIFICATION OF ABSTRACT	20. LIMITATION OF ABSTRACT
U	U	U	

THE OHIO STATE UNIVERSITY

Stability and Transition On Swept Wings

Th. Herbert
Department of Mechanical Engineering

Air Force Office of Scientific Research
Bolling Air Force Base, D.C. 20332-6448

Contract No. AFOSR-91-02-62
Final Report

March 1994

THE OHIO STATE UNIVERSITY

Stability and Transition On Swept Wings

Th. Herbert
Department of Mechanical Engineering

Air Force Office of Scientific Research
Bolling Air Force Base, D.C. 20332-6448

Contract No. AFOSR-91-02-62
Final Report
RF Project No. 769031/724697

March 1994

Abstract

The thrust of this research program has been the improvement of our capabilities for analyzing stability and transition in compressible boundary-layers as they appear in technologically important flows. Examples of such flows are swept wings of commercial airplanes or the highly cambered blades of gas turbines. We have extended the parabolized stability equations (PSE) for these situations and developed methods for solving these equations in disturbance environments reaching from the low atmospheric levels to the volatile high levels in gas turbines. The extension required both a basic study on the stability analysis of 3D flows and formulating the equations in general curvilinear coordinates. Proper choices have been made to minimize the effect of the parabolization. Major efforts have been spent on characterizing the disturbance environment. More recently, emphasis has been directed toward the control of stability and transition using neural networks.

Contents

1 Objectives

This research program aimed at developing and applying theoretical, numerical, and graphical tools for the quantitative description and deeper understanding of stability and transition in technologically important flows. Much of the effort has been directed toward engineering methods for advanced design. Toward these goals, we have worked in the following areas:

(1) Optimum formulations and algorithms for solving the PSE in general curvilinear coordinates.

(2) High-order Hermitian finite-difference methods.

(3) Stability theory for 3D boundary layers.

(4) Basic-flow calculations with Euler and boundary-layer codes. Accuracy requirements.

(5) Transition mechanisms.

(6) Characterization of the disturbance environment. Receptivity studies.

(7) Transient growth of disturbances in stable regions.

(8) Modeling of nonlinear phenomena with neural networks. Aspects of flow control.

2 Achievements

The work in all areas has considerably progressed. We have developed two versatile PSE codes. The first code is very flexible to adapt to 2D or 3D convectively unstable flows. The code is restricted to simple (typically Cartesian) coordinate systems and primarily serves for producing benchmark results and exploring new concepts using exact or similarity solutions for the basic flow. The second code has been developed in cooperation with DynaFlow, Inc. and is written specifically for compressible boundary layers in general curvilinear coordinates to enable studies of flows in realistic geometries. This code is the basis for specific applications e.g. to transition and heat transfer analysis in gas turbines. The work with this code is supported by various other codes

to compute the inviscid flow over wings or through cascades and to obtain the boundary-layer flow from the inviscid surface-pressure distribution. The work under this contract has involved various graduate students one of whom will complete his Ph.D. in the near future. The difficulty of the research areas listed above has required, however, a major involvement of the principal investigator. Some details on progress in the various areas of interest are reported below.

2.1 PSE in General Curvilinear Coordinates

Previous work has either neglected or only partially accounted for the curvature effects on basic flow and stability characteristics. While the step-by-step inclusion of curvature in previous work has provided the opportunity for follow-up publications of minor value, we have decided to account for the curvature terms completely and from the beginning. In a first approach, we have derived the nonlinear incompressible stability equations including transverse and longitudinal curvature as functions of the distance from the wall. The linearized equations have been coded for use with both spectral method or compact finite-difference method. The coded insert files are consistent with the file format used by the stability code linear.x (Herbert 1990) and the more advanced and efficient stability code LISA developed at DynaFlow. These files can be directly incorporated in the PSE code.

A different approach has been developed for the compressible case. The full nonlinear equations which account for high Mach numbers (up to quartic terms) are formulated for Cartesian coordinates. This challenging set of equations is used for all configurations. Additional subroutines and insert files have been incorporated to account for the metric by a first transformation from the coordinates of the basic-flow computation to Cartesian coordinates and a second transformation from Cartesian coordinates to the coordinate system for the stability computation. The strict separation of the metrics from the physics makes the problem more manageable. The distinction of two transformations allows greater flexibility in adapting to the results of CFD codes with structured grids and choosing optimal coordinates for the PSE analysis. The choice of proper coordinates for solving the PSE is important since the normal-mode solutions of the linear stability and the extended form of the PSE solution involve approximations that depend on the coordinate system.

While concepts, modular structure, and many of the insert and data files are similar to previous codes, a special version of LISA and the compressible PSE code COPS have been developed in cooperation with G. Stuckert of DynaFlow. The testing of these codes has been challenging since there are rarely any reliable data to compare. To guarantee correct function, we have devised a suite of tests that solves the same group of problems in different coordinate systems. The results of these tests are not expected to completely agree but are within the known approximations involved in the analysis.

For flows in realistic geometries, various procedures have been coded and compared to obtain the metric terms and flow quantities as well as their derivatives as accurately as possible. This task is non-trivial since the finite-difference methods used for calculating the basic flow is usually only of second order in space. There are certain trade-offs between solving the stability problem with spectral or finite-difference methods. The spectral method is advantageous by requiring lower derivatives than the widely used 4th-order compact scheme. The compact scheme, however, can utilize the given data at the grid points directly while the spectral method uses less points in a different yet rigid distribution. Suitable procedures have been developed for both cases since the spectral method is far superior for calculating eigenvalue spectra needed to identify the complete set of unstable modes. Finite-difference methods, however, are more efficient for tracing a specific mode over variable parameters and for the marching procedure of the PSE code.

Formulation of the PSE equations and practical applications reveal two severe disadvantages of the compact method: the need for writing the equations as a first-order system and the additional differentiation of the equations required to reduce the truncation error. The first-order system introduces the inverse of the transverse velocity component of the basic flow into the coefficients of the differential equations. This transverse component is generally small and difficult to accurately obtain by finite-difference methods. Moreover, the transverse component can change sign and cause undesirable singularities of the problem. We have therefore performed extensive studies of high-order numerical methods suitable for boundary-layer, stability, and PSE calculations.

2.2 Hermitian Methods

The goal of our efforts was to find finite difference schemes that are of high order, can be applied to second- and third-order differential equations, lead to block-tridiagonal systems (for efficient solution), and work for nonuniform grids. The result of this work was the selection of Hermitian methods which involve only three neighboring points. The use of the function values and derivatives at these points introduces enough degrees of freedom to reduce the truncation error to a desirable order.

Hirsh (1975) has used Hermitian high-order finite-difference schemes to solve some fluid mechanics problems. He attributes the scheme to "a suggestion made by Kreiss, pertaining to a new compact differencing of fourth-order accuracy." The idea of formulating high-order finite-difference approximations in a compact way, i.e. by utilizing the values of derivatives instead of an increasing number of neighboring function values, dates in fact back to the work of Hermite (1912). Selected formulas are tabulated by Collatz (1966, Table III, pp. 538ff) who also discusses Hermite's method. Both Collatz and Hirsh give expressions only for equidistant grid points.

To maintain high order, special attention has to be paid to the boundary conditions. To achieve the same 4th-order approximation for interior and boundary points, Hirsh uses boundary formulas that involve more than the three neighboring points in the interior, although this procedure prevents the use of the highly efficient solvers for block-tridiagonal systems.

The use of Hermitian methods on coarse and nonuniform grids is discussed by Adam (1975). Adam uses boundary formulas of lower order than in the interior and uses nonuniform grids to improve the accuracy near the boundaries. He concludes that the lower-order boundary formulas have no detrimental effect on the accuracy of the solution. However, Adam's utilization of nonuniform grids is in conflict with our desire to use the grid spacing to account, and increase the resolution, for physical phenomena such as internal boundary layers.

We have developed a systematic procedure to generate all linearly independent Hermitian formulas using up to the third derivative. For a system of N second-order differential equations, two of these formulas are needed at every interior point, three at the boundary. By exploiting the null space of the governing system of Taylor expansions, we have constructed methods of at least sixth order which increases to seventh order as the number of grid

points increases. By an elimination procedure, the original dimension $3N$ of the blocks in the diagonal system can be reduced to $2N$, the same number as with the compact method. Unavoidable deviations from tri-diagonality at the boundaries require a dedicated subroutine for solving the algebraic system. In contrast to the usual solvers for banded matrices, our subroutine exploits the block structure and increases the accuracy of the solution by partial pivoting within blocks.

The Hermitian method has been completely developed for systems of second and third order. Special elimination procedures have been written for systems derived from the Navier-Stokes equations which have no boundary conditions on the pressure. The method matches the accuracy of a spectral method at a fraction, say 2-5% of the computer time and reduced demand for memory. The method is key to using the PSE code on workstations, a definite advantage for practical applications. A further advantage is the use of the governing equations in original form without conversion to a first-order system.

A report on this method including applications to challenging test cases and convergence studies has been prepared and will be refined for publication as time permits.

2.3 Stability of 3D Boundary Layers

Detailed studies have been conducted to find the correct solution to the problem of normal-mode evolution in 3D boundary layers. Controversial views on this subject have been presented by Cebeci, Mack, Malik, and Nayfeh in their papers and at a workshop of the US Transition Study Group. At this time, a clear answer has been found only for boundary layers with 3D velocity over 2D geometry, e.g. infinite or conical wings. Our findings are in essential agreement with Mack. For an infinite wing the spanwise wavelength of disturbances must remain constant. This constraint is violated by most stability codes for practical applications, in particular by all optional strategies of COSAL. We plan to analyze the effect of the 2D approximation by comparative analysis of the same boundary layer on an infinite and a conical wing.

For fully 3D boundary layers, we have performed various conceptual studies aiming at the linear stability (as a first step) of flows over highly tapered and twisted wings or turbine blades with hub and tip. These studies indicate

that the approach will be necessarily computational since the basic flow can only be provided by CFD. Two different computational methods have been drafted which differ in the spectral vs. finite-difference representation on spanwise direction. Implementation and validation of these methods would require at least two man years and is beyond the working period and budget for this contract.

2.4 Support Codes

An unexpected amount of work has been required to analyze and satisfy the prerequisites for obtaining the basic flow for stability and transition analysis in realistic cases. The problem usually starts with the geometry of the body given as an extensive set of truncated coordinates. The metric terms of the body-fitted coordinate system must be extracted from these coordinates. The dense spacing together with the loss of significant digits causes intolerable errors in metric terms that involve higher derivatives of the body slope with respect to the arc length. Various utilities have been written and tested to smooth the data without loosing significant information. While these efforts were successful in some cases, the procedures failed in other situations. Since stability analysis deals with the sensitivity of the flow to small disturbances, significant results can only be obtained by keeping the input data, here the geometry, free of unnecessary disturbances by round-off errors. Once information is lost, it cannot be retrieved by densely spacing inaccurate coordinates. In this case, a sparser set of coordinates appears more appropriate. In any case, careful attention to details of geometry, curvature, and surface-pressure distribution are key to a successful stability analysis.

The second major problem area is the use of Navier-Stokes solvers versus a combination of an Euler solver with a boundary-layer code. The analysis of both Navier-Stokes solutions and Euler solutions for flows over wings and turbine blades has revealed unexpected flaws in these solutions. While our access to the variety of codes is very limited, the present status of computers and computational methods appears to prevent sufficiently accurate solutions for the boundary layer. In addition, the high cost of current DNS is unaffordable in engineering practice. This view is shared by various design engineers from industrial R&D labs.

The combination of an Euler code with a boundary-layer code is currently seen as the best way to obtain the basic flow. Of the results of an Euler code,

only the surface-pressure distribution is actually needed. The surface pressure is considered the easiest-to-get and most accurate result of these codes and has been the goal of much of the CFD development in the past. Velocities and stream-line orientation at the surface can be used for cross-checks with the boundary-layer calculation. Good boundary-layer codes are rare to find. Most codes are rather old and use finite-difference methods of only second order. We have analyzed the special version WING of the Kaups-Cebeci code commercially used in combination with COSAL and found unacceptable inaccuracies especially for wings with small taper. The accuracy was improved by recoding sections of the code. We have designed a new code that solves an extended set of flow problems with Hermitian finite-difference methods. Extensions concern primarily the boundary conditions that account for suction and prescribed temperature or heat flux at the body. The implementation of the design is not intended within this project since we want to dedicate our resources to the fundamental aspects of transition prediction in practice.

2.5 Transition Mechanisms

With the PSE research code, we have focused on establishing a catalogue of transition mechanisms originating from different input models for 2D and 3D boundary layers. The mechanisms in 2D boundary layers without wall curvature caused by secondary instability or direct mode interaction have been analyzed with special emphasis on the details of the coupling mechanism. Prototype results are discussed in the AGARD course notes on "Parabolized Stability equations" in Appendix A. For flows with primary Görtler or crossflow instability the transition picture is less well understood. Both types of instability lead to disturbance growth with larger rates than the feeble TS instability. Nonlinear terms act stabilizing at large amplitudes in excess of 5%, say. The internal shear layers that are considered the cause of inviscid secondary instabilities form only in highly nonlinear stages of the evolution. The secondary instability analysis of these nonlinear stages, though straightforward by accounting for a number of harmonics or using two-dimensional eigenfunctions, is computationally expensive and time-consuming because it has to be repeated at numerous levels of the nonlinear evolution. Some results of such analyses have been obtained by Malik at NASA Langley.

Most of our analyses were conducted to obtain an overview over the nonlinear characteristics of Görtler vortices and steady or unsteady cross-flow

vortices. Detailed calculations were performed for the swept-wing flows experimentally studied by Radetztski et al. at ASU (Saric 1993). Although the experimental flow is practically incompressible, the compressible code COPS was employed to account for curvature effects. The detailed comparison of PSE results with the experimental data is still ongoing (M. Wang, forthcoming thesis). The qualitative agreement is obvious. The study of interactions between nonlinear cross-flow vortices and unsteady disturbances that should lead to secondary instabilities and the breakdown of the disturbed flow required some modifications of the PSE research code. Although these changes have been made, the computations with the new version were not completed within the working period of this contract.

2.6 Disturbance Environment and Receptivity

Currently, the PSE codes are developed to solve the initial-boundary-value problems of linear and nonlinear disturbance evolution in quasi-3D (three velocity components depending on two spatial coordinates) flows over simple or realistic geometries.

To apply these codes for practical benefit, the initial and boundary conditions must be specified to characterize the proper disturbance environment in atmospheric flight, different wind tunnels, or gas turbines. Very limited measurements are available for wind tunnels (typically the turbulence level) while the operating environment of airplanes and gas turbines is largely unknown. The work in this area essentially involves the construction of model-data sets as input to the codes based on mechanisms and scales of instabilities and comparison of the results with observed transition points. Uncertainty arises both from insufficient knowledge of the environmental disturbances at the boundary (vibrations, roughness, waviness) or in the free stream and the receptivity of the flow which determines the associated disturbance amplitudes inside the boundary layer.

We have studied different types of model data. A first type accounts only for initial data while the boundary conditions remain homogeneous. This model closely follows the approach in most of the DNS work. The model consists of a combination of stability modes with proper frequencies and wavelength (calculated using LISA) and empirically specified amplitudes. Use of this model in the analysis of a group of problems associated with the flow in gas turbines has been largely successful (Herbert et al. 1993). The

work also revealed some shortcomings of this first type of input model in flows which have an extended region of accelerated and hence stable flow, such as the suction side of turbine blades. In these cases, the initial disturbances decay although the turbulent fluctuations in the core flow should maintain a certain disturbance level in actual flows. We have studied, and in simple flows, implemented the concept of area distributed receptivity into a second type of input model. PSE runs for different physical disturbances at the edge or at the body have been performed to account for different aspects of the disturbance environment. The successful implementation of inhomogeneous boundary conditions in the PSE code was enabled by the greater flexibility of the Hermitian methods and has lead to receptivity studies as a broad area of application for the PSE codes. Receptivity, instabilities, and transition can be covered in a single continuous PSE run.

In various runs, we have replaced the generation of initial data by inhomogeneous conditions at the initial position. This approach is similar e.g. to the introduction of wave packets in experiments or DNS runs. A pulse, for example, introduces a two-dimensional spectrum of disturbance waves, all in proper phase relation (a problem in Gaster's (1975) analysis), and allows detailed studies of the transient evolution and ultimate growth or decay. A PSE run to "repeat" the experiment of Gaster and Grant (1975) is completely set up. The run has not yet been executed since the post-processing of the data will be time-consuming and we currently have insufficient disk space to hold the data on-line.

A more tractable problem is the disturbance field generated by a harmonic point source. For this case, experimental data of Gilev et al. (1981), Kachanov (1985), Kendall (1993a,b), and Watmuff (1993) are available as well as linear stability calculations by Mack (1984) and Balakumar & Malik (1992). Linear PSE runs have been performed with more than 200 modes to provide sufficient resolution near the source. The still ongoing analysis of the various data is performed in cooperation with L. Mack. Good agreement has been found between theoretical results for the farfield provided the heuristic energy correction is suppressed. This correction has been introduced by Gaster to "account" for nonparallelism and led to a better agreement between theoretical and experimental data in previous comparisons. The current picture of the experimental data is somewhat confusing. From the few DNS solutions for the near field, it has become clear so far that size and type of the source have an unexpectedly strong influence on the field. These result

are relevant for the modeling of disturbances such as roughness elements exposed to sound or actuators in flow control applications. The DNS results also show certain shortcomings in the initial data for the PSE analysis. We expect that larger DNS runs for the different experimental conditions will help to clarify the picture. These runs will be performed and analyzed once additional computer resources (memory, disk space) become available.

Other studies relate to the possible causes for the characteristic differences between wave packets originating from free-stream turbulence and pulsed blowing/suction at the wall (Kendall 1993). It is likely that the narrow free-stream packets "ride" on a streaky structure that is simultaneously created by a convected source. The source can only be explained as a statistical event in the free-stream turbulence. We have performed some PSE analyses of models for this situation but were unable to complete these studies within the working period.

2.7 Transient Disturbance Growth

It has recently been found (Henningson & Schmid 1992, Butler & Farrel 1992, Trefethen 1992) that disturbances in shear flow can grow to considerable amplitudes even if they are not associated with unstable eigenvalues of the stability equations. This transient growth and ultimate decay is strongest for disturbances with spanwise periodic streamwise vorticity. The linear growth process is characteristic of initial-boundary-value problems for non-selfadjoint differential equations. While previous work considered the temporal evolution of a given initial field in parallel flows, we have studied the spatial evolution of disturbances introduced by inhomogeneous boundary conditions (spanwise periodic suction, waviness, or pressure variation at the initial position) with the PSE technique. A first set of results has been reported by Herbert & Lin 1993. The analysis has provided a detailed explanation for the occurrence of steady and low-frequency Klebanoff modes (Klebanoff 1971) in the flat-plate boundary layer. Depending on Reynolds number, frequency, and spanwise wave number, boundary disturbances can create Klebanoff modes, TS waves, or fast-traveling modes concentrated at the edge of the boundary layer, as observed in Kendall's experiments. By accounting for streamwise wall curvature, our results show a stabilizing effect of convex curvature while sufficiently strong concave curvature prevents the decay of the modes: Klebanoff modes are analytically connected to Görtler

vortices and continue to grow exponentially. In Falkner-Skan-Cooke flow, the introduction of sweep permits to show the analytical connection between Klebanoff modes and cross-flow vortices. All these modes share similar receptivities. The pure effect of pressure gradients has not yet been investigated. A vague connection to the observed streamwise vortices penetrating the stagnation plane in the flow over circular cylinders (or blunt leading edges) requires further strengthening.

We have concluded that other phenomena such as the "instability" of pipe and pipe-entrance flow and the occurrence of cross-flow vortices in rotating flows are closely associated with the transient growth mechanism. Analysis of these phenomena of scientific as well as practical interest could not be pursued with the available manpower.

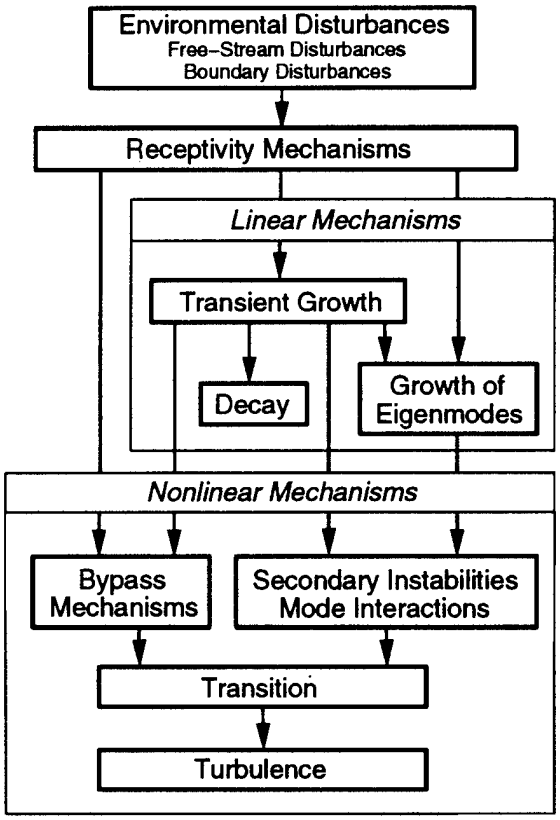

Figure 1: Pathways to Transition and Turbulence.

The transient growth mechanism has been incorporated into a new overview of pathways to turbulence shown in figure 1. This figure is the draft of the key figure for a discussion of the transition issue by Morkovin, Reshotko & Herbert to be submitted to Science.

Various other receptivity studies are in direct context with flow control and the analysis of actuator concepts. The insight into the transient flow originating from an actuator is important for the layout of the experimental arrangement of the flow-control system. Details of these studies will be reported under contract F49620-93-1-0135.

2.8 Adjoint Linear Problems

The adjoint problem to the Orr-Sommerfeld equation has often been solved to determine Landau constants in perturbation series for nonlinear stability problems. The theory of transient disturbance growth in shear flows heavily rests on the non-selfadjoint nature of the initial-boundary-value problem. Zhigulev & Fedorov (1987) used the biorthogonal system of eigenfunctions (of the original and adjoint problem) to study the boundary-layer receptivity to acoustic disturbances. At the APS meeting 1991, Hill reported on a theoretical approach for analyzing the restabilization of the wake behind a circular cylinder based on the solution to the adjoint linearized Navier-Stokes equations (Hill 1992). This latter work showed that the adjoint problem possesses not only formal mathematical properties but also a deep physical meaning: the adjoint solution describes the sensitivity (or receptivity) of the flow to small forcing of different nature. Therefore, the adjoint solution provides a rigorous tool to the analysis of receptivity and flow-control strategies.

We have started to investigate the use of adjoint solutions and to formulate and code the equations in increasingly general situations. The initial work is for incompressible 3D boundary layers. Starting from the linearized Navier-Stokes equations, it becomes immediately clear that adjoint solutions can be generated for the local analysis in parallel flows solving ordinary differential equations. In nonparallel boundary layers the adjoint PSE can be formulated and solved by marching upstream. For given wave numbers and frequency and the associated adjoint eigenfunction at some initial position, contour lines of appropriate components of the solution directly indicate where to place a disturbance generator to obtain the strongest disturbance at the (downstream) initial position. Application to the Blasius boundary layer

provides, e.g. the intuitively clear recommendation to place the vibrating ribbon near the critical layer at branch I to obtain the largest TS wave. Analyzing proper integrals involving the adjoint solution provides the effects of finite-size weak sources of momentum, mass, or vorticity in the interior or at the boundaries. The effects of pressure sources are not yet fully understood.

Hill (1993) has recently presented results for receptivity in parallel flows and locally parallel boundary layers. He has also used the 2D PSE to compute the adjoint solution in the nonparallel Blasius boundary layer (Hill 1993b). We consider a coordination of efforts or a cooperation on this promising new area. Since his continued funding at CTR is uncertain and receptivity issues are not a focus of this center, Dr. Hill may be available to work with us either at the University or at DynaFlow.

2.9 Flow Control and Neural Networks

During a part of the working period, our activities have been redirected from the analysis of transition to the control of transition in boundary layers. The work of two students in this area is supported by AFOSR-AASERT Fellowships.

Our capability to simulate transitional flows efficiently has been exploited to prepare a joint theoretical/computational/experimental study of flow control. The experiments are conducted by J. Haritonidis. Under this contract, we have concentrated on neural networks for flow control, specifically on suitable architecture, training methods, fault tolerance, and self-adaptivity. Various nonlinear dynamical systems such as the Lorenz equations have been modeled with as simple as possible networks. The Neuralworks Professional II software has been acquired to simulate networks on one of our workstations. With three inputs, three outputs, and six "neurons" in a single hidden layer, the Lorenz equations can be well modeled. Besides standard dynamical systems, we have successfully modeled a nonlinear feedback system for engine speed control.

For training, we had the best experience with DRS (direct random search) which is relatively slow but does not settle in local minima like back propagation. A problem that virtually found little attention in the literature is to measure the quality of a trained network or to compare the quality of different networks. The residual rms error is not a good quality indicator. We have used various statistical methods to analyze the discrete response

of the original system and of the neural network for the same input data. While the development is continuing, we have now tools at hand to compare network function and to measure the deterioration of the network response for increasing prediction times and the degradation through failure of connections or complete neurons. Interestingly, the loss of a heavily weighted connection can be more devastating than the loss of the whole neuron to which it is connected. A report on these studies has been given at the AIAA Shear-Flow Conference in Orlando (Fan & Herbert 1993).

After studies on fundamentals, we have concentrated on a flow-control situation that can be both simulated and tested in a wind tunnel. For simplicity, we have chosen the 2D problem of wave packets periodically generated by a ribbon or point source. Each packet consists of a mix of 2D waves with different frequencies. The mixture of phases and phase speeds poses a far more challenging control problem than the simple wave cancellations in earlier work. The test case has been used to study number and arrangements of sensors, actuators, and feedback connections. The preliminary design developed by computer has been successfully tested in the experiment. In this way, we have not only tested the concept and function of neural-network control but also our design capabilities prior to attacking more complex situations.

3 Personnel

The following personnel has participated in the work and has been partially supported under this contract:

Th. Herbert, Principal Investigator

Rihua Li, Postdoctoral Associate

Mengjie Wang, Ph.D. Student

Xuetong Fan, Ph.D. Student

Eugene Kalinin, M.S. Student

Charlotte Herbert, Systems Programmer 2

Lorenz Hofmann (MS Student) has cooperated in this program under an AFOSR-AASERT Fellowship. Rihua Li who accepted another position in

March 1993 and Mengjie Wang have worked on aspects and applications of the PSE. M. Wang will receive his Ph.D. in the near future. Xuetong Fan and Lorenz Hofmann have worked on neural networks and their application to flow control. Their work continues under contract F49620-93-1-0135. Eugene Kalinin cooperates in the analysis and physical interpretation of solutions to the adjoint linearized Navier-Stokes equations.

4 Publications

The following publications were completed or originated from work under support by this contract:

"Nonlinear Evolution of Secondary Instabilities in Boundary-Layer Transition," by J. D. Crouch and Th. Herbert, *J. Theor. Comp. Fluid Dynamics* (1992), in press.

"Exploring Transition by Computer," by Th. Herbert, *J. Appl. Num. Math.*, Vol. 7, No. 1, pp. 3-27 (1991).

"Analysis of the Linear Stability of Compressible Boundary Layers using the PSE," by F. P. Bertolotti and Th. Herbert, *J. Theor. Comp. Fluid Dynamics*, Vol. 3, pp. 117-124 (1991).

"A Note on the Calculation of Landau Constants," by J. D. Crouch and Th. Herbert, *Phys. Fluids A*, Vol. 5, pp. 283-285, (1993).

"Computation of Laminar Flow over a Long Slender Axisymmetric Blunted Cone in Hypersonic Flow," by V. Esfahanian, Th. Herbert, and O. R. Burggraf, AIAA Paper No. 92-0756 (1992).

"Stability of Hypersonic Flow over a Blunt Body," by Th. Herbert and V. Esfahanian, Proc. AGARD Symposium *Theoretical and Experimental Methods in Hypersonic Flows*, Torino, Italy. (1992). To appear.

"Linear and Nonlinear Stability of the Blasius Boundary Layer," by F. P. Bertolotti, Th. Herbert, and P. R. Spalart, *J. Fluid Mech.* Vol. 242, pp. 441-474 (1992).

"Stability and Transition on Swept Wings," by G. K. Stuckert, Th. Herbert, and V. Esfahanian, AIAA Paper No. 93-0078 (1993).

"Effects of Free-Steam Turbulence on Boundary-Layer Transition," by Th. Herbert, G. K. Stuckert, and V. Esfahanian, AIAA Paper No. 93-0488 (1993).

"Parabolized Stability Equations," by Th. Herbert, in: Special Course on *Progress in Transition Modeling*, AGARD Report No. 793 (1993).

"Studies on Boundary-Layer Receptivity with Parabolized Stability Equations," by Th. Herbert and Nay Lin, AIAA Paper No. 93-3053 (1993).

"Active Flow Control with Neural Networks," by X. Fan, L. Hofmann and Th. Herbert, AIAA Paper No. 93-3273 (1993).

"Nonlinear Analysis of Swept Wing Transitional Boundary Layers," by G. K. Stuckert and Th. Herbert, SAE Paper Klebanoff Modes," by Th. Herbert,

Bull. Amer. Phys. Soc., Vol. 38, p. 2207.

"Neural Networks for Active Flow Control," by X. Fan, L. Hofmann, and Th. Herbert, Bull. Amer. Phys. Soc., Vol. 38, pp. 2251-2252.

"Transition Control Using Neural Networks," by J. H. Haritonidis, M. Avery, X. Fan, and Th. Herbert, Bull. Amer. Phys. Soc., Vol. 38, p. 2251.

"PSE Analysis of Receptivity and Stability in Swept Wing Flows," by M. Wang, Th. Herbert, and G. K. Stuckert, AIAA-94-0180 (1994)

5 Technical Presentations

"Spatial Evolution of Boundary-Layer Transition," by Th. Herbert, Symposium on *Boundary Layer Stability and Transition to Turbulence*, First Joint ASME-JSME Fluids Engineering Conf., Portland, Oregon (June 1991).

"Engineering Methods for Transition Analysis," by Th. Herbert, Dornier GmbH Research Lab, Friedrichshafen, Germany (September 1991).

"Efficient Simulation of Boundary-Layer Transition," invited lecture, by Th. Herbert, 4th Int. Symp. on *Computational Fluid Dynamics*, Davis, California (September 1991).

"Computation and Stability Analysis of the Compressible Flow over a Blunt

Cone," by Th. Herbert and V. Esfahanian, 44th Annual Meeting, Division of Fluid Dynamics, American Physical Society Tempe, Arizona (November 1991).

"Computation of Laminar Flow over a Long Slender Axisymmetric Blunted Cone in Hypersonic Flow," by V. Esfahanian, Th. Herbert, and O. Burggraf, 30th Aerospace Sciences Meeting, Reno, Nevada (January 1992).

"Transition Prediction in High-Speed Boundary Layers," by Th. Herbert, Fluid Dynamics Laboratory, NASA Ames Research Center, Mountain View, California (January 1992).

"Analysis of Transition and Heat Transfer in Gas Turbines," by Th. Herbert, NASA Lewis Research Center, Cleveland, Ohio (March 1992).

"Stability of Hypersonic Flow over a Blunt Body," by Th. Herbert and V. Esfahanian, AGARD Symposium on *Theoretical and Experimental Methods in Hypersonic Flows*, Torino, Italy (May 1992).

"Transition Analysis with Parabolized Stability Equations," by Th. Herbert, DLR Göttingen, Germany (May 1992).

"Modern Developments in Numerical Simulation of Flow and Heat Transfer," keynote lecture, by Th. Herbert, 1992 National Heat Transfer Conference, San Diego, California (August 1992).

"Transition and Heat Transfer in Gas Turbines," by Th. Herbert and G. K. Stuckert, NASA Lewis Research Center, Cleveland, Ohio (March 1992).

"Boundary-Layer Transition on Aerodynamic Configurations," by Th. Herbert, International Symposium on *Computational Fluid Dynamics for Air Vehicle Technology*, Wright-Patterson AFB, Ohio (September 1992).

"Studies on Swept Wing Transition," by Th. Herbert and G. K. Stuckert, SAE Aerotech '92, Anaheim, California (October 1992).

"Stability and Transition on Swept Wings," by G. K. Stuckert and Th. Herbert, NASA Ames Research Center, Moffett Field, California (October 1992).

"Use of Parabolized Stability Equations for Transition and Heat Transfer Studies in a Gas Turbine," by Th. Herbert and G. K. Stuckert, Workshop on

Bypass Transition, NASA Lewis Research Center, Cleveland, Ohio (November 1992).

"Transition Studies on Realistic Configurations," by Th. Herbert and G. K. Stuckert, 45th Meeting of the American Physical Society, Division of Fluid Dynamics, Tallahassee, Florida (November 1992).

"Stability and Transition on Swept Wings," by G. K. Stuckert, Th. Herbert, and V. Esfahanian, 31st Aerospace Meeting & Exhibit, Reno, Nevada, January 11 - 14, 1993.

"Effects of Free-Steam Turbulence on Boundary-Layer Transition," by Th. Herbert, G. K. Stuckert, and V. Esfahanian, 31st Aerospace Meeting & Exhibit, Reno, Nevada, January 11 - 14, 1993.

"Parabolized Stability Equations," by Th. Herbert, AGARD Special Course on "Progress in Transition Modeling," Madrid, Spain, March 22-25, 1993.

"Parabolized Stability Equations," by Th. Herbert, AGARD Special Course on "Progress in Transition Modeling," Brussels, Belgium, March 29 - April 1, 1993.

"Active Flow Control with Neural Networks," by X. Fan, L. Hofmann, and Th. Herbert, AIAA Shear Flow Conference, Orlando, Florida, July 6 - 9, 1993.

"Studies of Boundary-Layer Receptivity with Parabolized Stability Equations," by Th. Herbert and N. Lin, AIAA 24th Fluid Dynamics Conference, Orlando, Florida, July 6 - 9, 1993.

"Simulations of Boundary-Layer Transition," by Th. Herbert, Workshop on "End-Stage Transition," Blue Mountain Lake, New York, August 15 - 18, 1993.

"Receptivity and Transition on Turbine Blades," by Th. Herbert, AFOSR Meeting on "Turbulence and Heat Transfer," Flagstaff, Arizona, 25-27 August 1993.

"Active Flow Control Using Neural Networks," by Th. Herbert and J. H. Haritonidis, AFOSR Meeting on "Turbulence and Heat Transfer," Flagstaff, Arizona, 25-27 August 1993.

"A PSE Code for Transition Analysis," by Th. Herbert, The First Bom-

bardier International Workshop, Montreal, Canada, September 20 - 21, 1993.

"Nonlinear Analysis of Swept Wing Transitional Boundary Layers," by G. K. Stuckert and Th. Herbert, SAE Aerotech '93, Costa Mesa, California, September 27 - 30, 1993.

"A PSE Code for the Analysis of Transition and Heat Transfer," by Th. Herbert, G. K. Stuckert and Nay Lin, Workshop on Bypass Transition, NASA Lewis Research Center, Cleveland, Ohio, November 18 - 19, 1993.

"Appearance and Metamorphosis of Klebanoff Modes," by Th. Herbert, 46th Meeting of the APS-DFD, Albuquerque, New Mexico, November 21 - 23, 1993.

"Neural Networks for Active Flow Control," by X. Fan, L. Hofmann, and Th. Herbert, 46th Meeting of the APS-DFD, Albuquerque, New Mexico, November 21 - 23, 1993.

"Transition Control Using Neural Networks," by J. H. Haritonidis, M. Avery, X. Fan, and Th. Herbert, 46th Meeting of the APS-DFD, Albuquerque, New Mexico, November 21 - 23, 1993.

"A PSE Code for the Analysis of Receptivity, Stability, and Transition," by Th. Herbert, G. K. Stuckert, and N. Lin, Boeing Commercial Airplane Group, Seattle, Washington, December 13, 1993.

6 References

Adam, Y. 1975 "A Hermitian finite-difference method for the solution of parabolic equations," *Comp. & Maths. with Appls.*, Vol. 1, pp.393-406.

Balakumar, P. and Malik, M. R. 1992 "Waves produced from a harmonic point source in a supersonic boundary-layer flow." *J. Fluid Mech.*, Vol. 245, pp. 229-247.

Butler, K. M. and Farrel, B. F. 1992 "Three-dimensional optimal perturbations in viscous shear flow," *Phys. Fluids A*, Vol. 4, pp. 1637-1650.

Collatz, L. 1966 *The Numerical Treatment of Differential Equations*, Springer-Verlag.

Fan, X., Hofmann, L. and Herbert, Th. 1993 "Active flow control with neural networks," AIAA-93-3273

Gaster, M. 1975 "A theoretical model of a wave packet in the boundary layer on a flat plate," *Proc. Roy. Soc. Lond.* A, Vol. 347, pp. 271-289.

Gaster, M. and Grant, I. 1975 "An experimental investigation of the formation and development of a wave packet in a laminar boundary layer," *Proc. Roy. Soc. Lond.* A, Vol. 347, pp. 253-269.

Gilev, W. M., Kachanov, Yu. S., and Kozlov, V. V. 1981 "Growth of spatial wave packets in a boundary layer." Preprint No. 34-81, Inst. Theor. and Appl. Mech., USSR Acad. Sci., Novosibirsk (In Russian).

Henningson, D. S. and Schmid, P. J. 1992 "Vector eigenfunction expansions for plane channel flows," *Stud. Appl. Math.*, preprint.

Herbert, Th. 1990 "Linear.x - A code for linear stability analysis," in: *Instability and Transition*, Vol. II, (Eds.) M. Y. Hussaini, R. G. Voigt, pp. 121-144, New York: Springer-Verlag.

Herbert, Th. and Lin, N. 1993 "Studies of boundary-layer receptivity with parabolized stability equations," AIAA-93-3053.

Hermite 1912 Oeuvres, Vol. 3, pp. 438ff.

Hill, D. C. 1992 "A theoretical approach for analyzing the restabilization of wakes," AIAA-92-0067

Hill, D. C. 1993a "Adjoint systems and their role in the receptivity problem for boundary layers," CTR Manuscript 146.

Hill, D. C. 1993b "Receptivity in the boundary layer: a role for adjoint solutions," Bull. Amer. Phys. Soc., Vol. 38, pp. 2207-2208.

Hirsh 1975 "Higher order accurate difference solutions of fluid mechanics problems by a compact differencing technique," *J. Comp. Phys.*, Vol. 19, pp. 90-109.

Kachanov, Yu. S. 1985 "Development of spatial wave packets in boundary layer." In: *Laminar-Turbulent Transition*, Ed. V. V. Koslov, Springer Verlag, pp. 115-123.

Kendall, J. M. 1993a "Boundary-layer receptivity to weak free-stream turbulence," Notes, Workshop on End-Stage Transition, Blue Mountain Lake, NY, September 1993.

Kendall, J. M. 1993b "Experimental methods and results on the generation of Tollmien-Schlichting wave packets by freestream turbulence," Bull. Amer. Phys. Soc., Vol. 38, p. 2208.

Klebanoff, P. S. 1971 "Effect of free-stream turbulence on a laminar boundary layer," *Bull. Amer. Phys. Soc.,* Vol. 16, and Personal Communication, 1985.

Mack, L. M. 1984 "Boundary-layer linear stability theory." In: *Special Course on Stability and Transition of Laminar Flow*, AGARD Report No. 709, pp. 3.1-3.81.

Saric, W. S. 1993 "Physical description of boundary-layer transition: experimental evidence," AGARD Report 793.

Trefethen, L. N., Trefethen, A. E., and Reddy, S. C. 1992 "Pseudospectra of the linear Navier-Stokes evolution operator and instability of plane Poiseuille and Couette flows," Techn. Report TR 92-1291, Dept. Computer Science, Cornell Univ.

Watmuff, J. H. 1993 "Interaction between instabilities originating from suction holes." *Bull. Amer. Phys. Soc.*, Vol. 38, p. 2237.

Zhigulev, V. N. and Fedorov, A. V. 1987 "Boundary-layer receptivity to acoustic disturbances," *J. PMTF*, Vol. 28, pp.30-37.

Appendix A

Parabolized Stability Equations

Thorwald Herbert

AGARD R-793

Special Course on

"Progress in Transition Modelling"

Madrid, Spain, 22-25 March, 1993

Brussels, Belgium, 29 March - 1 April, 1993

Parabolized Stability Equations

Thorwald Herbert
Department of Mechanical Engineering
The Ohio State University
206 West 18th Avenue
Columbus, Ohio 43210-1107, USA
and
DynaFlow, Inc.
3040 Riverside Drive, Suite 109
Columbus, Ohio 43221-0319, USA

1 SUMMARY

The parabolized stability equations (PSE) are a new approach to analyze the streamwise evolution of single or interacting Fourier modes in weakly nonparallel flows such as boundary layers. The concept rests on the decomposition of every mode into a slowly varying amplitude function and a wave function with slowly varying wave number. The neglect of the small second derivatives of the slowly varying functions with respect to the streamwise variable leads to an initial-boundary-value problem that can be solved by numerical marching procedures. The PSE approach is valid in convectively unstable flows. The equations for a single mode are closely related to those of the traditional eigenvalue problems for linear stability analysis. However, the PSE approach does not exploit the homogeneity of the problem and, therefore, can be utilized to analyze forced modes and the nonlinear growth and interaction of an initial disturbance field. In contrast to the traditional patching of local solutions, the PSE provide the spatial evolution of modes with proper account for their history. The PSE approach allows studies of secondary instabilities without the constraints of the Floquet analysis and reproduces the established experimental, theoretical, and computational benchmark results on transition up to the breakdown stage. The method matches or exceeds the demonstrated capabilities of current spatial Navier-Stokes solvers at a small fraction of their computational cost. Recent applications include studies on localized or distributed receptivity and prediction of transition in model environments for realistic engineering problems. The following describes the basis, intricacies, and some applications of the PSE methodology.

2 Introduction

The analysis of the transition process in shear flows is of both fundamental and practical interest. Over the past decade, much insight into this process has been gained from combined experimental, theoretical, and computational studies. However, this progress has little impact yet on the engineering methods used for aerodynamic design, since the successful research tools suffer from some shortcomings that prevent their application to practically relevant phenomena. The traditional engineering tools still rest on questionable concepts and rely on spotty empirical data bases which are costly to generate for advanced projects.

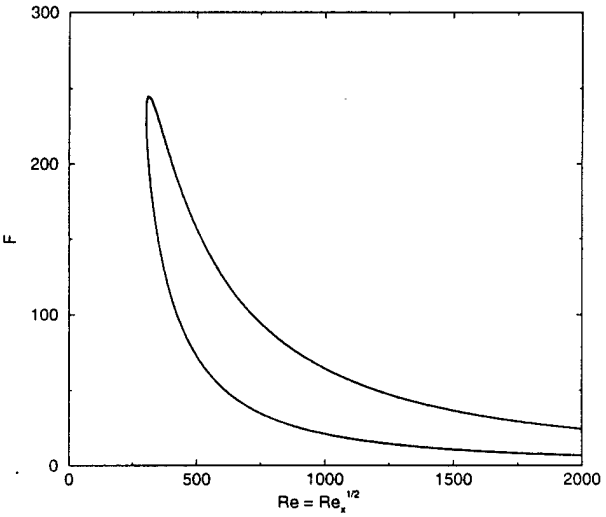

Figure 1: Stability diagram for the flat-plate boundary layer.

In low-speed experiments in wind tunnels of very low turbulence levels, "natural", i.e. uncontrolled and unavoidable transition in the flat-plate boundary layer occurs at length-Reynolds numbers Re_x below $4 \cdot 10^6$ or slightly higher in anechoic tunnels. A glance at the stability diagram for this flow in figure 1 shows that the occurrence of natural transition restricts experimental studies of the controlled disturbance evolution from branch I to branch II to Reynolds numbers $Re = Re_x^{1/2}$ well below $Re < 2000$

and hence to frequencies $F > 25$. In fact, the microscopic experiments are restricted to this range, where two-dimensional waves are "most dangerous" [1]. On the other hand, the common e^N criterion for the amplitude ratio and the correlation with experimental data show transition typically at $N \geq 10$ [2, 3]. To obtain an amplitude ratio of e^{10} at branch II, the frequency must be $F < 25$. At these lower frequencies, two-dimensional waves are no longer preferred. Consequently, the microscopic experiments do not necessarily reveal the transition process as it occurs in practice, let alone the different disturbance environments in free flight and in wind tunnels.

Theoretical and computational studies of transition and its inherent mechanisms have led to considerable progress in explaining and reproducing the results of the ribbon-controlled experiments. Accordingly, these studies have revolved around the same parameter range of relatively small Reynolds numbers, high frequencies, and low growth rates. The linear theory of primary instability is not restricted to this range, and the underlying parallel-flow approximation is commonly assumed to be better justified at lower frequencies and the associated higher Reynolds numbers downstream of branch I. Therefore, the e^N calculations are performed without major concern. However, nonparallel effects are indeed significant for certain three-dimensional disturbances, invalidate Squire's theorem and the normal-mode concept for long-wave disturbances, and may accumulate in the N factor integration. Even if streamwise variations of the boundary layer are properly included, the primary instability is only one of the important steps toward transition.

The development of the theory of secondary instability [4] has advanced our insight into the next step where strong vortical mechanisms are activated. In spite of some necessary approximations, the theory provides results in good agreement with experiments and enables systematic studies in a multi-dimensional parameter space. However, the potential for significant improvements in predicting the onset of transition is disappointing since the theory is still linear and hence cannot reveal the nonlinear coupling of primary and secondary disturbances that appears crucial for transition. A perturbation scheme has been developed to successfully analyze this nonlinear stage [5], but the method is not as well suited for routine applications as many other weakly nonlinear models and methods in this field.

Over the past decade, details and structure of the transition process have been studied with asymptotic theories for high Reynolds numbers [6]. These theories enlist impressive results for some linear and nonlinear problems and local phenomena that can be captured within a single asymptotic structure. The drastically simplified equations often allow closed-form solutions or ease numerical solutions to nonlinear problems. However, the quantitative features of the transition process that critically depend on the physical parameters, especially the Reynolds number, may not be accessible to these asymptotic methods. As in other asymptotic theories, it cannot be a priori assured that expansion parameters such as $\epsilon = Re_x^{-1/8}$ are sufficiently small for quantitative conclusions.

With increasing capability and availability of supercomputers, efforts have broadened to analyze the transition process by direct numerical solution of the Navier-Stokes equations (DNS) [7]. Computer simulations provide a wealth of detailed data, resolved in 3D space and time, for the idealized prototype problems of traditional stability theory, and can be viewed as a new type of "experiment" under well-controlled conditions. Extracting insight requires tedious post-processing yet is facilitated by the easy access to accurate information on quantities that are difficult to measure, e.g. vorticity. The effects of initial conditions or changes in geometry and basic flow on the transition location would be easy to extract. However, DNS is not yet feasible as an engineering method. The enormous computational costs in both memory and time prohibit parameter studies and have constrained transition simulations in boundary layers to a few runs, typically for the conditions of the benchmark experiments [8, 9, 10]. All simulations are for simple geometries, and only a few track the spatial evolution in streamwise varying boundary layers. Although current research focuses more on realistic simulations and algorithmic improvements, both research and engineering practices demand less expensive methods without intolerably compromising the quality of results. This demand is particularly strong for compressible flows, where the computational requirements increase easily by an order of magnitude. Even the Floquet analysis of secondary instability in a compressible flow can be a challenge for a supercomputer.

Here we discuss a less expensive method that has shown great potential for efficient transition simulations. This method rests on parabolized stability equations (PSE) and takes advantage of the efficient methods available for solving parabolic partial differential equations with marching procedures. The PSE approach can be viewed on one hand as a WKBJ extension of the theoretical approach to nonparallel flows and on the other as a simplification of the Navier-Stokes equations. The approach is based on earlier ideas for analyzing the stability of weakly nonparallel flows [11] and on the concept of convective instability [12] which excludes significant upstream influence of disturbances. While originally intended to capture nonparallel effects on linear stability characteristics of single modes, the nonlinear version of the PSE turned out to provide results on secondary instability and mode interactions that suggest the use of this approach for analyzing transition up to the

spike stage and beyond. The efficiency of the approach and the good agreement of PSE and DNS solutions encourage further development both as a research method and as an engineering tool for transition analysis and prediction.

The following describes the underlying formalisms, mathematical aspects, numerical procedures, and some applications to problems of increasing complexity in incompressible and compressible 2D and 3D boundary-layer flows. The applications to similarity solutions are chosen to exhibit the essential steps of the analysis as well as the potential of the approach. Some applications to realistic geometries are discussed to demonstrate the feasibility of PSE-based engineering methods and to shed some light on the requirements of transition predictions in practice.

3 PSE for Incompressible Flow

The motion of an incompressible fluid with constant density ρ and viscosity μ is governed by the continuity equation

$$\nabla \mathbf{v} = 0 \tag{1}$$

and the nonlinear momentum equations

$$\frac{\partial \mathbf{v}}{\partial t} + (\mathbf{v} \cdot \nabla)\mathbf{v} = -\frac{1}{\rho}\nabla p + \nu \nabla^2 \mathbf{v} \,, \tag{2}$$

where $\mathbf{v}$ is the velocity vector, p the pressure, and $\nu = \mu/\rho$ the kinematic viscosity. In Cartesian coordinates x, y, z, we use the velocity components $\mathbf{v} = (u, v, w)$ and

$$\nabla = \frac{\partial}{\partial x}\mathbf{i} + \frac{\partial}{\partial y}\mathbf{j} + \frac{\partial}{\partial z}\mathbf{k} \,, \tag{3}$$

where $\mathbf{i}, \mathbf{j}, \mathbf{k}$ are the unit vectors in the direction of x, y, z, respectively.

We consider the stability of steady laminar boundary-layer flows over the plane $y = 0$ with edge velocities $U_e(x)$ and $W_e(x)$ in the x and z direction, respectively. As common for stability analysis, we decompose the total flow field $\mathbf{v}, p$ into the steady laminar basic flow $\mathbf{V}, P$ and the deviation (or disturbance) $\mathbf{v}', p'$:

$$\mathbf{v} = \mathbf{V} + \mathbf{v}' \,, \; p = P + p' \,. \tag{4}$$

Owing to the uniformity in z, the steady basic flow takes the form $\mathbf{V} = (U(x,y), V(x,y), W(x,y))$ where V, U_x, and W_x are small and their derivatives U_{xx}, V_x, W_{xx} with respect to x are of order $\mathcal{O}(Re_x^{-1})$ and negligible. Here, the Reynolds number is $Re_x = U_r x/\nu$ with a proper reference velocity U_r. Under the boundary-layer approximation, the basic flow is governed by

$$U_x + V_y = 0 \,, \tag{5a}$$

$$UU_x + VU_y = -\frac{1}{\rho}P_x + \nu U_{yy} \,, \tag{5b}$$

$$0 = -\frac{1}{\rho}P_y \,, \tag{5c}$$

$$UW_x + VW_y = \nu W_{yy} \,, \tag{5d}$$

where $P_x = \rho(U_e dU_e/dx + W_e dW_e/dx)$ is given from potential-flow theory. Equations (5) are parabolic partial differential equations and can be solved as an initial-boundary-value problem in x. Boundary conditions are the no-slip conditions

$$U = V = W = 0 \text{ at } y = 0 \tag{6a}$$

and the asymptotic matching with the edge conditions,

$$U \to U_e \,, \; W \to W_e \text{ as } y \to \infty \,. \tag{6b}$$

The transverse velocity V is small but in general nonzero at the edge of the boundary layer. Of particular interest for theoretical studies are the exact similarity solutions to eqs. (5) and (6). These solutions are obtained from ordinary differential equations and thus do not require the specification of initial conditions. Similarity solutions are the two-dimensional Blasius, Falkner-Skan, or Hiemenz flows or the three-dimensional Falkner-Skan-Cooke or swept Hiemenz flows. For three-dimensional flows, the constant viscosity permits solving first the two-dimensional problem (5a) to (5c) for U and V and afterwards eq. (5d) for W. Little modification is required to extend the basic flows to two-dimensional mixing layers, jets, or wakes, or to axisymmetric cases. Nonsimilar solutions can be generated by numerical techniques.

For the disturbances $\mathbf{v}'$, p' we obtain the "stability equations"

$$u'_x + v'_y + w'_z = 0 \,, \tag{7a}$$

$$u'_t + Uu'_x + u'U_x + Vu'_y + v'U_y + Wu'_z + \frac{1}{\rho}p'_x$$
$$-\nu(u'_{xx} + u'_{yy} + u'_{zz}) = -(u'u'_x + v'u'_y + w'u'_z) \,, \tag{7b}$$

$$v'_t + Uv'_x + Vv'_y + v'V_y + Wv'_z + \frac{1}{\rho}p'_y$$
$$-\nu(v'_{xx} + v'_{yy} + v'_{zz}) = -(u'v'_x + v'v'_y + w'v'_z) \,, \tag{7c}$$

$$w'_t + Uw'_x + u'W_x + Vw'_y + v'W_y + Ww'_z + \frac{1}{\rho}p'_z$$
$$-\nu(w'_{xx} + w'_{yy} + w'_{zz}) = -(u'w'_x + v'w'_y + w'w'_z) \,, \tag{7d}$$

where we have neglected the small term $u'V_x$ in eq. (7c). For a given basic flow, and within the boundary-layer approximation, this system is equivalent to the Navier-Stokes equations and hence of elliptic type.

For the study of instabilities, we usually apply homogeneous boundary conditions

$$u' = 0, \; v' = 0, \; w' = 0 \text{ at } y = 0 \,, \tag{8a}$$

$$u' \to 0, \; v' \to 0, \; w' \to 0 \text{ as } y \to \infty \,, \tag{8b}$$

since any inhomogeneous conditions are already satisfied by the basic flow. In nonlinear problems,

however, the fluctuating components of the disturbance also create a distortion of the steady mean flow $(\bar{u}, \bar{v}, \bar{w})$. Since the mean flow and its distortion are governed by the boundary-layer equations, we must admit $\bar{v} \neq 0$ as $y \to \infty$ with

$$\bar{v}_y \to 0 \text{ as } y \to \infty \tag{8c}$$

and $\bar{p}_x = 0$. In general, the nonlinear stability equations (7) can also be solved under inhomogeneous boundary conditions to account for disturbances at the wall or in the free stream. Numerical simulations often use inhomogeneous boundary conditions to simulate disturbance generators such as a vibrating ribbon. Inhomogeneous boundary conditions are key to the study of forced oscillations and receptivity problems.

In the following we consider the equations in nondimensional form. For convenience we maintain the notation yet delete the factors $1/\rho$ and replace ν by $1/Re$, where Re is formed with a length scale δ_0^* related to the boundary-layer thickness and a characteristic velocity U_0^*. Henceforth the asterisk denotes dimensional quantities. Specific choices will depend on the application.

3.1 Linear Stability of Parallel Flow

To illustrate the conceptual difference between the traditional local stability analysis and the PSE approach, we consider the linear stability of a parallel flow $\mathbf{V} = (U(y), 0, W(y))$.

3.1.1 Local Analysis

For a strictly parallel flow, the linearized equations (7) reduce to the linear stability equations

$$u'_x + v'_y + w'_z = 0\,, \tag{9a}$$

$$u'_t + Uu'_x + v'U_y + Wu'_z + p'_x - \frac{1}{Re}(u'_{xx} + u'_{yy} + u'_{zz}) = 0\,, \tag{9b}$$

$$v'_t + Uv'_x + Wv'_z + p'_y - \frac{1}{Re}(v'_{xx} + v'_{yy} + v'_{zz}) = 0\,, \tag{9c}$$

$$w'_t + Uw'_x + v'W_y + Ww'_z + p'_z - \frac{1}{Re}(w'_{xx} + w'_{yy} + w'_{zz}) = 0\,, \tag{9d}$$

together with the homogeneous boundary conditions (8a), (8b).

Since the coefficients of these differential equations are either constant or depend only on the basic flow $\mathbf{V}(y)$, we can assume solutions in the form of normal modes:

$$\mathbf{q}'(x, y, z, t) = \mathbf{q}(y) e^{i\alpha x + i\beta z - i\omega t}\,, \tag{10}$$

where $\mathbf{q}' = [u', v', w', p']^T$ is the vector of flow variables and $\mathbf{q} = [u, v, w, p]^T$ is the vector of the associated amplitude functions. The exponential factor with wavenumbers α and β in x and z, respectively, and frequency ω describes the wave nature of the solution. Introducing the normal modes (10) into equations (9) yields the normal-mode equations

$$i\alpha u + i\beta w + Dv = 0\,, \tag{11a}$$

$$i(\alpha U + \beta W - \omega)u + (DU)v + i\alpha p - \frac{1}{Re}(D^2 - \alpha^2 - \beta^2)u = 0\,, \tag{11b}$$

$$i(\alpha U + \beta W - \omega)v + Dp - \frac{1}{Re}(D^2 - \alpha^2 - \beta^2)v = 0\,, \tag{11c}$$

$$i(\alpha U + \beta W - \omega)w + (DW)v + i\beta p - \frac{1}{Re}(D^2 - \alpha^2 - \beta^2)w = 0\,, \tag{11d}$$

with the boundary conditions

$$u = 0,\ v = 0,\ w = 0 \text{ at } y = 0\,, \tag{12a}$$

$$u \to 0,\ v \to 0,\ w \to 0 \text{ as } y \to \infty\,, \tag{12b}$$

and $D = d/dy$. These equations represent a homogeneous sixth-order system of ordinary differential equations for the natural variables u, v, w, and p. Depending on the specific problem and the numerical method of solution, various equivalent forms of the normal-mode equations are in use [13]. Here we mention only the system

$$\left\{\left[\frac{D^2 - \alpha^2 - \beta^2}{Re} - i(\alpha U + \beta W - \omega)\right](D^2 - \alpha^2 - \beta^2) + i(\alpha D^2 U + \beta D^2 W)\right\} v = 0\,, \tag{13a}$$

$$\left[\frac{D^2 - \alpha^2 - \beta^2}{Re} - i(\alpha U + \beta W - \omega)\right](\alpha w - \beta u) = -(\alpha DW - \beta DU)v\,, \tag{13b}$$

$$i(\alpha u + \beta w) = -Dv\,. \tag{13c}$$

The fourth-order differential equation (13a) for v with homogeneous boundary conditions on v and Dv is the generalized form of the Orr-Sommerfeld problem originally derived with $W \equiv 0$. This homogeneous problem provides eigenvalues and eigensolutions for v. The second-order differential equation (13b) for $\alpha w - \beta u$ with homogeneous boundary conditions on $\alpha w - \beta u$ is the generalized Squire problem that is inhomogeneous for given $v \neq 0$ but supports a separate set of eigensolutions for $v = 0$. Equation (13c) permits the calculation of u and w once v and $\alpha w - \beta u$ are known.

The derivation of eqs. (13) from eqs. (9) first involves the elimination of the pressure by taking the

curl $\nabla\times$ of the momentum equations which provides the vorticity transport equations. The Orr-Sommerfeld equation is obtained by subtracting the z derivative of the x-vorticity equation from the x derivative of the z-vorticity equation and eliminating w_z via continuity. The Squire equation is the z derivative of the y-vorticity equation. Equations (13) offer various benefits for theoretical studies, the first of which is the separation of the eigenvalue spectrum into Orr-Sommerfeld modes and Squire modes that are associated with different physical mechanisms. Squire modes are stable and usually disregarded. Since the interest in solving stability problems usually is in growth rates, not in the structure of the eigenmodes, the Squire equation (13b) is rarely used. In addition, the Orr-Sommerfeld problem for oblique waves with $\beta \neq 0$ can be reduced to the problem for two-dimensional waves with $\beta = 0$ by using Squire's transformation [13]. Otherwise, the preference for a specific formulation is largely determined by the choice of a numerical method for solution. Within numerical errors, the results are independent of the formulation.

It is worth noting that the Orr-Sommerfeld equation requires D^2U and D^2W which are absent from eqs. (9). While this requirement is easy to satisfy in studies of similarity solutions, higher derivatives of flow quantities may be inaccurate or difficult to obtain if the basic flow is computationally generated. Also, the separation of modes is specific to incompressible problems. In compressible problems, the choice is between the formulation in natural variables or a first-order system of equations. In both cases, the separation of classes of modes requires *a posteriori* study.

Independent of the formulation and for given U and W, the eigenvalue problem can be reduced to solving a complex characteristic equation of the form

$$\mathcal{F}(Re, \alpha, \beta, \omega) = 0 \qquad (14)$$

which yields two quantities per eigenmode, provided all others are given. For boundary layers, it is most appropriate to specify the real quantities Re, β, and ω and determine $\alpha = \alpha_r + i\alpha_i$ from eq. (14) to obtain the spatial growth rate $-\alpha_i$ in x-direction. Unfortunately, different powers of α appear in the equations which causes difficulty for many eigenvalue solvers. Therefore, the problem is often solved with the eigenvalue ω for real Re, α, and β to obtain the temporal growth rate ω_i.

Let us assume we solve the homogeneous boundary-value problem with Newton's method for a single eigenmode. Besides Re, β, ω, U, and W, we provide an initial guess $\tilde{\alpha}$ for the eigenvalue and $\tilde{\mathbf{q}}$ for the eigenfunction, e.g. the results from a previous solution for different parameters. Typically, the Newton iteration converges after a few steps within a given convergence criterion to an approximation $\alpha = \alpha(Re, \beta, \omega)$, $\mathbf{q}(y)$ of the eigensolution. In a strictly parallel flow, this solution is valid for any x.

In a boundary layer, the situation is more complicated. Owing to the streamwise variation of the flow, the stability characteristics change, and the computation has to be repeated at numerous streamwise positions x_n for appropriate input data and local velocity profiles $\mathbf{V}$. The choice of wavenumbers and frequency at a new position is ambiguous. It is tempting to use the parameters of the previous position, but since the length and time scale usually involve the x-dependent boundary-layer thickness, a fixed value of β, for example, describes different physical wavelengths at different positions. On the other hand, the stability analysis aims at finding the total amplification and the amplitude growth of the "most dangerous" modes that evolve in the streamwise direction and thus requires maintaining the physical properties of the modes. In the traditional linear stability analysis, the physical connection between the solution at different streamwise stations is obviously lost by the assumption of a parallel flow which implies the same solution for all x. Retrieving this physical connection in general three-dimensional boundary layers is a rather intricate and controversial matter.

For the z-independent flows considered here, it can be shown [14] that the dimensional frequency f^* and spanwise wavelength λ_z^* of a mode must be independent of x. With these physical constraints, we can calculate a sequence of eigenvalues $\alpha(x_n)$ and obtain the amplitude ratio $A(x)/A_0$ from

$$\ln \frac{A(x)}{A_I} = -\int_{x_I^*}^{x^*} \alpha_i^* dx^* \,, \qquad (15)$$

where the asterisk denotes dimensional quantities and A_I is the amplitude of the mode at the first neutral point x_I^*. Within a linear framework, the modes are independent and the "most dangerous" modes, i.e. those with the largest amplitude ratios at any position can be identified from the envelope of all amplitude growth curves for different values of f^* and λ_z^*.

3.2 PSE Concept in Natural Variables

The PSE concept was originally pursued [15] to clarify the different results of Bouthier [16, 17], Gaster [11], and Saric & Nayfeh [18] on the nonparallel stability of the Blasius flow to two-dimensional TS waves. For nonparallel flows, the normal-mode solutions (10) are not strictly valid since the coefficients of the linearized equations (7) depend weakly on x. Both the amplitude function $\mathbf{q}$ and the wavenumber α change according to nonparallel effects. Following a WKBJ analysis, we maintain the decomposition of $\mathbf{q}'$ into an amplitude function $\mathbf{q}$ and a wave function χ and write the disturbances in the form

$$\mathbf{q}'(x, y, z, t) = \mathbf{q}(x, y)\chi(x, z, t) \,, \qquad (16a)$$

$$\chi = \exp(i\theta(x) + i\beta z - i\omega t)\ ,\ \theta_x = \alpha(x)\ . \qquad (16b)$$

Similar expressions have been applied in the cited earlier work. We note that

$$\mathbf{q}'_x = (i\alpha\mathbf{q} + \mathbf{q}_x)\chi\ , \qquad (17a)$$

$$\mathbf{q}'_{xx} = (-\alpha^2\mathbf{q} + 2i\alpha\mathbf{q}_x + \mathbf{q}_{xx} + i\alpha_x\mathbf{q})\chi\ , \qquad (17b)$$

and by substituting the components of (16) into the linearized eqs. (7) we obtain in nondimensional form

$$i\alpha u + Dv + i\beta w + u_x = 0\ , \qquad (18a)$$

$$\left\{-\frac{1}{Re}[D^2 - (\alpha^2+\beta^2)]u + i(\alpha U + \beta W - \omega)u + DUv + i\alpha p\right\} + \{U_x u + VDu\}$$
$$+\left\{(U - \frac{2i\alpha}{Re})u_x + p_x\right\} - \left\{\frac{i\alpha_x}{Re}u\right\} = \frac{1}{Re}u_{xx}\ , \qquad (18b)$$

$$\left\{-\frac{1}{Re}[D^2 - (\alpha^2+\beta^2)]v + i(\alpha U + \beta W - \omega)v + Dp\right\} + \{DVv + VDv\}$$
$$+\left\{(U - \frac{2i\alpha}{Re})v_x\right\} - \left\{\frac{i\alpha_x}{Re}v\right\} = \frac{1}{Re}v_{xx}\ , \qquad (18c)$$

$$\left\{-\frac{1}{Re}[D^2 - (\alpha^2+\beta^2)]w + i(\alpha U + \beta W - \omega)w + DWv + i\beta p\right\} + \{W_x u + VDw\}$$
$$+\left\{(U - \frac{2i\alpha}{Re})w_x\right\} - \left\{\frac{i\alpha_x}{Re}w\right\} = \frac{1}{Re}w_{xx}\ , \qquad (18d)$$

where now $D = \partial/\partial y$. The left-hand side of eqs. (18b) to (18d) each contains four groups of terms enclosed in braces. The terms in the first group are retained by the normal-mode equations (11) for parallel flow. The second group originates from the streamwise changes of the basic flow: the streamwise gradients of U and W and the transverse velocity component V associated with the growth of the boundary layer. The third group contains the streamwise derivatives of the amplitude functions (u, v, w, p). One of these derivatives also appears in the continuity equation (18a). The last group originates from the streamwise changes of the wavenumber α.

For a proper function $\alpha(x)$, the streamwise variation of $\mathbf{q}'$ is governed by the wave function χ while the derivatives $\mathbf{q}_x$ and α_x are small. The PSE approximation assumes the variation of $\mathbf{q}$ and α as sufficiently small to neglect $\mathbf{q}_{xx}$, α_{xx}, products $\alpha_x\mathbf{q}_x$, and their higher derivatives with respect to x. Hence we obtain the parabolized stability equations by neglecting the terms on the right hand side of eqs. (18b) to (18d).

It is convenient to rewrite the parabolized eqs. (18) in the more compact form

$$L\mathbf{q} + M\frac{\partial\mathbf{q}}{\partial x} + \frac{d\alpha}{dx}N\mathbf{q} = 0\ , \qquad (19)$$

where the operators L, M, and N act only in y. Within the PSE approximation, the streamwise derivatives of $\mathbf{q}'$ take the form

$$\frac{\partial^k\mathbf{q}'}{\partial x^k} = i^k[\alpha^k\mathbf{q} - ik\alpha^{k-1}\frac{\partial\mathbf{q}}{\partial x}$$
$$-i\frac{k(k-1)}{2}\alpha^{k-2}\frac{d\alpha}{dx}\mathbf{q}]\chi \qquad (20)$$

and hence

$$M = -i\frac{\partial L}{\partial\alpha}\ ,\ N = \frac{1}{2}\frac{\partial M}{\partial\alpha} = -\frac{i}{2}\frac{\partial^2 L}{\partial\alpha^2}\ . \qquad (21)$$

These relations simplify the derivation of the PSE or can serve as a useful check.

Obviously, we can rewrite eqs. (18) in the form of a first-order system or in a form similar to the Orr-Sommerfeld-Squire formulation (12) [19]. After parabolization, we obtain equations in the generic form (19), (21) with different operators L, M, N. While the parabolized first-order system involves exactly the same approximation as the parabolized eqs. (18), the additional differentiations with respect to x necessary to obtain the Orr-Sommerfeld-Squire form lead to a slightly different effect of the PSE approximation.

3.2.1 Mathematical Character of the PSE

At first sight, eqs. (19) appear suitable for solution as an initial-boundary-value problem. In fact, the parabolic character of closely related equations has been mentioned by Gaster [11]. Disturbing is the appearance of α_x since α affects the operators yet is a priori unknown. The next section will discuss how to overcome this problem. The ad hoc numerical solution of the PSE (19) for various two-dimensional boundary layers is in fact successful [19]. However, numerical instabilities occur for small marching steps and indicate a residual ellipticity of the PSE.

Ellipticity of the stability equations is necessary to describe instabilities in the form of waves, e.g. TS waves. Any attempt to obtain TS waves on the basis of the boundary-layer equations or parabolized Navier-Stokes equations (PNS) must fail since $\mathbf{q}'_{xx} = \mathcal{O}(|\alpha|^2)$ is not negligible. The traditional normal-mode analysis for parallel flows fully accounts for the ellipticity although the separation of variables leads to ordinary differential equations. Through the decomposition (16), the PSE account for the essential part of ellipticity and remove it from the equations for the amplitude functions $\mathbf{q}$. Any residual ellipticity must be associated with the small deviation of waves in nonparallel flows from normal modes.

Depending on the formulation, different procedures reveal the mathematical character of the partial differential equations (19). We use a modification of the analysis presented by Haj-Hariri [20] for a strictly parallel flow that is directly applicable to eqs. (18). We collect all derivatives of $\mathbf{q}$ on the left hand side and indicate all other terms by the dots on the right hand side:

$$c_1 u_x + v_y = 0 \,, \tag{22a}$$

$$-\frac{1}{Re}u_{yy} + Vu_y + (U - \frac{2i\alpha}{Re})u_x + c_2 p_x - c_0 \frac{1}{Re}u_{xx} = \dots \,, \tag{22b}$$

$$-\frac{1}{Re}v_{yy} + Vv_y + (U - \frac{2i\alpha}{Re})v_x + p_y - c_0 \frac{1}{Re}v_{xx} = \dots \,, \tag{22c}$$

$$-\frac{1}{Re}w_{yy} + Vw_y + (U - \frac{2i\alpha}{Re})w_x - c_0 \frac{1}{Re}w_{xx} = \dots \,, \tag{22d}$$

where the constants $c_i = 1, i = 0, 1, 2$, have been introduced for convenience. We replace $\mathbf{q}_x$ by $\lambda\mathbf{q}$ and $\mathbf{q}_y$ by $\mu\mathbf{q}$ to obtain the system in the form $\mathbf{Aq} = \dots$ with

$$\mathbf{A} = \begin{pmatrix} c_1\lambda & \mu & 0 & 0 \\ C & 0 & 0 & c_2\lambda \\ 0 & C & 0 & \mu \\ 0 & 0 & C & 0 \end{pmatrix} \tag{23a}$$

and

$$C = -c_0 \frac{1}{Re}\lambda^2 + (U - \frac{2i\alpha}{Re})\lambda - \frac{1}{Re}\mu^2 + V\mu \,. \tag{23b}$$

The ellipticity of the original equations is completely removed if the roots $\lambda = \lambda(\mu)$ of the determinant $\det \mathbf{A} = 0$ are real for all real values of μ. We obtain

$$\det \mathbf{A} = (c_1 c_2 \lambda^2 + \mu^2) \times \frac{[c_0\lambda^2 - (ReU - 2i\alpha)\lambda + \mu^2 - ReV\mu]^2}{Re^2} \tag{24}$$

and immediately realize that there are two imaginary roots

$$\lambda = \pm i\mu \,, \tag{25}$$

except if either $c_1 = 0$, $c_2 = 0$, or both. Parabolization, $c_0 = 0$, has no effect on these roots of acoustic origin. To remove this source of ellipticity, we can neglect either u_x in the continuity equation or p_x in the x-momentum equation. The upstream propagation of information is not related to the convective terms, as suggested by Chang et al. [21].

For the complete equations, the second set of roots of multiplicity 2 is

$$\lambda = -\frac{1}{2}[(ReU - 2i\alpha) \pm \sqrt{(ReU - 2i\alpha)^2 - 4\mu(\mu - ReV)}] \tag{26}$$

which are in general complex. For the parabolized equations, $c_0 = 0$, these roots reduce to

$$\lambda = \frac{\mu(\mu - ReV)}{ReU - 2i\alpha} \tag{27}$$

which for $\alpha_r \neq 0$ are still complex, though with a very small imaginary part. It is interesting to note that the sign of U does not affect the imaginary parts of the roots (25), (27) of the parabolized equations.

The situation we find for the PSE is in fact very similar to the parabolized Navier-Stokes equations (PNS). The equations can be solved with marching techniques as an ill-posed initial-boundary-value problem provided the step size is sufficiently large to "skip" over the weak and rapidly decaying upstream propagation of information. Alternatively, additional approximations can be introduced to arrive at a well-posed parabolic problem that can be solved without restriction on the size of the marching step. Contrary to other conclusions [21], well-posedness of the problem cannot be enforced by a proper choice of the wavenumber α but only by neglecting small terms to suppress acoustic sources and even smaller terms to suppress viscous sources of ellipticity. The effect of these steps can be demonstrated by numerical results. Other formulations of the problem such as the velocity-vorticity formulation studied by Haj-Hariri [20] exhibit similar propagation characteristics. Bertolotti (personal communication, 1993) has not found any step-size restriction in his work with the Orr-Sommerfeld-Squire formulation [19, 22].

3.2.2 Closure and Norm

Solving eqs. (19) as an initial-boundary value problem is not straightforward. The appearance of $d\alpha/dx$ is disturbing and α affects the operators, yet is a priori unknown. Key to determining $\alpha(x)$ is the ambiguity in the partition (16) of $\mathbf{q}$ which permits the incorporation of streamwise changes of the wave function χ into $\mathbf{q}$. Given some $\Delta\alpha$, we can write eq. (16) as well as

$$\mathbf{q}'(x, y, z, t) = \hat{\mathbf{q}}(x, y)\hat{\chi}(x, z, t) \,, \tag{28a}$$

where

$$\hat{\mathbf{q}} = \mathbf{q}\exp(i\Delta\alpha) \,, \; \hat{\chi} = \chi\exp(-i\Delta\alpha) \,. \tag{28b}$$

An additional equation is necessary to remove this ambiguity. We note that $\Delta\alpha$ affects the derivatives $\hat{\mathbf{q}}_x$ and $\hat{\mathbf{q}}_{xx}$. To reduce the effect of the PSE approximation, we aim at finding a relation that removes the oscillatory behavior from $\hat{\mathbf{q}}$. We realize, though, that with the choice of an appropriate $\Delta\alpha$, we can achieve this goal only locally at some point y_m or in an average sense across the y domain.

In the absence of any information on streamwise changes, we can impose the restriction

$$\alpha_x = 0 \tag{29}$$

and absorb all streamwise changes into $\hat{\mathbf{q}}(x,y)$. This choice is most convenient for the first step of the numerical integration of eq. (19). However, application of eq. (29) for all x would maintain the error owing to the neglect of higher streamwise derivatives at $\mathcal{O}(\Delta\alpha^2)$ and prevent convergence to the correct solution.

The second choice imposes a streamwise independent norm on $\mathbf{q}$. Such a norm could be applied locally at a fixed position $y = y_m(x)$ as suggested by Bertolotti [19], where y_m is the position of the maximum streamwise rms fluctuation $\sqrt{2}|u|$. The deformation of the function $|u|$ (especially in nonlinear problems) may lead to jumps of y_m and undesirable effects on the solution procedure. We, therefore, prefer an integral norm that is both physically and mathematically meaningful.

The complex wave number α in eq. (10) is given by the logarithmic derivative

$$-i(\ln \mathbf{q}')_x = -i\frac{\mathbf{q}'_x}{\mathbf{q}'} = \alpha \ . \tag{30}$$

From eq. (16), we obtain

$$-i(\ln \mathbf{q}')_x = \alpha - i\frac{\mathbf{q}_x}{\mathbf{q}} \ , \tag{31}$$

where the last term causes a dependence of the local wave number on y, except if $\mathbf{q}_x = 0$. To remove this dependency, we multiply eq. (31) with the weight $|\mathbf{q}|^2$, integrate over the domain Ω in y, and divide by the integral of $|\mathbf{q}|^2$. These steps yield

$$-i\frac{\int_\Omega |\mathbf{q}|^2(\ln \mathbf{q}')_x dy}{\int_\Omega |\mathbf{q}|^2 dy} = \alpha - i\frac{\int_\Omega \mathbf{q}^\dagger \mathbf{q}_x dy}{\int_\Omega |\mathbf{q}|^2 dy} \ , \tag{32}$$

where the dagger denotes the complex conjugate. We now choose

$$\int_\Omega \mathbf{q}^\dagger \mathbf{q}_x dy = 0 \tag{33}$$

to normalize $\mathbf{q}$ and consider eq. (32) the definition of $\alpha(x)$.

Eq. (33) minimizes the streamwise change $\partial\mathbf{q}/\partial x$ in a weighted sense across the y domain. Alternative conditions can be formulated using different weighting functions or deleting certain components of $\mathbf{q}$. Particularly useful is the definition of α obtained from eq. (32) by deleting the pressure and replacing $\mathbf{q}$ by the vector $\mathbf{v}$ of velocity amplitudes. The denominator then is the kinetic energy integral, and the norm is

$$\int_\Omega \mathbf{v}^\dagger \mathbf{v}_x dy = 0 \ . \tag{34}$$

The even simpler condition

$$\int_\Omega u^\dagger u_x dy = 0 \tag{35}$$

has been successfully applied in previous work [19, 22].

Equations (19) together with one of the conditions (33) to (35), or any other suitable norm are the closed system of parabolized stability equations (PSE). This system permits the simultaneous calculation of $\alpha(x)$ and $\mathbf{q}(x,y)$ in a streamwise marching procedure. Different norms lead to different partitions (16) of the solution $\mathbf{q}'$ and to similar yet different results for $\alpha(x)$ and $\mathbf{q}(x,y)$. The physical solution $\mathbf{q}'$, however, is the same to within small effects of the norm on the PSE approximation. Work is currently conducted to implement an optimal norm that would minimize the effect of the PSE approximation.

In parallel flows, $V = 0$, the choice of different norms has no effect on the asymptotic result $\lim_{x\to\infty} \alpha = \tilde{\alpha}$, $\lim_{x\to\infty} \mathbf{q} = \tilde{\mathbf{q}}$ since the wavenumber is independent of y and the same for all components of $\mathbf{q}$. For parallel flows, it can be shown that the PSE approach leads to the correct solution of the elliptic problem provided $\Delta\alpha = \tilde{\alpha} - \alpha_0$ and $\Delta\mathbf{q} = \tilde{\mathbf{q}} - \mathbf{q}_0$ are sufficiently small, where α_0 and $\mathbf{q}_0$ are initial estimates similar to those used for the iterative solution of the local eigenvalue problem.

3.2.3 Local Analysis of Weakly Nonparallel Flow

All previous work on stability theories for weakly nonparallel flows has reduced the problem to ordinary differential equations for local solutions. These theories have been criticized for not being rational perturbation expansions since the lowest order, the Orr-Sommerfeld problem for parallel flow, includes terms of the same order $\mathcal{O}(Re^{-1})$ as the nonparallel correction. Based on the parabolized equations, we can develop a local formulation that does not exhibit this shortcoming.

Let us approximate α, $\mathbf{q}$, and the basic flow by their lowest-order Taylor expansions with respect to x in the neighborhood of some x_0:

$$\alpha(x) = \alpha(x_0) + (x - x_0)\left.\frac{d\alpha}{dx}\right|_{x_0}$$

$$= \alpha_0 + (x - x_0)\alpha_1 \ , \tag{36a}$$

$$\mathbf{q}(x,y) = \mathbf{q}(x_0,y) + (x - x_0)\left.\frac{\partial \mathbf{q}}{\partial x}\right|_{x_0}$$

$$= \mathbf{q}_0(y) + (x - x_0)\mathbf{q}_1(y) \ . \tag{36b}$$

Introducing these expansions into eq. (19) and requiring the equations to be valid for varying x we obtain two coupled ordinary differential equations,

$$\begin{bmatrix} L_0 + L_1 + \alpha_1 L_3 & L_2 \\ L_4 + \alpha_1 L_2 & L_0 \end{bmatrix} \begin{Bmatrix} \mathbf{q}_0 \\ \mathbf{q}_1 \end{Bmatrix} = \begin{Bmatrix} 0 \\ 0 \end{Bmatrix} \tag{37}$$

where the operators are obtained from L, M, N in the following way: partial differentiation is replaced by ordinary differentiation; α is replaced by α_0; L_0 is the strictly parallel part of L, L_1 the nonparallel

correction of L, $L_2 = M$, $L_3 = N$, and L_4 originates from the expansions of U and W in L. The homogeneous boundary conditions on the velocities in $\mathbf{q}$ apply separately to $\mathbf{q}_0$ and $\mathbf{q}_1$.

The homogeneous system associated with eqs. (37) represents a coupled system of equations for the unknown quantities α_0, α_1, $\mathbf{q}_0$, and $\mathbf{q}_1$ subject to two (complex) normalizations. The first norm removes the ambiguity in the eigensolution. The second norm governs the split of the x dependence between $\mathbf{q}$ and α as with eq. (19).

In the simplest case, we can apply the restriction (29), $\alpha_1 = 0$, and solve

$$\begin{bmatrix} L_0 + L_1 & L_2 \\ L_4 & L_0 \end{bmatrix} \begin{Bmatrix} \mathbf{q}_0 \\ \mathbf{q}_1 \end{Bmatrix} = \begin{Bmatrix} 0 \\ 0 \end{Bmatrix} \qquad (38)$$

subject to homogeneous boundary conditions and a norm on the eigenvector. The modified complex wavenumber can be obtained from eq. (31). As usual in nonparallel flows, the growth rate is different for different flow quantities and depends on the y location.

As an alternative, one can assume that the solution of the weakly nonparallel problem differs only by small terms from the solution of the strictly parallel problem $L_0\mathbf{q}^* = 0$ and attempt an iterative solution of the system (37). This procedure requires separate norms on $\mathbf{q}_0$ and $\mathbf{q}_1$ and α_1 is determined by a solvability condition. The first iteration loop is identical with the method described by Saric and Nayfeh [18].

Determining the solution of the nonparallel problem by solving eqs. (37) accounts simultaneously for the terms of orders $\mathcal{O}(1)$ and $\mathcal{O}(Re^{-1})$ and is, therefore, not subject to the criticism mentioned above. The direct relation to the method of Saric & Nayfeh shows on the other hand, that accounting for the terms of $\mathcal{O}(Re^{-1})$ at different orders of approximation is no shortcoming of their method.

The local analysis of weakly nonparallel flows is applicable for waves with sufficiently large wavenumbers, i.e. if the changes of the basic flow over one wavelength are sufficiently small. The procedure breaks down for long waves as they appear at low Reynolds numbers or low frequencies [22]. The parabolized stability equations are well suited to analyze long and short waves.

3.2.4 Some Formal Properties

Convergence of the PSE solution to the correct result is nontrivial and cannot be expected for all stability problems. An obvious counter-example is the streamwise evolution of an initial disturbance in circular Couette flow, where, after integrating over the circumference, the condition of periodicity would be violated. The neglect of the second and higher derivatives of α and $\mathbf{q}$ with respect to x and the change of the mathematical character of the governing partial differential equations from elliptic to quasi-parabolic is only permitted if the stability problem is governed by downstream propagating information while the upstream propagation can be neglected.

The use of parabolic differential equations for analyzing problems of basically elliptic nature with small feedback is successful in some other areas, e.g. in the analysis of acoustic wave propagation [23]. In the field of flow instabilities, the propagation characteristics of disturbances have been studied in detail and led to the classification into absolute and convective instabilities [12]. In these terms, the PSE approach is valid for convectively unstable flows. This class contains pipe and channel flows and the technologically important boundary layers, mixing layers, far wakes, and others that make it worthwhile pursuing this new avenue.

The convective nature of linear instabilities can be assured by analytical studies. For nonlinear problems such as the later stages of transition, the role of upstream propagating information can only be estimated from experimental or numerical evidence. Our applications of the PSE approach suggest that the transition process in boundary layers is largely governed by downstream propagating information.

In contrast to the normal-mode approach, the PSE formulation and marching solution neither exploits nor requires the homogeneity of the problem. This property permits both inhomogeneous boundary conditions and a forcing function instead of zero on the right hand side of eq. (19). The approach can, therefore, handle forced and natural oscillations of the flow within a largely unified numerical approach. Receptivity, the reaction of the basic flow to small forced disturbances, is a yet insufficiently explored field of transition research which can benefit from the PSE approach. Certain types of bypass transition that are associated with strong transient energy growth although linear stability would predict stability [24, 25, 26, 27] are directly accessible to the PSE approach. The forcing function can also describe the nonlinear coupling in the simultaneous evolution of a group of modes distinguished by their frequencies and spanwise wavenumbers. These properties of the PSE permit the analysis of transition from the ingestion of small disturbances through primary and higher instabilities to the breakdown of the laminar basic flow. Together with efficient marching techniques, the PSE appear as a suitable basis for applications in both research and engineering practice.

3.2.5 Solution Procedure

Before solving eqs. (19) and (34), we need to specify initial and boundary conditions. For comparison with the local analysis in section 3.1.1, we specify Re, β, ω, and $\mathbf{V}$, provide the same estimates α_0 for the eigenvalue and $\mathbf{q}_0$ for the eigenfunction as initial conditions at x_s, and apply the homogeneous boundary

conditions (11).

To solve the PSE, the differential operators (21) and boundary conditions are converted into algebraic form by any method suitable for the Orr-Sommerfeld problem. We use a spectral collocation method with Chebyshev polynomials, together with a domain transformation if appropriate. Alternatively, we use two-point or three-point Hermitian high-order finite-difference methods on nonuniform grids. These methods lead to algebraic systems with banded or block-tridiagonal matrices which can be more efficiently solved for the relatively large system (18) in natural variables.

The streamwise derivative is in the simplest case approximated by the two-point finite difference

$$\mathbf{q}_x \approx \frac{1}{\Delta x_j}(\mathbf{q}_{j+1} - \mathbf{q}_j) \,, \tag{39}$$

where $j \geq 0$ is the step index and $\mathbf{q}_j = \mathbf{q}_j(y) = \mathbf{q}(x_j, y)$. Since α appears in the differential operators, the system is nonlinear, and a predictor-corrector approach is employed to find the solution at x_{j+1}. The explicit forward difference formula leads to numerical instability. Although second-order accurate, the central difference formula which evaluates $\mathbf{q}_x$ at the midpoint $x_{j+1/2}$ has not been found advantageous in comparison with the first-order accurate backward difference

$$(\mathbf{q}_x)_{j+1} \approx \frac{1}{\Delta x_j}(\mathbf{q}_{j+1} - \mathbf{q}_j) \,. \tag{40}$$

Equation (19) then assumes the form

$$[\Delta x_j L^n_{j+1} + M^n_{j+1} + (\alpha_x)^n_{j+1} N^n_{j+1}]\mathbf{q}^n_{j+1}$$

$$= M^n_{j+1}\mathbf{q}_j \,, \tag{41}$$

where $(\alpha_x)^n_{j+1} = \alpha^n_{j+1} - \alpha_j$, and the index n counts the iterations. Starting with $\alpha^0_{j+1} = \alpha_j$ according to eq. (29) or with any better initial estimate, we obtain $\mathbf{q}^0_{j+1}$ and henceforth exploit eq. (32) to obtain an updated wavenumber

$$\alpha^{n+1}_{j+1} = \alpha^n_{j+1} - \frac{2i}{\Delta x_j}\frac{\int_\Omega (\mathbf{q}^n_{j+1})^\dagger(\mathbf{q}^n_{j+1} - \mathbf{q}_j)dy}{\int_\Omega |\mathbf{q}^n_{j+1}|^2 dy} \,. \tag{42}$$

The integration-update cycle is repeated until eq. (33) is satisfied within a given error limit and the solution has converged to $\alpha_{j+1}, \mathbf{q}_{j+1}(y)$. We then proceed to the next step in x where a better estimate for α and α_x is known. The marching procedure terminates if the convergence criterion is not satisfied within a given number of iterations.

A simultaneous iteration of $\mathbf{q}^n_{j+1}$ and α^n_{j+1} can be implemented e.g. by using Newton's method on the coupled equations (41) and (42).

3.2.6 Scaling Considerations

Similar to DNS, the solution of the PSE refers to fixed scales U^*_0 and $\delta^*_0 = \delta^*_r(x_0)$ for velocity and length, where $\delta^*_r(x) = (\nu^* x^*/U^*_0)^{1/2}$ and $x = x^*/\delta^*_0$ (the star denotes dimensional quantities). The Reynolds number $Re_0 = U^*_0\delta^*_0/\nu^*$ is fixed. The reference position x_0 is not necessarily the initial position x_s. In contrast, local stability analyses commonly use the local length scale δ^*_r and the Reynolds numbers $Re_x = U^*_r x^*/\nu^*$, $Re = Re_x^{1/2}$. For example, the frequency $\omega = \omega^*\delta^*_0/U^*_0$ in the PSE formulation describes a wave of fixed physical frequency, and there is no need to refer to the usual nondimensional frequency F. To avoid confusion between the differently scaled quantities, we use the caret to indicate local scales, e.g. $\hat{\omega} = \omega^*\delta^*_r(x)/U^*_r$.

For Blasius flow, the two scalings provide $F = \omega/Re_0 = \hat{\omega}/Re$ and the relations

$$\hat{\alpha} = \alpha\frac{Re}{Re_0} \,,\ \hat{\beta} = \beta\frac{Re}{Re_0} \,,\ \hat{\omega} = \omega\frac{Re}{Re_0} \,. \tag{43}$$

Since x is scaled with δ^*_0, we also have the relations

$$Re_x = xRe_0 \,,\ Re = \sqrt{xRe_0} \,. \tag{44}$$

Similar relations can be established for other basic flows.

In nonparallel flow, additional corrections to $\hat{\alpha}$ may be necessary to account for specific quantities and/or positions y. The results reported in the following are based on the norm (34) and the amplitude $A = (\int_\Omega |\mathbf{v}|^2 dy)^{1/2}$. For comparison with experiments, we convert to the local magnitude of velocity components (for steady modes) or the rms value (for oscillatory modes).

The nature of the primary results obtained by the PSE approach and linear stability theory (LST) is different and their comparison involves proper conversion. Since the PSE results for the flow field in space and time (similar to DNS solutions) are closer to the answers sought by the analysis than eigenvalues as a function of the local Reynolds number, we prefer the fixed scaling and present the evolution over x or Re_x according to eq. (44).

3.3 Some Linear Studies

As an introduction to PSE applications, we consider some applications of the linear equations. Thes applications concern both instability and receptivity of 2D and 3D boundary layers.

As a generic example, we first analyze the 2D boundary-layer flow over a flat plate at zero pressure gradient. The examples can be considered as a "test suite" for the development of a PSE code.

3.3.1 Strictly Parallel Blasius Flow

As a first test of the PSE concept, we apply the solution procedure to a strictly parallel flow which is in-

dependent of x. We choose the Blasius profile and a two-dimensional mode with $\omega = 0.0344$ at $Re_0 = 400$ ($F = 86 \cdot 10^{-6}$). The basic flow is held fixed, independent of x. We start the computation at $x_s = x_0 = 400$ and choose as an initial condition the results of the local analysis (a) for the same conditions, (b) for $\omega = 0.0172$ at the same Reynolds number. Giving the value of α for case (b) as an initial guess for the local analysis at $\omega = 0.0344$ leads to convergence to some other eigenvalue with strong damping. Indices s and 0 distinguish the starting position for the PSE run and the reference position, respectively. The results of the PSE calculation for the streamwise evolution of α_r and α_i are shown in figure 2.

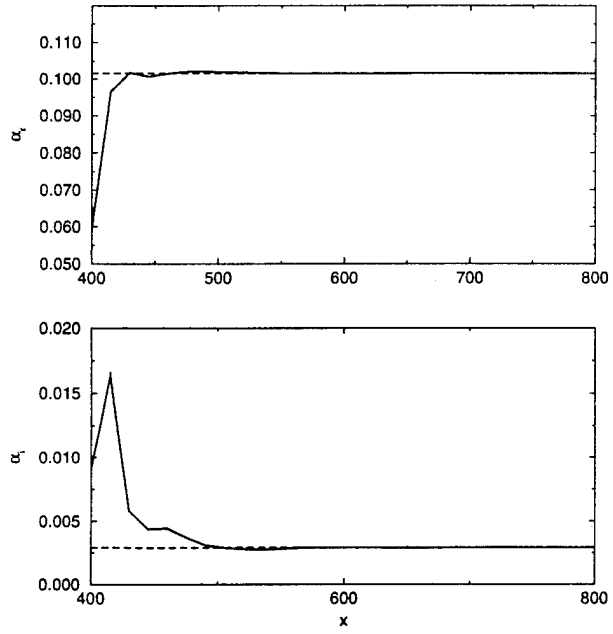

Figure 2: Evolution of the wave number α for different initial conditions.

Case (a) (dashed) is a valid test of the integrity of the PSE code which should maintain the correct result over the marching domain. The other case serves to demonstrate the proper function of the wavenumber update by using a suitable norm. For initial condition (b), the first few marching steps provide a rapidly decaying transient and the PSE result asymptotes to exactly the same value of α obtained with the local analysis at comparable numerical resolution. As an advantage we recognize that even poor initial conditions lead to convergence to the most unstable mode. Since $|\alpha_i|$ is typically much smaller than α_r, the initial transients of the growth rate appear stronger. The results are largely insensitive to changes of the marching step Δx and the choice of alternative integration schemes. The transient solution closely approximates the physical behavior provided the initial equation error is sufficiently small.

Since neither the derivation nor the solution procedure for the PSE requires the problem to be homogeneous, we can introduce disturbances not only through the initial conditions but also through boundary conditions or forcing inside the flow domain, as in laboratory experiments. In the second test, we leave the initial conditions identically zero and apply a small v component at the wall to generate a disturbance of frequency $\omega = 0.0344$ at the same values of Re_0 and x_s as before, while $v_{wall} = 0$ for $x > x_s$. Figure 3 shows the result for the evolution of α in this case. After a short period of "wild" transient behavior, the solution settles at the same values given by the previous runs and the local analysis. The capability to force disturbances in the absence or presence of initial conditions is key to many studies on receptivity and transition.

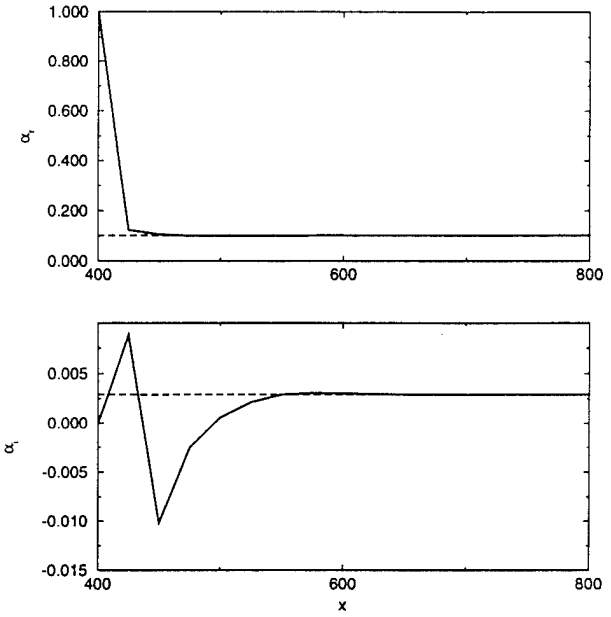

Figure 3: Disturbance introduced by a small v component at the initial position x_s.

The application of the PSE to parallel flows is a demonstration of the concept and a verification of the stability and robustness of the marching procedure. Considering the effort for marching with a step size of $\Delta x \approx 20$ over the range of x shown in figures 2 and 3, the direct solution of the eigenvalue problem is indeed more efficient. However, this comparison changes drastically if the basic flow is nonparallel and the coefficients of the stability equations change with the marching variable x.

3.3.2 Nonparallel Blasius Flow

To illustrate some advantages of the PSE technique, we consider the evolution of a two-dimensional wave at frequency $\omega = 0.0344$ with $Re_0 = 400$ for $x > x_s = 400$. The initial conditions are given by the local analysis at x_s.

Figure 4 shows the wavenumbers and growth rates obtained from the local analysis in comparison with

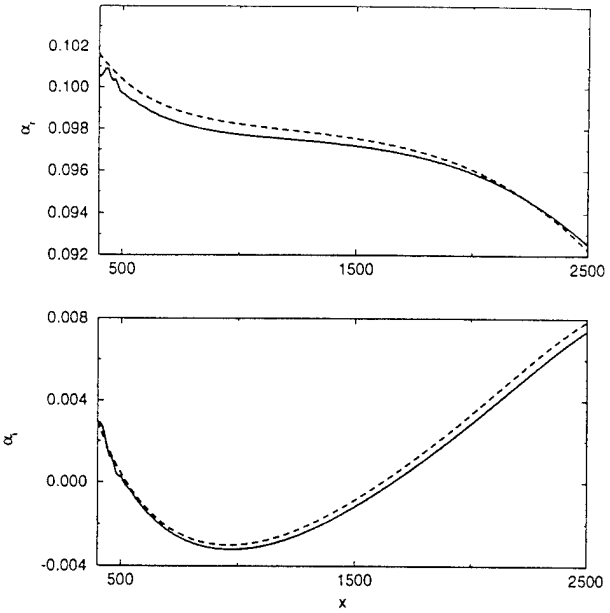

Figure 4: Evolution of the wavenumber α in a Blasius boundary layer. LST (dashed) and PSE (full line).

the result of the PSE. With LST we refer to the traditional linear stability theory for locally parallel flow while the "modified LST" includes the transverse velocity V and the derivative U_x.

We observe only small differences in the growth rates. We also find that the variation of α is very small, as reported by Mack [13], and the effect of α_x is negligible. The variation of $\hat{\alpha} = \alpha Re/Re_0$ in results of the traditional analysis is largely due to the streamwise variation of the length scale $\delta_r^*(x)$ while the PSE results refer to the fixed length scale $\delta_0^* = \delta_r^*(x_0)$. The jiggles near the starting position are caused by the marginal step size of $\Delta x = 10$ and disappear as α_r decreases.

To illustrate the changes in the amplitude functions over the large x domain in figure 4, figure 5 compares the normalized streamwise rms fluctuations u'/u'_{max} at different positions. The modest changes justify the neglect of the derivatives $\mathbf{v}_{xx}$ in the PSE.

For the numerical work, it is important to note that the boundary layer actually grows in the Cartesian coordinates used here. The numerical grid and its extent to some y_{max} must be carefully chosen to cover the boundary layer at the end of the run yet to maintain sufficient resolution for the amplitude functions of the disturbance near the wall.

In general, the results of the PSE runs are very sensitive to small changes in basic flow, initial conditions, and numerical treatment. This property often makes it difficult to find agreement between results of different codes or different authors for virtually the same case. This fact is especially true for the amplitude-growth curves which are more relevant in practical applications than the growth rates provided by the local analysis. Small deviations in

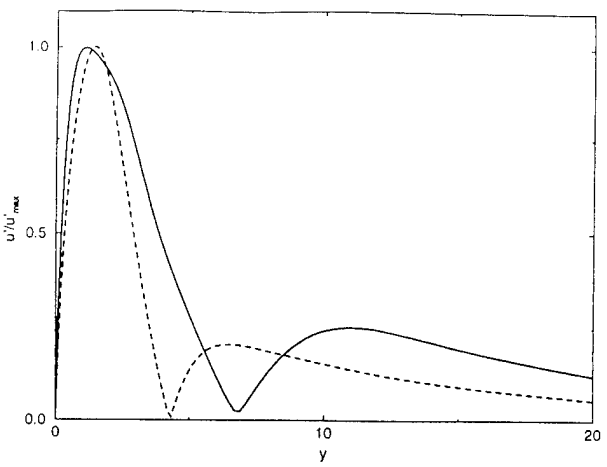

Figure 5: Normalized rms profiles of the amplitude function u at $x = 500$ (dashed) and 2000 (full line).

growth rates accumulate by integration over an extended streamwise distance. The PSE approach provides these amplitude-growth curves directly together with α and the spatial growth rates α_i.

The previous comparison of local and PSE results for two-dimensional waves seems to indicate a rather small effect of the nonparallelism. This conclusion changes, however, for oblique or three-dimensional waves with $\beta \neq 0$.

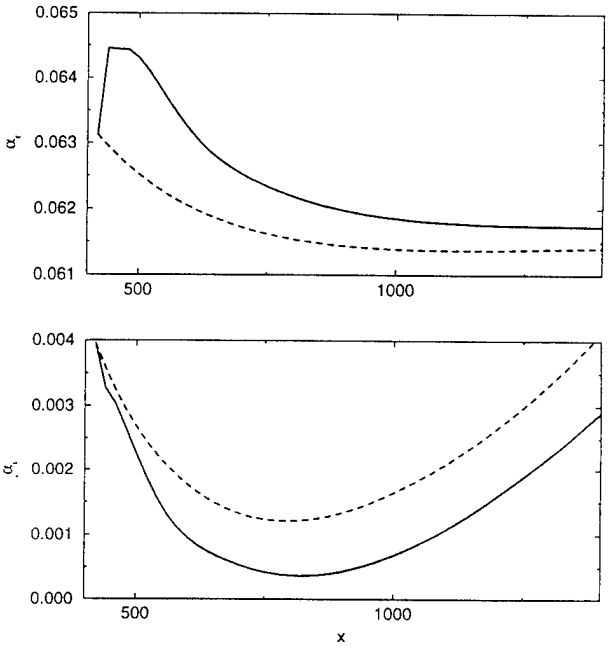

Figure 6: Comparison of results for the wavenumber of a three-dimensional disturbance. LST (dashed) and PSE (full line).

The streamwise variation of α for a wave with $\omega = 0.02604$ and $\beta = 0.14$ at $Re_0 = 400$ (the subharmonic wave in the Kachanov-Levchenko experiment [10]) is shown in figure 6. Starting from the initial value given by the local analysis, the growth

rate develops to a more unstable level which it maintains throughout the run. For smaller β, the PSE analysis exhibits instability while the wave remains stable according to the locally parallel theory.

The local theory for weakly nonparallel flows of section 3.2.3 can retrieve some of the effects of boundary-layer growth, provided the wavenumber α_r is not too small. As the wave angle increases, this condition is not satisfied and the local theory fails. This failure has been shown by Hall [28] for the case of Görtler vortices (wave angle 90°). Hall demonstrated that Görtler vortices are governed by an initial value problem for parabolic stability equations. These equations are derived from the boundary-layer equations, and therefore, the pressure terms p and p_x in the x-momentum equation (18b) are absent. Since Görtler vortices are steady, the analysis can set $\alpha = 0$ and absorb the growth into the amplitude function.

3.3.3 Vortices in Blasius Flow

In the flat-plate boundary layer, steady disturbances have not been revealed by the local stability analysis although quasi-steady regular spanwise modulations of the basic flow have been observed in numerous experiments since Dryden [29] and studied in detail [30, 31, 32]. Even in wind tunnels with low turbulence levels, these "Klebanoff modes" can grow with $\approx x^{1/2}$ to amplitudes of 5% before the onset of TS instability. Similar modulations have been observed in channel flow [33] where the amplitude varies slowly. The modulations in channel flow are associated with the stable yet very weakly damped longitudinal vortices and u-modes [34] that are eigensolutions of the Orr-Sommerfeld and Squire equation, respectively, for $\alpha = 0$, $\beta \neq 0$. In the Blasius flow, these modes are hidden in the continuous spectrum and the local analysis cannot provide initial data for the marching technique.

With proper boundary conditions, the PSE analysis for steady modes, $\omega = 0$, can be performed with zero initial conditions. To introduce u-modes, which in a parallel flow have $v = w = 0$, disturbances can be generated by a small, spanwise periodic variation of the wall-shear stress, $Du = \epsilon$ at $y = 0$, $x = x_s$. Test runs show the rapid formation of a streamwise u and weaker v and w components that decay with $\alpha_i = \mathcal{O}(10^{-4})$. Owing to the nonparallelism of the basic flow and the nonzero derivative u_x, pure u-modes cannot appear in the Blasius flow. Since neither the streamwise amplitude variation nor the u profile is consistent with observations, the spanwise modulations are likely associated with other mechanisms.

To study the generation and evolution of forced longitudinal vortices, disturbances can be generated by a small, spanwise periodic variation of the normal velocity component at the wall, $v(0) = \epsilon$ at $x = x_s$. Figure 7 shows the evolution of the amplitude for three initial positions, $x_s = 25, 100, 400$, with $\beta = 0.14$, $Re_0 = 400$, and $\epsilon = 10^{-4}$. The spanwise wavenumber is larger than the value $\beta \approx 0.105$ ($\hat{\beta} \approx 0.25$ at $Re = 941$) observed by Klebanoff et al. [8] and about half the value $\beta \approx 0.33$ ($\hat{\beta} \approx 0.6$ at $Re = 717$) reported by Kendall [35, 32]. The small initial disturbances monotonically grow to considerable amplitudes. The growth rate increases with x_s. The velocity profiles of the disturbances closely resemble those of Görtler vortices, with a pronounced u component and v and w typically two orders of magnitude smaller. The amplitude evolution of disturbances with different spanwise wave numbers is given in figure 8 for $x_s = 25$ and the previous values of Re_0 and ϵ. The curves for the larger wavenumbers show that the initial growth ultimately changes into decay. The maximum amplitude is higher and appears at lower x as β increases.

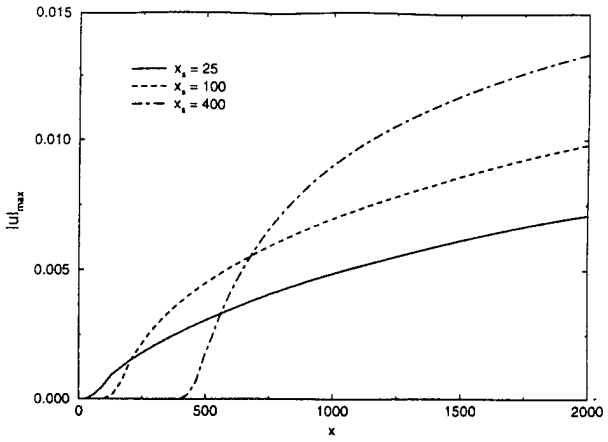

Figure 7: Growth of longitudinal vortices forced at different initial positions.

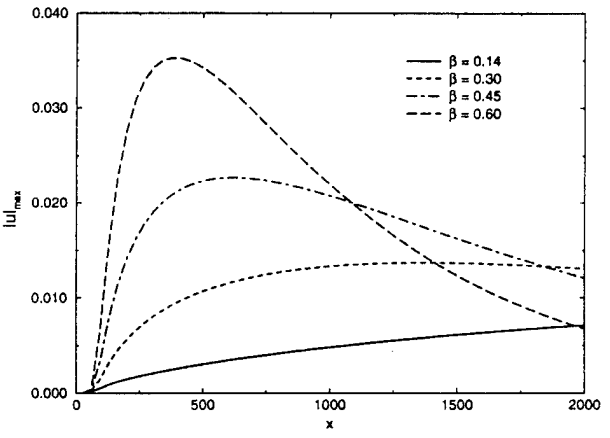

Figure 8: Growth curves of forced longitudinal vortices for different spanwise wavenumbers

At $x = 1285$, $Re = 717$, the position of Kendall's detailed measurements, the largest amplitude occurs for $\beta \approx 0.5$, in the same range as in the experiments. The profile of the calculated u disturbance shown in

figure 9 with its maximum near $\eta = yRe_0/Re = 2.2$ is similar to the observed distribution (crosses) in figure 10. The accompanying curve would result from a spanwise thickening and thinning of the boundary layer, as pointed out by Taylor [36] and Klebanoff [30].

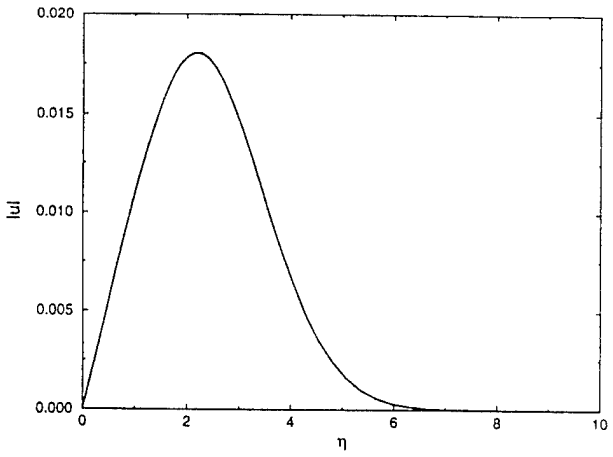

Figure 9: Calculated velocity distribution of the Klebanoff mode.

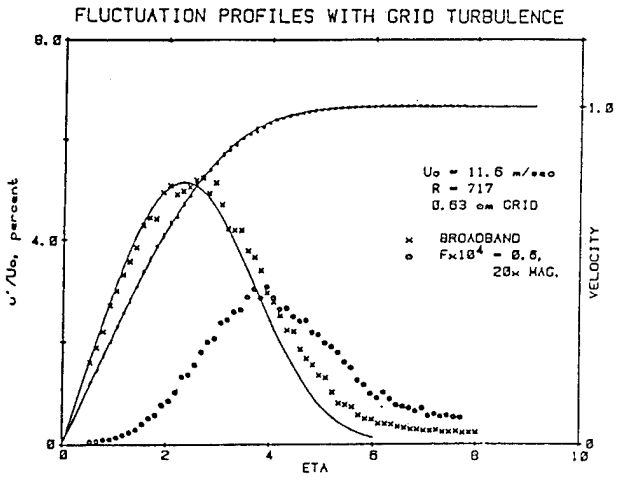

Figure 10: Measured velocity distribution of the Klebanoff mode.

The single disturbance introduced at $Re = 25$ decays at the position $Re = 717$ of the observation. In the experiment, however, the disturbances are continuously seeded by area-distributed receptivity to a wide spectrum of wavenumbers. To better reproduce the experimental conditions, a discrete spectrum of modes in z and proper inhomogeneous boundary conditions in some range of x should be applied. Besides through $v(0)$, the Klebanoff modes can be introduced through inhomogeneous conditions on Dw at the wall, and most efficiently, through spanwise variations of the wall pressure $p(0)$. While the strongest response is for steady modes, the mechanism covers a broad band of low frequencies. For a smooth plate, generation of Klebanoff modes by spanwise pressure variations associated with free-stream turbulence is the most likely scenario.

The significant transient amplitude (or energy) growth of steady and low-frequency disturbances in the absence of linear instability is an example of the bypass mechanism described by Gustavsson [24] and Henningson [25] for channel flow. Related studies of optimal energy growth in a crude model of Blasius flow by Butler & Farrel [26] show that the optimum is associated with steady disturbances of a spanwise wavelength similar to those found in the experiments of Kendall and in our PSE analysis of forced disturbances. While previous studies of the transient growth mechanism were restricted to the temporal evolution, the PSE are well suited to analyze the spatial evolution and properly account for the nonparallelism of the flow.

3.3.4 Effect of Curvature

The similarity between the velocity distributions of Klebanoff modes and Görtler vortices suggest that they may be strongly affected by curvature. Also, the occurrence of Görtler vortices on concave walls may be related to the same receptivity mechanisms. To analyze the effect of curvature, the PSE have been derived from the Navier-Stokes equations for a surface-oriented coordinate system with streamwise varying radius of curvature $R(x)$ [37]. While these equations permit interesting studies on the disturbance evolution on wavy walls or airfoils, we consider here walls with a constant (dimensional) radius of curvature and $\kappa = \delta_0/R(x) = \text{const.}$ with respect to the reference length at $Re_0 = 400$. As before, we introduce disturbances through a small, spanwise periodic wall velocity $v(0) = 10^{-4}$ at $x_s = 25$.

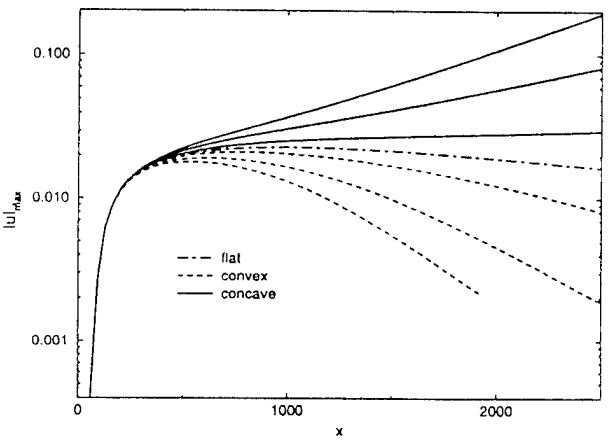

Figure 11: Growth curves of forced longitudinal vortices for different convex and concave wall curvature in comparison with the result for a flat wall.

Figure 11 shows the growth curves for values of $\kappa \cdot 10^6 = -25(10)25$ together with the result for the

flat plate, $\kappa = 0$, for $\beta = 0.36$. After initial growth, the amplitudes for $\kappa > -5 \cdot 10^{-6}$ decrease with increasing x, the amplitude for $\kappa = -5 \cdot 10^{-6}$ remains nearly constant, while the amplitudes for larger concave curvature ($\kappa < 0$) increase with varying rate.

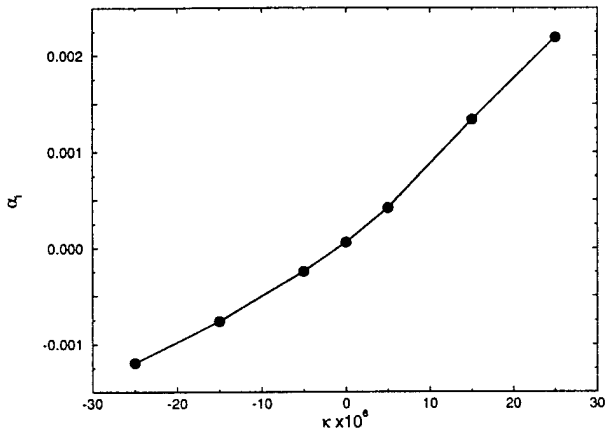

Figure 12: Growth rate of forced longitudinal vortices vs. curvature at $x = 1600$.

The growth rates as a function of κ are given in figure 12 for $x = 1600$. The data from PSE runs are shown by the circles. The growth rate varies monotonically as κ increases. After rescaling the data for $\kappa = -25 \cdot 10^{-6}$ to the local conditions at $Re = 800$, the growth rate $\hat{\alpha}_i = -0.002386$ agrees surprisingly well with the value $\hat{\alpha}_i = -0.002382$ of the local analysis of a Görtler vortex at the proper parameters $\hat{\beta} = 0.72$, $\hat{\kappa} = -5 \cdot 10^{-5}$. Some of this agreement is incidental since a PSE analysis for locally parallel flow, which is more consistent with the local analysis, provides $\hat{\alpha}_i = -0.002056$. However, growth characteristics and comparison of velocity profiles leave no doubt that the forced vortices at $\kappa = -25 \cdot 10^{-6}$ are Görtler vortices. The PSE analysis clearly shows the existence of these vortices in the form of Klebanoff modes on a flat plate and increasingly damped modes on convex walls of increasing curvature. The stabilizing effect of convex curvature on longitudinal vortices is a new result outside the scope of the linear stability theory. In spite of the close relation between Klebanoff modes and Görtler vortices, it is appropriate to maintain the different names since Görtler vortices are inherently associated with centrifugal instability.

3.3.5 Wave Packets

Besides the single modes studied above, the PSE code allows tracking the evolution of waves distinguished by their frequency and spanwise wave number. In a linear framework, the waves can be analyzed sequentially or simultaneously. The latter approach has been chosen since it enables easier post-processing of the data. Test runs with coarsely spaced modes have been performed for two-dimensional wave packets [38], a periodic point source [39], and a three-dimensional wave packet [40]. More detailed studies with higher resolution are performed in cooperation with L. Mack to compare with experimental and earlier theoretical results. Figure 13 shows the wave pattern created by a harmonic point source at $x_s = x_0 = 475$ with $\omega = 0.0285$ ($F = 60 \cdot 10^{-6}$).

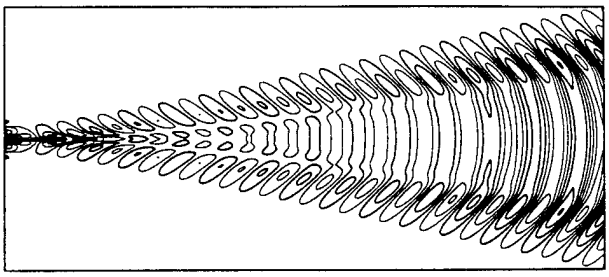

Figure 13: Contours of equal streamwise disturbance velocity for $0 \leq x - x_s \leq 1000$ at $y = 2.5$.

The initial disturbance is modeled by 201 modes with equal initial amplitudes and phases and $b_m = 0.0075 \cdot m$, $m = 0, \cdots, 200$. Alternatively, the initial conditions could be derived from a Fourier decomposition of the disturbance source at the initial position by applying proper boundary conditions and including selective receptivity mechanisms. The PSE analysis is time consuming yet otherwise straightforward since the physical constraints during the downstream evolution of the waves are maintained by the governing equations. The analysis does not require the heuristic corrections for the disturbance-energy distribution across the boundary layer. Accounting for a larger number of modes is only a matter of patience and disk space.

3.3.6 Three-Dimensional Boundary Layers

The examples so far were for two-dimensional boundary layers. The parabolized equations (19) can be directly applied to three-dimensional boundary layers in Cartesian coordinates, such as the Falkner-Skan-Cooke flows over a swept wedge or the swept Hiemenz flow along and towards the sides of a stagnation line. For other cases such as the boundary layer over a rotating disk, the PSE can be reformulated in cylindrical coordinates [41]. Alternatively, a coordinate transformation between Cartesian and cylindrical coordinates can be prescribed and the proper equations can be generated during the computation. This latter procedure permits a modular split of the metric terms from the formulation of the PSE.

For the flow over a rotating disk, the nondimensional radius is used as the marching variable. Figure 14 shows the variation of the growth rate for a disturbance with $n_\beta = 30$, where n_β is the number of vortices over the circumference. The result is similar to the data presented by Malik & Balakumar [42, fig. 1a] who also compare with results of various other

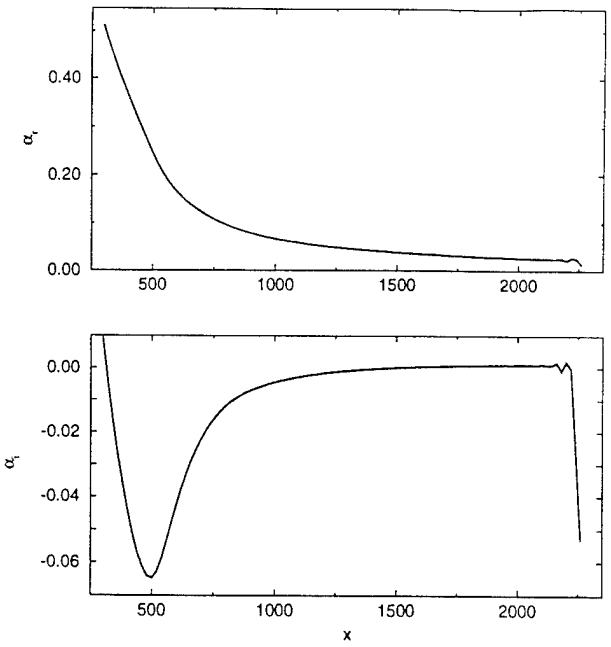

Figure 14: Wave number and growth rate of cross-flow vortices with $n_\beta = 30$ in the boundary layer on a rotating disk.

approaches to the controversial stability of this flow. Additional discussion of the results can be found in ref. [43]. The figure also shows some oscillations at high Reynolds number that ultimately terminate the run. Although the wave number α_r decreases, the oscillations are caused by a strong numerical instability for the step size used for this run. With larger step size or control of the elliptic influence, the run can be continued to higher Reynolds numbers.

The originally strong interest in the stability of the boundary layer over a rotating disk as a prototype of boundary layers on realistic swept wings has faded since the stability properties are in fact more complex than in swept-wing flows. Falkner-Skan-Cooke and swept Hiemenz flow are more closely related to different aspects of swept-wing flows and we present only a few results for the latter case. Based on eqs. (19), the marching variable is x. There is no need to work in coordinate systems that adapt one axis to the inviscid streamline direction, as it is common in traditional N factor calculations. There is also no problem with the controversial in-plane curvature terms which have been the topic of various papers [43, 44]. Given the wavenumber β in the spanwise z direction, the streamwise wavenumber α_r adapts properly to the local orientation of the disturbances. Since the basic flow is independent of z, β must be constant during the run [14].

Although Hiemenz flow has a constant boundary-layer thickness, the flow is non-parallel, as shown by the streamlines. Figure 15 shows the amplitude growth of steady cross-flow vortices in the swept Hiemenz flow with $Re = 500$, $\beta = -0.4$, a case studied with DNS by Spalart [45]. Re is formed with the spanwise velocity W_e and the reference length $(\nu/A)^{1/2}$, where $U_e(x) = Ax$. The marching variable x is the Reynolds number formed with U_e. In general, the linear stability characteristics provided by the local theory are in good agreement with the PSE results. Accounting for the variation of the basic state causes some differences but no dramatic change. We note, however, that these observations cannot be generalized to other, more realistic flows.

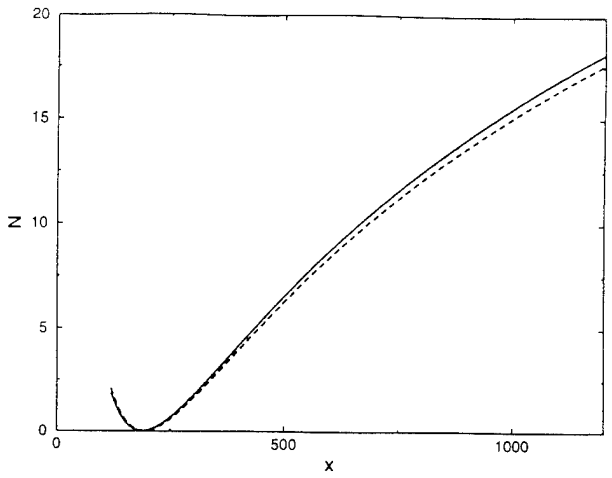

Figure 15: Amplitude growth curves (N factors) for swept Hiemenz flow. PSE results with and without (dashed) accounting for nonparallel terms.

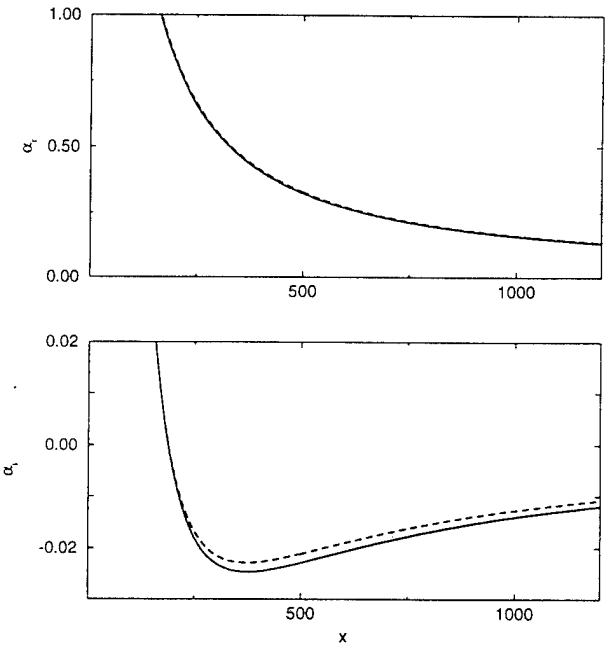

Figure 16: Wavenumber and growth rate of steady cross-flow vortices in swept Hiemenz flow according to LST (dashed) and PSE approach.

The wave numbers α_r and growth rates α_i obtained by linear theory and PSE analysis are compared in

figure 16. Similar results have been presented by Malik & Li [46, 47].

3.3.7 Receptivity of Hiemenz Flow

While the PSE approach allows a more efficient, accurate, and reliable analysis of growth rates and N factors, it also provides new capabilities for analyzing and understanding the receptivity of three-dimensional boundary layers. Fedorov [48] studied the excitation of cross-flow vortices in subsonic boundary layers over swept wings and found that microroughness of the height of 1% of the displacement thickness or spanwise periodic suction/injection with $v(0) = 10^{-4}$ can excite cross-flow vortices with an initial amplitude of 0.1%. Radeztsky et al. [49, 50] report a strong effect of small roughness elements on transition in swept-wing flows. Crouch[51] extended his local nonlinear approach to the receptivity of the Falkner-Skan-Cooke flow to steady and unsteady cross-flow vortices and obtained results consistent with the experiments of Müller & Bippes[52]. There are at least some aspects of these studies that can be qualitatively reproduced by modeling the roughness elements by a disturbance of the v component of the velocity normal to the wall.

Figure 17 shows the amplitude of forced cross-flow vortices of $\beta = -0.4$ at $x = 500$ depending on the position x_s of the v disturbance. In all cases, $v(0) = 10^{-4}$ at x_s. The response is strongest if the disturbance (or the roughness in the experiments) is placed shortly upstream of the neutral point for the onset of instability. The small spanwise irregularity in the wall velocity is amplified by a factor 7000 which is the result of subcritical transient growth combined with subsequent growth due to instability. The amplitude ratio at $x = 500$ is $A/A_I = 654$ (figure 15).

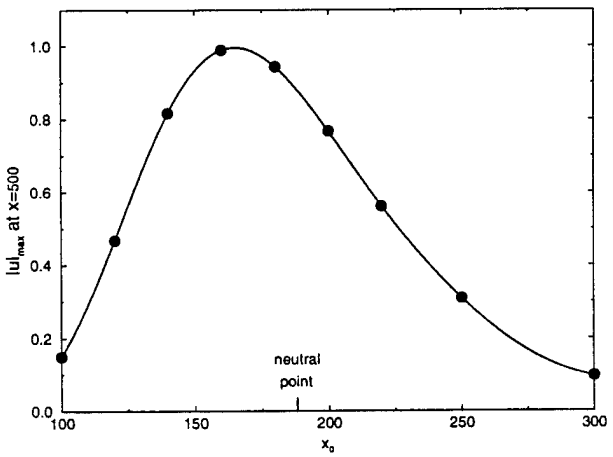

Figure 17: Amplitude of cross-flow vortices at $x = 500$ in response to forcing at different upstream positions, $\beta = -0.4$.

In general, an isolated or spanwise periodic roughness element is characterized by a Fourier decomposition not only in the spanwise direction, but also in the marching direction x. A more sophisticated analysis, therefore, would allow for both spanwise and streamwise wave numbers. Preliminary results show the highest receptivity for the wave numbers and streamwise position of the critical disturbance for onset of cross-flow instability.

3.4 Nonlinear PSE

The previous section has shown that the linear PSE approach is an efficient and accurate method and exceeds the capabilities of the local stability theory especially with respect to inhomogeneous problems. Inhomogeneities can not only enter through boundary conditions but also as a distributed force on the right-hand side of eqs. (19). Such distributed forces most naturally occur if we retain the nonlinear terms on the right-hand side of eqs. (7).

Similar to a spectral method, we assume the flow field $\mathbf{q}'$ as periodic in time t with a period $T = 2\pi/\omega_1$ and in spanwise direction z with wavelength $\lambda_z = 2\pi/\beta_1$. We expand the initial conditions and the solution for $x > x_s$ in a double Fourier series

$$\mathbf{q}'(x,y,z,t) = \sum_{n=-\infty}^{\infty} \sum_{m=-\infty}^{\infty} \mathbf{q}'_{nm}(x,y) e^{im\beta_1 z - in\omega_1 t} \,. \qquad (44)$$

The choice of ω_1 and β_1 is analogue to choosing the computational domain in Navier-Stokes simulations. Some guidance is given by controlled experiments and the theory of primary and secondary instability.

To exploit the PSE concept, we write every mode in terms of slowly varying functions of x,

$$\mathbf{q}'_{nm}(x,y) = \sum_{l=0}^{\infty} \mathbf{q}_{nml}(x,y)\, e^{i\theta_{nml}(x)} \,, \qquad (45a)$$

$$\frac{d\theta_{nml}}{dx} = \alpha_{nml}(x) \,, \qquad (45b)$$

such that every amplitude function $\mathbf{q}_{nml}(x,y)$ is associated with the wave function

$$\chi_{nml} = \exp(i\theta_{nml}(x) + i\beta_m z - i\omega_n t) \,, \qquad (46)$$

where $\beta_m = m\beta_1$ and $\omega_n = n\omega_1$. With the proper indices attached to the various quantities, relations (17), the linear left-hand side of eqs. (18), and relations (19) to (21) carry over to the nonlinear problem except that eq. (19) now becomes a system of inhomogeneous equations,

$$L_{nml}\,\mathbf{q}_{nml} + M_{nml}\,\frac{\partial \mathbf{q}_{nml}}{\partial x} + \frac{d\alpha_{nml}}{dx} N_{nml}\,\mathbf{q}_{nml} = \mathbf{r}_{nml} \,, \qquad (47)$$

where the right-hand side $\mathbf{r}_{nml} = \mathbf{r}_{nml}(x,y)$ is the sum over all terms that contribute to the mode

(n, m, l). To collect these terms from the sixfold summation (for the quadratic nonlinearity) is straightforward with respect to z and t, yet not in x. The first component of $\mathbf{r}_{nml}$ is zero since the continuity equation (7a) is linear. The terms that contribute to the second component of $\mathbf{r}_{nml}$ are obtained from eq. (7b) as

$$-[u_{n-\nu,m-\mu,\lambda}\,(i\alpha_{\nu\mu\kappa}u_{\nu\mu\kappa}+\frac{\partial u_{\nu\mu\kappa}}{\partial x})$$

$$+v_{n-\nu,m-\mu,\lambda}\,\frac{\partial u_{\nu\mu\kappa}}{\partial y})+w_{n-\nu,m-\mu,\lambda}\,i\beta_\mu u_{\nu\mu\kappa}]$$

$$\times\exp(i\theta_{n-\nu,m-\mu,\lambda}+i\theta_{\nu\mu\kappa}-i\theta_{nml})$$

Eqs. (7c) and (7d) provide similar expressions for the remaining terms.

With respect to the x direction, the decision is yet open which term contributes to which mode since there is no simple relation between the indices λ, κ, and l. To minimize the effect of the PSE approximation and to close the system of equations, every mode is subject to a proper norm, e.g.

$$\int_\Omega \mathbf{v}^\dagger_{nml}\,\frac{\partial \mathbf{v}_{nml}}{\partial x}dy=0 \qquad (48)$$

in analogy to eq. (34). This norm determines α_{nml} and θ_{nml} to make $\mathbf{q}_{nml}$ a slowly varying function of x. To maintain this property in the presence of $\mathbf{r}_{nml}$, we observe that the terms in square brackets are slowly varying and select l such that for given n and m

$$\Delta_l=\min_l|\alpha_{n-\nu,m-\mu,\lambda}+\alpha_{\nu\mu\kappa}-\alpha_{nml}|\,, \qquad (49)$$

i.e., the term contributes to the "nearest neighbor" with respect to the streamwise wavenumber to reduce the residual variation with x. This residual variation is absorbed into the amplitude function. Intuitively it is clear that the effect of the PSE approximation can be reduced by providing a large number of choices for the selection (49) of l though at higher computational expense.

In previous studies of ribbon-controlled transition [19], successful runs were performed with only a single wavenumber α_{nm0} per mode and the difference $\theta_{n-\nu,m-\mu,0}+\theta_{\nu\mu0}-\theta_{nm0}$ has been neglected. However, this approach is too limited for a broader range of applications. The need for more wavenumbers α_{nml} can be determined by monitoring Δ_l.

While it is desirable to solve the nonlinear PSE system in a uniform procedure for all modes, the mode q'_{00} requires certain exceptions. This special role of the mean-flow distortion arises since it is governed – like the basic flow – by the boundary-layer equations, not the Navier-Stokes equations. In general, the wavenumber associated with the mean-flow distortion is unnecessary, $\alpha_{00l}=0$. The growth of the distortion caused by all terms is absorbed into a single amplitude function $\mathbf{q}_{000}(x,y)$. The boundary conditions on the mean-flow distortion are different from those of all other modes since the growth of disturbances in the boundary layer causes changes in the displacement thickness and hence $v_{000}\neq 0$ as $y\to\infty$.

In contrast to unsteady modes with $n\neq 0$, steady modes (including the mean-flow distortion) exhibit a pronounced dependence on history and accumulate small differences or changes during the marching solution. Since the mean-flow and its derivatives strongly affect the stability characteristics, utmost care has to be paid to the treatment of the mean flow and its nonlinear distortion. Also note that quantities such as the skin friction coefficient $C_f(x)$ (and heat transfer coefficient $St(x)$ in compressible flows) are solely governed by the mean flow. All periodic components average to a zero contribution when the local mean is taken over t and z.

3.4.1 Implementation

For numerical applications, the Fourier series (44) is truncated at prescribed values of $|n|<N$, $|m|<M$ and the physical flow field takes the form

$$\mathbf{q}'(x,y,z,t)=\sum_{n=-N}^{N}\sum_{m=-M}^{M}\mathbf{q}'_{nm}(x,y)e^{im\beta_1 z-in\omega_1 t}\,. \qquad (50)$$

Further, a limit $l\leq L$ is specified to restrict the number of modes with different α_{nml} at given n,m. While the summation includes modes with $n<0$, it is unnecessary to compute these modes since the physical field must be real and hence

$$\mathbf{q}'_{-n,-m}=\mathbf{q}'^{\dagger}_{n,m} \qquad (51)$$

where $\dagger$ denotes the complex conjugate. For two-dimensional basic flows such as Blasius flow, the computation can be further reduced by the assumption of symmetry in z,

$$\mathbf{q}'_{n,-m}=[u_{nm},v_{nm},-w_{nm},p_{nm}]^T \qquad (52)$$

This symmetry can be derived from the governing equations but may be used only if initial and boundary conditions are symmetric. Without assuming symmetry, the PSE code can track the evolution of asymmetric initial conditions, e.g. of a single oblique wave. For three-dimensional boundary layers, eq. (52) is invalid if both $\omega\neq 0$ and $\beta\neq 0$.

The "best approach" to the treatment of the nonlinear terms during the marching procedure requires the usual compromise between accuracy and efficiency. For many calculations it is sufficient to treat the terms explicitly. The explicit treatment is more efficient since the computation of the nonlinear interaction terms can be time consuming. To increase the accuracy of the results, the marching step for the explicit integration should be small. Small marching steps may require suppression of the term p_x to remove the small upstream influence. For more accurate calculations and studies far into the transition

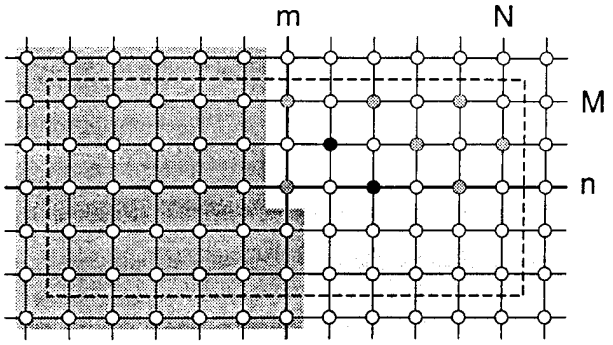

Figure 18: Schematic of the modes. The modes in the dashed frame constitute the physical field. The dark shaded area is excluded from the computation. The modes in the light shaded area can be generated by symmetry in two-dimensional flows.

regime, the implicit treatment is preferable although the cost per iteration step is higher. Often it is necessary to recalculate the nonlinear terms and the mean-flow distortion after updating the wavenumber for every single mode to achieve convergence for strongly growing modes. The increased effort per iteration step is often outweighed by more rapid convergence and the opportunity to use larger marching steps.

Initial data are usually given only for a few modes, e.g. for modes (2,0) and (1,0) as indicated by the dark circles in figure 18. The other modes (shaded circles) are generated as the nonlinear forcing terms come into play. To avoid strong transients for initial data with large amplitudes, it is useful to calculate the nonlinear terms and generate at every position the yet missing modes using the inhomogeneous version of the local stability equations if the forcing exceeds a low threshold. This procedure provides reasonable starting values for the first wavenumber update. For the mean-flow distortion, this approach is inapplicable. Various methods of generating the distorted mean flow at the starting position have been tested and compared. Since the mean flow (and other steady modes) exhibit a pronounced memory, different choices at the initial position have a lasting effect on the nonlinear evolution of the flow which may be significant in runs with large initial amplitudes. It appears best to assume the mean flow distortion to be zero upstream of the initial position. This choice is well justified for runs with small initial amplitudes.

Many applications such as the example in figure 18 leave certain modes unused (white circles). In the interest of studying advanced problems with limited resources, this fact can be exploited by a flexible memory allocation. For research applications, it is useful to associate the modes with two tables, the first of which keeps track of existence and status of each mode while the second table indicates pre-determined properties. By assigning special properties, modes can receive special treatment or be prohibited to participate in nonlinear interactions.

Most results shown in the following have been produced as tutorial examples to illustrate capabilities and phenomena. No special care has been applied to produce archival results. Initial conditions have been generated by the modified LST with the transverse velocity terms included.

3.4.2 Nonlinear Effects on Single TS Modes

The nonlinear evolution of single modes was once the focus of weakly nonlinear theories which were limited by the inability to incorporate both nonlinearity and nonparallelism [53, 55]. This inability especially affected the mean-flow distortion and prevented higher-order perturbation analysis. The nonlinear evolution of a TS wave was also the corner stone of spatial Navier-Stokes solutions [56]. Therefore, this case has also been chosen as a first application of the PSE approach [19, 57, 22]. The PSE results for a TS wave with $\omega_1 = 0.0344$ and an initial rms amplitude of 0.25% at $Re_0 = 400$ were found in excellent agreement with DNS results. Results for the same case were also presented by Chang et al. [21] and also found in agreement with DNS results although their maximum amplitude is somewhat higher than the value reported by Bertolotti et al. [22].

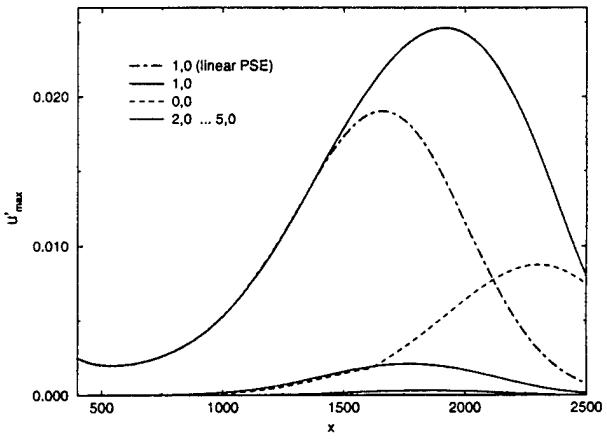

Figure 19: Linear and nonlinear evolution of a TS wave of frequency $\omega_1 = 0.0344$ with $u'_{max} = 0.0025$ at $x_s = Re_0 = 400$. The various modes are labeled n, m for their frequency ω_n and spanwise wavenumber β_m as in figure 18 (l is omitted if $L = 0$).

Figure 19 shows a similar result obtained with $N = 5$ for the same case in comparison with the linear result. Although nonlinearity is small, as shown by the low amplitudes of the harmonics, it causes a significant change in the peak amplitude and the location of branch II. The destabilization near branch II is consistent with the results of the weakly nonlinear theory [53, 54], direct numerical simulation [58], and asymptotic theory [59]. Notable is the evolution of the mean-flow distortion, $(0,0)$. The "kink" near

$x = 1700$ is an artifact of plots of the maximum absolute value for oscillatory functions. Different parts of the curve are associated with peaks at different distance from the plate. While plots of local amplitudes are often necessary to compare with measurements, plots based on the amplitude A or the kinetic energy A^2 are in general easier to interpret.

The mean-flow distortion assumes a maximum further downstream than the nonlinear TS wave. In other words, the mean-flow distortion continues to accumulate the nonlinear effects in the presence of a finite-amplitude wave even if this wave decays. While traveling waves quickly adapt to local conditions, the mean-flow distortion and other steady modes possess a pronounced memory. This memory cannot be modelled by the local weakly nonlinear analysis but requires solving an initial-value problem.

The maximum amplitude of the TS wave in figure 19 is slightly lower than the result of Bertolotti et al. [22]. This difference is largely due to the use of different initial conditions; we use a linear stability mode while results of the local weakly nonlinear or nonparallel theories were used in earlier work. The sensitivity of the solution to initial conditions is a fundamental property of the stability and transition problems we deal with. Every small change in initial conditions or numerical treatment causes minute changes in the growth rates which accumulate over the long distance downstream to small yet noticeable differences in the amplitude. Different initial conditions also have caused the different results of Bertolotti [19] and Chang et al. [21] (M. R. Malik, personal communication, 1993).

A second principal difference between the earlier and present approach is the update of the wave number. Leaning on the weakly nonlinear theory for parallel flow [60], the earlier formulation implemented the restriction

$$(\alpha_r)_{n0} = n(\alpha_r)_{10} \tag{53}$$

on the wavenumber and updated only the growth rate from an integral norm. In nonparallel flows there is no rigorous justification for this property. Therefore, our analysis determines both wavenumber and growth rate by the norm. In the case shown above, relation (53) is satisfied only within about 1% once the initial transients decayed. Although this deviation may be negligible and the use of eq. (53) saves the cost for iterating on the higher wavenumbers, this approach is not generally applicable and the assumption of a single dominating ("ribbon-induced") mode is too restrictive.

3.4.3 Secondary Instabilities

The next major test for the PSE approach and its implementation is the ability to track the simultaneous evolution of multiple modes and their interactions, especially for the parametric resonance mechanisms that lead to secondary instabilities [4].

Earlier PSE studies [19, 57] considered the effect of a finite-amplitude TS wave on a subharmonic mode of secondary instability, i.e. the initial conditions for the subharmonic mode were obtained from the Floquet analysis of secondary instability. Suppressing the feedback of the subharmonic mode on the TS wave, the subharmonic mode evolved in close proximity to the predictions of the Floquet theory.

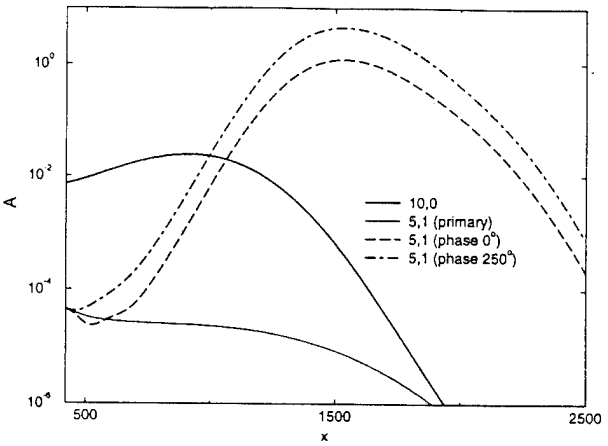

Figure 20: Linear subharmonic secondary instability and influence of the initial phase.

Figure 20 shows a similar result for the conditions of the experiment of Kachanov & Levchenko [10], $x_s = Re_0 = 420$, $\omega_1 = 0.005208$, $\beta_1 = 0.14$. Here, however, the initial data are given by the two primary modes $(10, 0)$ and $(5, 1)$ with rms amplitudes of 0.46% and 0.0035%, respectively. Two cases with different phase shifts between the two modes are shown. The feedback of the three-dimensional wave on the two-dimensional mode and the mean-flow distortion are suppressed.

In absence of the TS wave, the primary mode $(5, 1)$ would decay as shown. Affected by the TS wave, the three-dimensional mode exhibits a strong transient, and the wavenumber settles near twice the wavenumber of the TS wave while the growth rate strongly increases. The perfect synchronization of both waves obtained by Floquet analysis (and enforced in earlier work) is not achieved in the nonparallel flow with streamwise varying TS amplitude. The near-synchronization is lost at $x \approx 2000$ and the subharmonic mode develops on its own while the parametric excitation has faded away. The subharmonic growth rates are slightly smaller than the theoretical predictions. The transient evolution and the maximum amplitude of the subharmonic mode depend on the phase relation to the TS wave.

Closely related to subharmonic secondary instability is the mechanism of combination resonance in the presence of the TS wave $(10, 0)$ and a detuned mode $(4, 1)$ with amplitudes and other parameters as above,

and the same phase. As figure 21 shows, the one-sided nonlinear interaction introduces the mode $(6,1)$ such that the sum of the frequencies of the three-dimensional modes equals the frequency of the TS wave. For $700 < x < 1300$ the combination modes develop with similar large growth rates. Further downstream, where the rms amplitude of the TS wave is less than 0.3%, each of the three-dimensional modes is governed by its own linear stability characteristics. The maximum amplitudes due to combination resonance is less than for subharmonic resonance. A similar result is obtained by specifying mode $(6,1)$ instead of $(4,1)$ by the initial conditions.

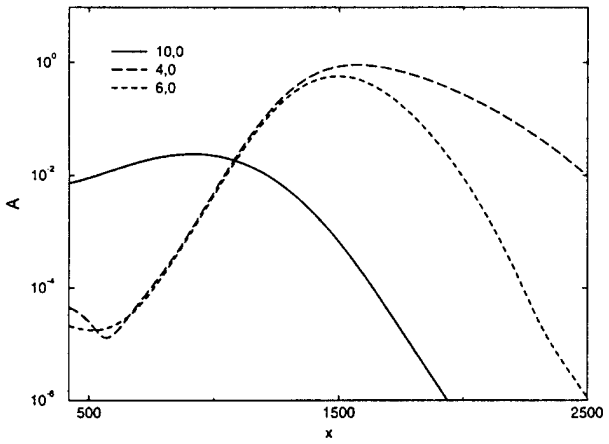

Figure 21: Combination resonance.

The third type of secondary instability, fundamental or principal parametric resonance is rather weak at the relatively low TS amplitudes in the Kachanov-Levchenko experiment. We, therefore, consider this type at lower frequency where the TS waves experience stronger growth. Most of the microscopic experiments on K-type breakdown [8, 64] were performed at these lower frequencies.

The K-type of secondary instability is caused by the interaction of a TS wave (1,0) with either a pair of oblique waves (1,1) or a longitudinal vortex (0,1). The latter interaction is favored by Klebanoff modes (caused by "spacers" underneath the ribbon in experiments).

Figure 22 shows the evolution of the amplitudes from initial modes (1,0), (1,1) with $x_s = Re_0 = 600$, $\omega_1 = 0.03$, $\beta_1 = 0.15$, and small initial rms amplitudes of 0.1% and 0.01%, respectively. The interaction generates mode (0,1), a steady, spanwise periodic mode. Because of the different streamwise wavenumbers of the initial modes, the amplitude oscillates and increases in the mean as the TS amplitude grows. As modes (0,1) and (1,1) reach comparable magnitude, they engage in an interaction with each other and with the TS wave. Mode (1,1) synchronizes with the TS wave and the oscillations of mode (0,1) disappear, leaving a longitudinal vortex mode. The spanwise periodic disturbance grows rapidly ($\alpha_i \approx 0.035$) to large

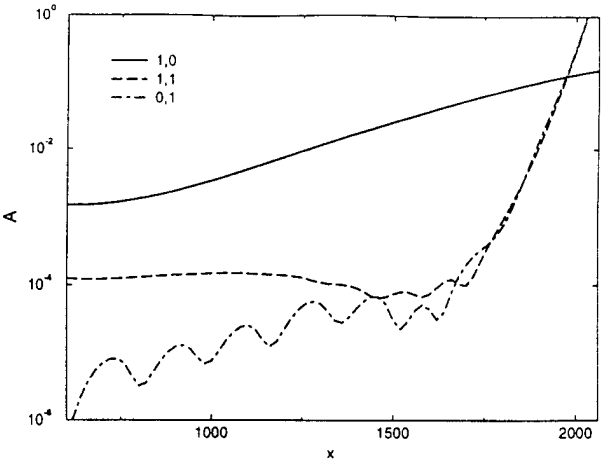

Figure 22: Fundamental (K-type) secondary instability originating from initial modes (1,0) and (1,1).

amplitude. The unrealistic amplitudes in these runs appear because the effects of the secondary disturbances on the TS wave and the generation of harmonics are suppressed.

3.4.4 Nonlinear Receptivity Studies

Another application of the nonlinear PSE is the study of certain receptivity mechanisms that involves the interaction of small disturbances at the boundaries, such as the interaction of sound with a wavy wall. Based on the local theory, these mechanisms have been analyzed by Crouch [61] and Choudhari & Street [62] for two-dimensional boundary layers. Nonlinearity is necessary to combine the Stokes wave of frequency ω and the steady component of wavenumber $\bar{\alpha}$ induced by the waviness into a forcing term for TS waves.

Local and PSE results have been compared by Crouch & Bertolotti [63] and found in good agreement. Small differences are attributed to nonparallelism. In these PSE computations, the forced TS wave maintains the wavenumber $\bar{\alpha}$ and the growing difference between $\bar{\alpha}$ and the wavenumber α_{TS} of a TS eigenmode is absorbed into the amplitude function.

Analysis of the simple forced linear oscillator discussed by Crouch [61] shows, that $\bar{\alpha}$ dominates the behaviour of the forced mode only in the stable domain. After passing through resonance (at or near the neutral point), the wavenumber of the forced mode approaches that of the eigenmode. Therefore, we prefer to update the wavenumber of the forced component and extract the oscillatory behaviour from the amplitude function.

The results in figure 23 are for $Re_0 = 400$, $x_s = 300$, $\omega = 0.0224$ ($F = 56 \cdot 10^{-6}$) and a wall waviness with $\bar{\alpha} = 0.0696944$ (as in [63]). The difference between the two evolutions with and without updating the wavenumber of the forced TS wave is consider-

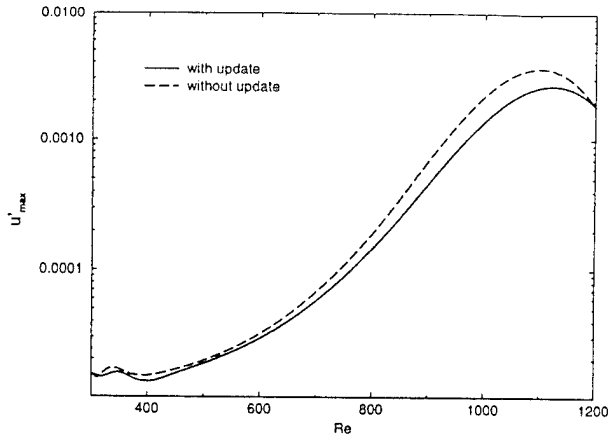

Figure 23: Interaction of sound with a wavy wall. Effect of the wavenumber update.

able and cannot be attributed to different effects of the PSE approximation. At small Reynolds numbers up to $Re \approx 700$, the smaller response with wavenumber update is due to the changing phase difference between the forced wave and the forcing term which also causes an ondulation of the amplitude that diminishes as the natural oscillation takes over and $\alpha \rightarrow \alpha_{TS}$. Although the difference in the wavenumbers $\bar{\alpha}$ and α_r is small, it causes different growth characteristics at higher Re as shown by the shift in the branch II position.

3.5 Ribbon-Controlled Transition

A more severe test of the nonlinear PSE is the reproduction of the microscopic experiments of Klebanoff, Tidstrom & Sargent [8], Kachanov & Lechenko [10], Cornelius [64], and others on transition in the flat-plate boundary layer. These experiments are also the benchmark cases for spatial DNS codes and serve to analyze the nonlinear development of transition from different types of secondary instability. Besides for these test cases, the PSE can be used to study related problems, in particular problems that involve numerous modes such as wave packets.

PSE studies for these test cases have been performed by Bertolotti [19, 57] and compared with experiments and Navier-Stokes solutions. Good agreement has been found except for some experimental data as the $2f$ mode (4,0) of Kachanov & Levchenko. For this mode, both PSE and DNS show a continuous rise while the experiment found a significant decline followed by a steep rise near onset of transition. The discrepancy was attributed to experimental error.

Of the various analyses of transition arising from H-type, K-type, or combination resonance or interaction of two oblique modes (1,1) and (1,-1), we show only one example[1] that helps to clarify the earlier discrepancy between the experiment of Kachanov & Levchenko [10] and computations [65, 19, 57].

PSE studies of this case by Bertolotti used a dominant TS wave and a subharmonic secondary mode from Floquet analysis as initial conditions. Both modes were in the correct phase and synchronization. Here we continue our study of subharmonic secondary instability (section 3.4.3) by fully accounting for nonlinearity. Deviating from previous work, we use a primary mode to introduce a subharmonic component. This choice allows tracing the synchronization process between two-dimensional and three-dimensional components and the effect of the phase difference between the initial modes. All wavenumbers are determined by the norm without any assumption on synchronization.

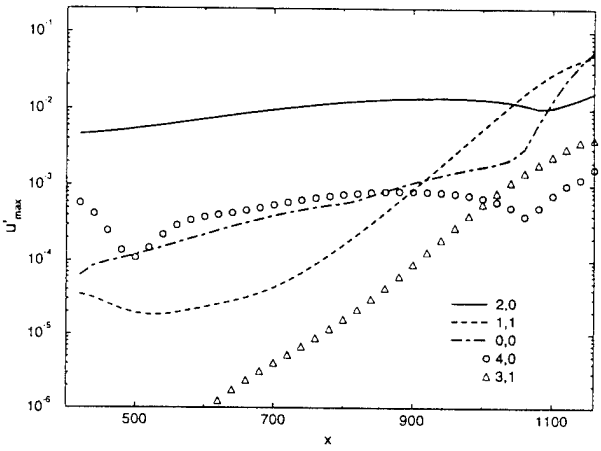

Figure 24: Amplitude growth of selected modes in a PSE simulation of the Kachanov-Levchenko experiment.

Figure 24 shows the nonlinear evolution ($N = 4, M = 2$) of selected modes from the same initial conditions as for figure 20 (phase 0^o). With full interaction permitted, the growing subharmonic mode (1,1) prevents the decline of the TS wave. Here and in other runs with different truncations and initial phase, mode (4,0) behaves as in the experiment. The earlier disagreement between PSE results and experimental data is apparently due to the particular choice of initial amplitudes and the enforced resonance from the outset.

3.6 Nonlinear Vortices

Transition evolving from Görtler vortices or cross-flow vortices is still a matter of experimental and computational research. These types of disturbances do not initiate secondary instabilities at small amplitudes where the approximations of the Floquet analysis [4] are justified. Instead, vortices grow to large amplitudes and develop strong harmonics before secondary instabilities develop on the embedded layers of high shear.

[1] to meet the deadline for submission of the manuscript.

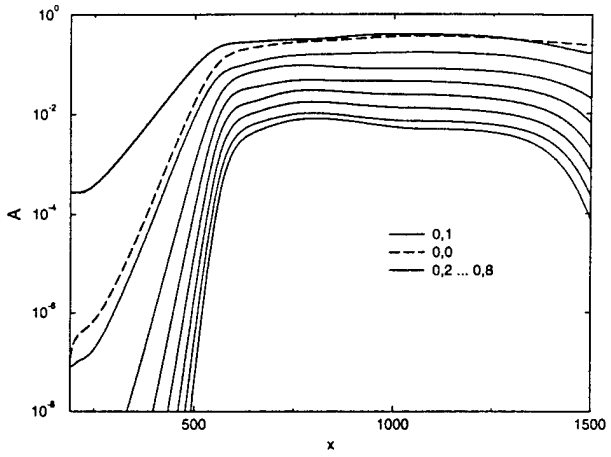

Figure 25: Nonlinear growth of a steady cross-flow vortex in swept Hiemenz flow.

The nonlinear evolution of a steady cross-flow vortex in swept Hiemenz flow for the conditions of figure 15, $Re = 500$, $\beta = -0.4$, $x_s = 190$, an initial amplitude of $|u|_{max} = 10^{-4}/\sqrt{2}$, and $M = 8$ is shown in figure 25. The rapid growth of mode (0,1) causes the rise of harmonics until saturation is reached near $x \approx 600$. For $x > 700$, the maximum of the mean-flow distortion $|u_{00}|$ exceeds 10% and the spanwise periodic component $|u_{01}|$ exceeds 17% of the reference velocity W_e. These ratios are smaller with respect to $U_e = xW_e/Re$. The saturation level is insensitive to the initial amplitude. For higher initial amplitudes, saturation is reached at smaller x. Similar characteristics have been found for unsteady cross-flow vortices (see also [46, 47]).

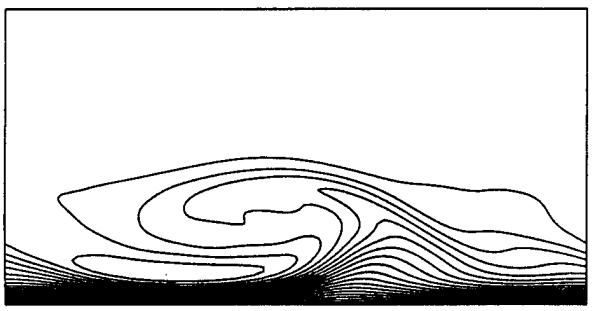

Figure 26: Contour lines of equal u velocity at $x = 716$. The contour levels are multiples of 5% of the edge velocity U_e.

Figure 26 shows a cross section of the vortex at $x = 716$ over one period in z and $y \leq 8$ (to scale). The different spacing of the contour lines near the wall indicates a strong spanwise variation of the wall-shear stress. A vertical cut near the center reveals a strongly inflectional velocity distribution.

While the general features of figure 25 can be obtained with $M = 2$, the detailed structure of the cross-flow vortex after saturation depends on the number of harmonics taken into account. The relatively strong influence of harmonics raises questions on the validity of secondary instability results obtained at low truncation. Floquet analysis of the flow at fixed x under neglect of the streamwise variation but accounting for all relevant harmonics is a computationally expensive task. Alternatively, the linear primary instability of the three-dimensional flow at fixed x can be analyzed using two-dimensional eigenfunctions in z and y, but the computational demand remains high. At this time, reliable results on the instability of highly nonlinear cross-flow vortices are unavailable. As a consequence, the breakdown of these vortices and the resulting transition process have not yet been analyzed. Work toward closing this gap is in progress.

4 PSE for Compressible Flows

The successful application of the PSE for incompressible flows and the demand for improved predictive tools in aerodynamic design suggest the extension to compressible flows. While this extension appears straightforward, it faces a series of hurdles and decisions:

- The sheer size of the nonlinear stability equations and associated code that need careful checks and support by symbolic manipulation even in the simplest case of Cartesian coordinates.
- The implementation of general curvilinear coordinates to adapt to realistic geometries.
- The choice of the "best" set of variables between p, T, or ρ, primitive or conservative variables, covariant or contravariant velocity components.
- The choice of models for the thermodynamic properties of the working gas at high Mach numbers.
- The failure or inefficiency of proven numerical methods.
- The uncertain accuracy of the basic flow and its derivatives generated by traditional computational methods and boundary-layer codes for flows over aerodynamic bodies.
- The need for consistent interpolation methods to obtain the basic-flow data on the grid used for stability analysis from the data given on some other computational grid.
- The unavailability of detailed test data from microscopic experiments or spatial DNS at high speeds.
- The lack of physical understanding for mechanisms and results.

As a rule of thumb, the difficulties increase with the Mach number and the complexity of geometry and disturbance environment.

4.1 Stability Equations

The PSE for compressible flow in Cartesian coordinates up to quadratic nonlinear terms were developed by Bertolotti and applied to study the nonparallel linear stability of the flat-plate boundary layer [19, 66, 67]. Based on his work, the PSE approach was also adopted by Chang et al. [21] to perform a nonlinear analysis of this flow. While the choice of variables and coordinates for the traditional stability analysis is important because of the effect on the parallel-flow assumption, it is less critical for the linear PSE. However, the use of ρ and T is advantageous for the nonlinear formulation. The complete nonlinear formulation including cubic and quartic nonlinearities in general curvilinear coordinates has been developed by Stuckert et al. [68]. The velocity field is described by the contravariant velocity components.

Our implementation of the nonlinear compressible PSE is rather general. Different sets of disturbance variables, e.g. $\mathbf{q} = [p, T, (\rho u)^k]^T$ or $\mathbf{q} = [\rho, T, u^k]^T$ can be chosen for the analysis. Different models of the thermodynamic properties can be chosen, which is helpful in comparing with previous work. Two separate time-dependent coordinate transformations $\xi^k = \xi^k(x, y, z, t)$, $k = 1, 2, 3$ can be specified: for the computational grid of the basic flow and for the grid used in the PSE analysis. This capability enables use of the same core modules for diverse problems such as flat plate or rotating disk, swept wings or blunt cones. Grouped around this core are application-dependent modules as well as interfaces to similarity solutions, boundary-layer codes, and the Plot3D files produced by most computations of the basic flow.

4.2 Numerical Aspects

While the incompressible problem spends most of the computer time in solving linear algebraic systems, the setup of these systems for nonlinear compressible analysis consumes a major fraction of the total time. Obviously, the setup time increases with the number of grid points needed to resolve the flow in ξ^2 normal to the boundary and with the order of approximation (quadratic, cubic, or quartic) to the nonlinear terms.

The reliable and accurate single-domain spectral method successfully used for the incompressible formulation in terms of Orr-Sommerfeld and Squire equation [19] loses advantage for the compressible problem because the dimension of the algebraic system with a completely filled matrix increases from $2J$ to $5J$ where J is the number of collocation (or grid) points normal to the boundary. At high Mach numbers, the inflexible arrangement of the collocation points near the boundary makes it difficult to resolve details of higher modes with critical layers near the edge of the thick boundary layers. Bertolotti (personal communication, 1993) has adopted a multi-domain spectral method to overcome these shortcomings. While the multi-domain approach reduces the matrix size, it demands additional numerical specifications which need optimization and distract from the physical problem.

The fourth-order compact (Euler-Maclaurin) method favored by Chang et al. [21] requires the tedious reformulation of the PSE equations as a system of first-order differential equations in ξ^2 and leads to numerous terms involving the inverse $(V^2)^{-1}$ of the small transverse component V^2 of the basic flow. In computational basic flows, this component is usually inaccurate. Moreover, V^2 can change sign and lead to unpleasant divisions by zero.

We maintain the single-domain spectral method for special-purpose studies such as obtaining spectra of eigenvalues or highly accurate results for comparisons. The routine calculations are based on Hermitian finite-difference methods [70] for second-order differential equations. For nonuniform grids, two-point formulas permit overall accuracy up to fourth order, three-point formulas up to seventh order. Nonuniform grids with moderate stretching reduce the number of grid points needed to achieve a certain accuracy at lower Mach numbers. Equidistant grids are preferable at high Mach numbers.

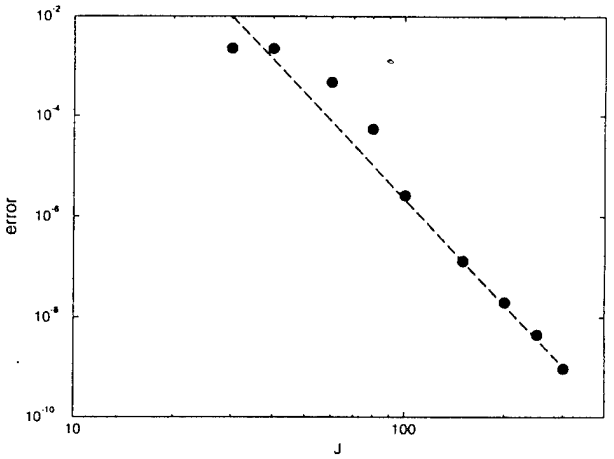

Figure 27: Error of the temporal eigenvalue calculated with the three-point Hermitian method at high Mach number. The dashed line indicates seventh-order accuracy.

Figure 27 shows the result of a convergence study for test case IV of Malik [69] at $Ma = 10$, $Re = 1000$, $T_e = 111.111^oK$, and $\alpha = 0.12$ for the compressible flat-plate boundary layer. Our "exact" result for the temporal eigenvalue was obtained by the spectral method with $J \geq 50$ as $\omega = 0.115861436 +$

$i0.000137657$ (different from the spectral results given in ref. [69]). The error comprises both the errors of the basic-flow calculation and stability analysis. To obtain the correct eigenvalue within an absolute error of 10^{-6} or 10^{-8} requires about 100 or 200 grid points, respectively. The spectral result is matched with 300 points. At lower Mach numbers, $Ma \leq 2$, good accuracy can be achieved with as few as 50 grid points.

We have compared application of the Hermitian formulas with and without elimination, and with block-tridiagonal or banded matrix solvers without finding a superior approach. Using banded matrix solvers without elimination requires more time to solve the system but saves the time for the elimination step during setup and for retrieving the second derivatives needed when calculating the nonlinear terms. A clear advantage, however, is the use of the LAPACK library subroutines and of the BLAS libraries which are optimized for various supercomputer and workstation architectures.

While we have overcome the numerical difficulties in solving the stability problem for exact or similarity solutions as basic flows, applications to computational solutions for realistic geometries face additional numerical problems. These problems often start with insufficient accuracy of the coordinates that define the shape of the body, e.g. an airfoil. Small oscillations in the pressure gradient and the curvature along the body cause strong oscillations in the stability characteristics.

Most computational methods for aerodynamic applications are second-order accurate and designed to provide reliable results for the pressure distribution at the surface. The stability characteristics, however, are governed by the whole flow field in the boundary layer and beyond. Our experience shows that satisfactory accuracy can be obtained with boundary-layer codes. Viscous flow solutions from Navier-Stokes or PNS solvers often lack the accuracy needed for a reliable stability analysis.

4.3 Validation of the PSE Code

To guarantee proper function of the compressible PSE code, extensive tests have been performed for the speed range from $Ma \approx 0$ to $Ma = 10$. These tests range from comparison with independent results to solving the same problem in different coordinate systems and with different sets of variables.

Figure 28 shows the comparison with results of El-Hady [71] for subharmonic secondary instability in the flat-plate boundary layer at $Ma = 1.2$. Two PSE runs were performed using Cartesian and similarity coordinates, respectively. Although the PSE runs have been tailored to match the locally-parallel flow assumption, the results deviate from El-Hady's due to a slight shift of the instability region for the primary mode toward higher Reynolds number R. Except for the initial transients, the PSE results agree. The transients are stronger in Cartesian coordinates because the initial data are more affected by the parallel-flow assumption of the LST.

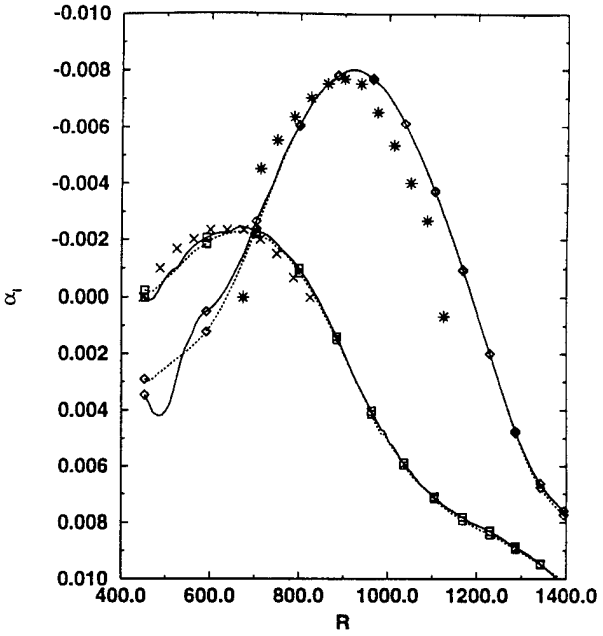

Figure 28: Subharmonic secondary instability at $Ma = 1.2$. Comparison of the PSE solution in Cartesian (solid) and similarity coordinates (dashed) with results of El-Hady (symbols). □: PSE, primary mode (2,0), ◇: PSE, subharmonic mode (1,1). ×: El-Hady, primary mode (2,0), ∗: El-Hady, subharmonic mode (1,1).

5 Practical Applications

While most of our work on compressible flows has served to develop and implement the PSE approach together with efficient and accurate numerical methods for integration and interpolation, to validate the code, and gain an overview of the differences between LST and PSE results, we have also performed feasibility studies and tested the code in some real-world applications.

5.1 Flow over Swept Wings

Flows over the swept wings of airplanes are routinely analyzed for the transition location using the e^N criterion [2, 3]. The N factor is obtained by one of a series of proprietary or restricted stability codes. The e^N code COSAL by Malik [72] is in widespread use in the U.S.[2]

We have performed a detailed comparison of amplitude-growth curves (N factor versus arclength)

[2] COSAL was provided by NASA Langley Research Center for our study.

obtained with different options of COSAL, our own stability code LISA, and the linear PSE code [68]. An infinite wing with a 64A010 airfoil and sweep angles of 0^o, 25^o, 53^o, and 70^o was considered at $Ma = 1.5$ and an altitude of 55,000 feet.[3] The modified version WING of the boundary-layer code by Kaups & Cebeci [73] which is provided with COSAL was used to compute the basic flow for all stability computations. The flow over this slender airfoil exhibits weak TS instability at 0^o sweep and is otherwise dominated by cross-flow instability.

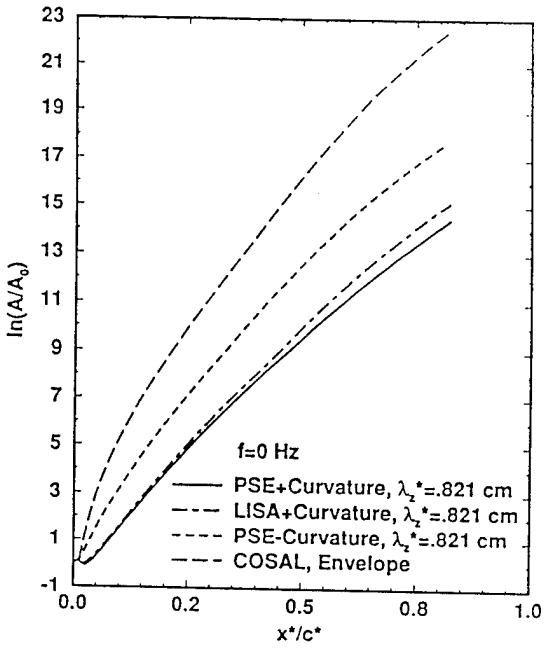

Figure 29: Amplitude growth curves for cross-flow vortices obtained with COSAL (envelope method), PSE without curvature effect, LISA, and PSE.

Figure 29 compares the amplitude growth of steady cross-flow vortices at 53^o sweep obtained with the envelope option of COSAL, the PSE without accounting for curvature effects, LISA, and the PSE. COSAL does not account for curvature. The largest deviation between the results is caused by the violation of physical constraints by the envelope method which at any point selects the spanwise wavenumber for maximum growth while physical solutions have fixed spanwise wavenumber [14]. Although our version of COSAL provides alternative strategies, the physical constraints cannot be satisfied. The second major change is the strong stabilizing effect of surface curvature. (The PSE approach does not suffer from the inconsistency between in-plane curvature and parallel-flow approximation [44, 43].) The discrepancy between results of LISA and PSE code reflects the small effect of nonparallelism. While the discrepancy is small in this case, it is significant for other airfoils and the growth predicted by LISA may be substantially higher or lower than that obtained with the PSE code.

The comparison of the different results for N factors enhances the critical attitude toward e^N transition predictions and raises doubts in the value of the extensive database of N factors created by use of COSAL and other stability codes.

Other studies on swept wings [41] aim at comparing receptivity and disturbance evolution with the low-speed experiments of Radetztsky et al. [49, 50] on a 45^o swept wing with an NLF(2)-0415 airfoil.[4] The flow over this airfoil is one of the cases where LISA predicts a substantially larger amplitude growth than the PSE code.

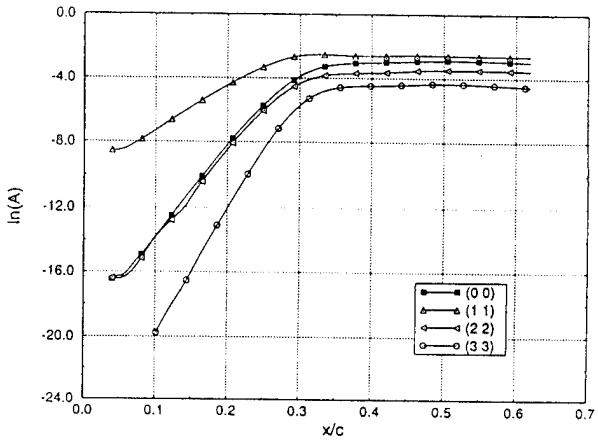

Figure 30: Nonlinear growth of an unsteady cross-flow vortex with $f = 180\ Hz$, $\beta = 0.4$, and an initial amplitude of $A_0 = 0.0002$ at the neutral point in the flow over the NLF(2)-0415 airfoil.

Figure 30 shows the amplitude growth of an unsteady cross-flow vortex calculated using $M = 3$. Owing to the large growth rate, the vortex reaches early saturation near 30% of the chord. Steady vortices of the same initial amplitude saturate downstream of 60% chord at a higher amplitude level. Nevertheless, unsteady vortices create a stronger mean-flow distortion. As in swept Hiemenz flow, the saturation amplitude is largely independent of the initial amplitude, however, it varies with the spanwise wavenumber β. A detailed comparison with the experimental data of Radeztski et al. is forthcoming.

5.2 Flow over a Blunt Cone at $Ma = 8$

The stability of the flow over a blunt cone at $Ma = 8$ has been experimentally studied by Stetson et al. [74] for different nose bluntness. The cone has a half angle of 7^o, a length of 40 inches, and a base diameter

[3] The Euler solutions for the various cases were provided by G. Klopfer, NASA Ames Research Center.

[4] The geometry and computational results for the pressure distribution at -4^o angle of attack were provided by W. S. Saric.

of 9.823 inches. The stability of the mean flow over the blunt cone with a 0.15-inch nose tip is considered here, because this case is controversial and has developed into a benchmark case for application of basic-flow and stability codes. While the computational tools provide converging results, the discrepancy between stability results for sharp and blunt cones in the same experimental facility and the disagreement of the blunt cone results with stability calculations remain unexplained.

The basic flow has been calculated using two different codes: a Thin Layer Navier-Stokes (TLNS) code developed by Esfahanian [75, 76, 77] and the AFWAL Parabolized Navier-Stokes (PNS) code. The TLNS solution has been computed to serve as an accurate benchmark.

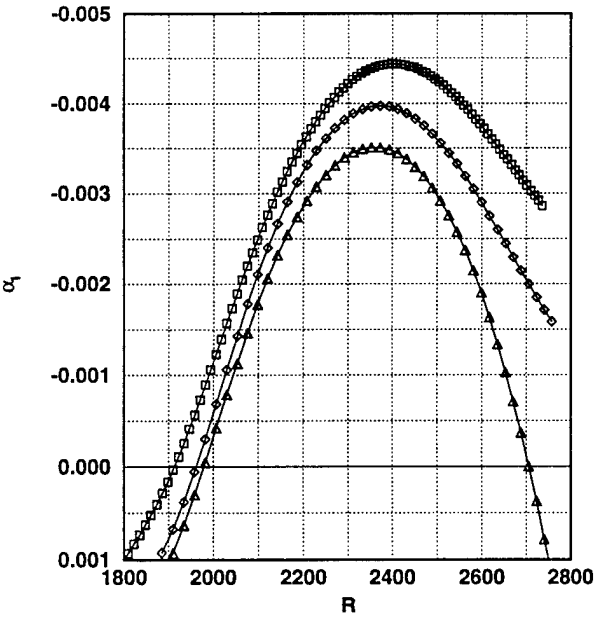

Figure 31: Comparison of spatial growth rates as a function of arc length using different solutions for the basic flow. $F = 82.7 \cdot 10^{-6}$. □: TLNS solution, 200 wall normal points. ◇: AFWAL PNS solution, 501 radial points. △: AFWAL PNS solution, 251 radial points.

Figure 31 compares the spatial growth rates for the two-dimensional second mode at $F = 82.7 \cdot 10^{-6}$ obtained with different basic flows. Although the PNS code has been pushed to the limits with 501 radial points (and an automatic increase in the number of streamwise stations), there remains a significant difference from the growth rates obtained with the TLNS solution. This difference is enhanced by integrating the growth rates into N factors. Comparison of basic-flow quantities shows in general good agreement but differences near the edge of the boundary layer. Since the critical layer of the second mode is located in this region, the stability results are strongly affected by the accuracy of the solution.

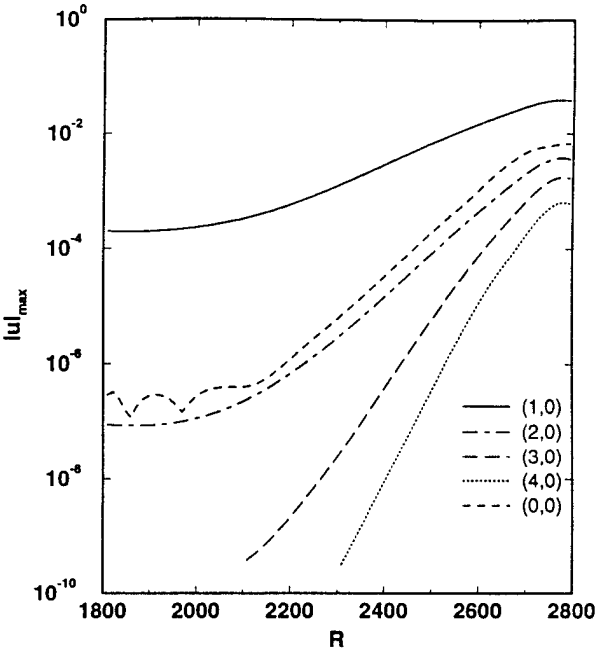

Figure 32: Nonlinear evolution of a 2D second Mode at $F = 82.7 \cdot 10^{-6}$ for an initial amplitude of 0.0002.

The nonlinear evolution ($N = 4$) of a two-dimensional second mode at $F = 82.7 \cdot 10^{-6}$ and a small initial amplitude of only $2 \cdot 10^{-4}$ is shown in figure 32. The TLNS solution has been used as basic flow. In the linear case (figure 31), the second mode exhibits growth well beyond $R = 2800$. Here the nonlinear terms cause a stabilization starting near $R \approx 2500$ and decay of the mode for $R > 2760$. In spite of the moderate maximum-amplitude, the disturbance causes a significant rise in the skin friction coefficient C_f that dramatically increases for larger amplitudes.

We have studied various second-mode and first-mode interactions to identify resonance mechanisms and drive the flow into transition. Temporal analysis of subharmonic transition at $Ma = 4.5$ [78, 79, 80] has shown a strong resonance between a two-dimensional second mode and a three-dimensional subharmonic first mode. In the blunt-cone flow, spatial analysis of this mechanism has only a weak effect. The growth of the subharmonic mode is enhanced only in a small range of Reynolds numbers, and as the second mode grows, it suppresses the growth of the first mode below the linear level until it decays. To clarify this unexpected observation, we performed various spatial simulations of the subharmonic "transition" at $Ma = 4.5$ in the flat-plate boundary layer. The parameters were chosen to match those of the temporal studies and later varied in their neighborhood. We found that the lack of a strong subharmonic resonance is not particular to the blunt-cone flow. In the spatial case, enhanced growth of the subharmonic is limited to a short region, too short to

increase the amplitude of the (assumed) small subharmonic mode to a level where it would strongly interact with the two-dimensional mode. As in the temporal case, we found no evidence for fundamental secondary instability.

Of all the cases studied in the flow over the blunt cone, the strongest interaction and growth was observed for an interacting pair of oblique second modes with $F = 82.7 \cdot 10^{-6}$ and an initial wave angle of 40^o. With initial amplitudes of $2 \cdot 10^{-4}$ at $R = 2000$, breakdown occurs near the end of the cone. The longitudinal vortex components exhibit strong growth.

5.3 Heat Transfer on Turbine Blades

This last group of PSE studies is concerned with the heat transfer in transitional flows and the prediction of transition in the highly disturbed boundary layers on the strongly curved surfaces of gas turbine blades [81]. Various experiments are available that address specific aspects such as the effect of the turbulence level on the transition location in the flow over a heated flat plate [82], the effect of curvature on transition in flows over heated plates [83, 84], and the effects of turbulence on the heat transfer of a rotating turbine model [85, 86].

We have chosen this set of experiments to explore the feasibility of formulating proper input models for the PSE computation that describe the disturbance environment and permit transition predictions without empirical N factors. This input model was intentionally kept as simple as possible.

Disturbances can be introduced into the PSE computation either by internal forcing, forcing at the boundaries, or through the initial conditions. The latter method has been chosen in most DNS studies such as the work of Rai & Moin [87] and was adopted for the first phase of our studies. In flows over realistic bodies this method reveals severe shortcomings when the computation proceeds through regions of strong stability.

The input model should introduce a proper spanwise scale and proper frequencies which are closely coupled with the streamwise scales. The spanwise scale can be either chosen from Kendall's observations on the scale of the Klebanoff mode or from secondary instability theory which predicts strongest K-type instability for spanwise scales smaller than the dominant streamwise scale [4], $\lambda_z \approx \lambda_x/\sqrt{2}$. This latter scale is usually smaller than the spanwise scale of the Klebanoff modes.

The proper frequencies, in particular at lower turbulence levels, are associated with unstable modes of the Orr-Sommerfeld equation since small disturbances must be enhanced by instability to cause transition. In general, these unstable modes are waves in a certain band of spanwise and streamwise wavenumbers.

Since nonlinear interactions, secondary instabilities, and the onset of transition require fluctuation amplitudes to exceed some threshold, the amplification must be larger at lower disturbance levels. Since the total amplification between branch I and branch II decreases as the frequency increases, the relevant frequencies decrease with the disturbance level. This shift and the streamwise distance necessary to achieve sufficient amplification are obvious reasons for the increase of the transition Reynolds number with decreasing disturbance level. For high turbulence levels, the weak amplification at high frequencies may be sufficient to initiate transition. At even higher levels, instability is unnecessary, since the initial disturbances are large enough to nonlinearly interact without additional amplification and cause bypass transition.

We conclude that one of the key ingredients in the transition model is a pool of 2D waves of different frequency which can be analyzed simultaneously or separately for their interaction with the Klebanoff mode. The upstream shift of transition as the turbulence level increases will be a combination of the upstream shift at fixed frequency and the earlier onset at higher frequency. The broad band of frequencies present in the pool of disturbances is a remarkable difference from the traditional vibrating ribbon experiments.

The simplest model consists of a Klebanoff mode of spanwise wavenumber β and a TS wave of frequency ω. The frequency can be estimated using amplitude growth curves for one baseline case (grid 0 of Sohn & Reshotko [82]) which also provides an estimate for the initial amplitude. The amplitude estimate can be replaced as soon as receptivity coefficients for free-stream turbulence are established. The amplitude of the Klebanoff mode is less critical because this mode serves primarily to establish a spanwise scale, except if the surface is concave and causes instability to Görtler vortices. After a series of estimates we chose $\omega = 0.05$, $\beta = 0.6$ and amplitudes of 0.3% and 0.1% at $Re_x = 1.25 \cdot 10^5$ for modes (1,0) and (0,1), respectively, for the baseline case with 0.4% turbulence level. Since receptivity is considered a largely linear process, both amplitudes are linearly scaled for other turbulence levels.

For our analysis we chose the minimum of the skin friction coefficient C_f or the minimum of the Stanton number St as an operational definition of the transition location. This definition necessarily requires a nonlinear analysis since linear disturbances cannot cause any changes in skin friction or heat transfer coefficients. The runs shown were performed with low truncation ($N = M = 1$) until shortly downstream of the transition location.

The boundary layer for a heated flat plate with an unheated leading edge was used to study the effect of the turbulence level. Figure 33 shows the effect of turbulence levels of 1.2% and 2.4% in comparison with

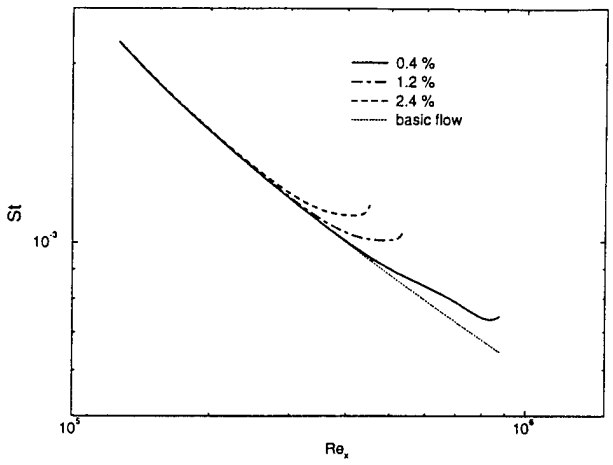

Figure 33: Stanton number vs. Re_x for different disturbance levels reflecting approximately the turbulence levels for grids 0, 1, and 2 of Sohn & Reshotko.

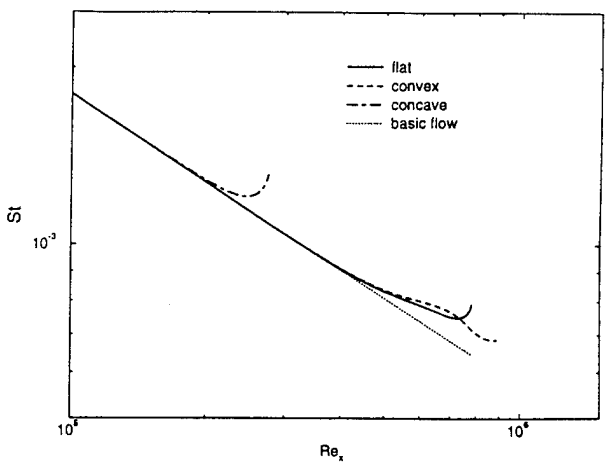

Figure 34: Variation of the Stanton number with the Reynolds number Re_x for convex, flat, and concave plates at comparable turbulence levels.

the baseline case, 0.4%. The transition location for 0.4% is at $Re_x \approx 8.3 \cdot 10^5$, close to the value found by Sohn & Reshotko. The shift to lower values as the turbulence level increases is clearly demonstrated. The shift is not as large as observed because we have maintained the same frequency for these runs. Accounting for a pool of waves with different frequencies would improve the quantitative agreement. Another important consideration is the streamwise decay of the turbulence level. Rai & Moin observed a decay from 9.6% to 2.4% over the length of their first computational domain.

To analyze the effect of curvature we selected three cases, a flat plate at 0.68% turbulence level, a concave plate with a radius of 0.97 m at 0.6%, and a convex plate with a radius of 0.90 m at 0.68% from the experimental studies [83, 84]. Although the turbulence level for the flat plate is higher, transition in this experiment occurs at a higher Re_x than in the baseline case of Sohn & Reshotko. The effect of the unheated leading edge has been neglected since the experimental conditions are not specified.

Figure 34 compares results of the three runs which are in good agreement with the observations. Remarkable is the higher transition Reynolds number on the convex plate which originates from the stabilizing effect of convex curvature on the longitudinal vortex (see figure 11) and delayed onset of secondary instability. The significant upstream shift of the transition location is not caused by bypass transition, but by strong amplification of the longitudinal vortex. The change in heat transfer occurs in a still laminar but highly disturbed flow without participation of the TS wave.

5.3.1 Analysis of a Gas-Turbine Blade

The analysis of the heat transfer on the first stator blade used in the experiments performed at United Technologies Research Center (UTRC) involved all aspects of performing PSE runs under realistic conditions.

The geometry of this stator blade at midspan was obtained in the form of 134 nondimensional coordinates with an absolute error of $\pm 10^{-5}$. The geometry is shown in figure 35.

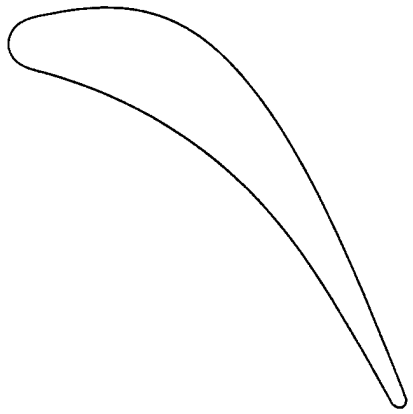

Figure 35: The airfoil of the UTRC first stator at midspan.

The inviscid flow in the cascade was computed using the PCPANEL code.[5] In this code, the maximum number of points to describe the blade geometry is limited to 99. An attempt to extend this limit was discontinued since the closer spacing of the points caused undesirable oscillations of the results. Flow parameters were selected for the test run R53PD1 [86] that has been analytically studied at UTRC. The turbulence level for this test run is 0.5%.

The pressure coefficient C_p is shown in figure 36. The scatter of the data in the leading-edge region is caused by roundoff errors in the coordinates which

[5] This code was provided by E. R. McFarland, NASA Lewis Research Center.

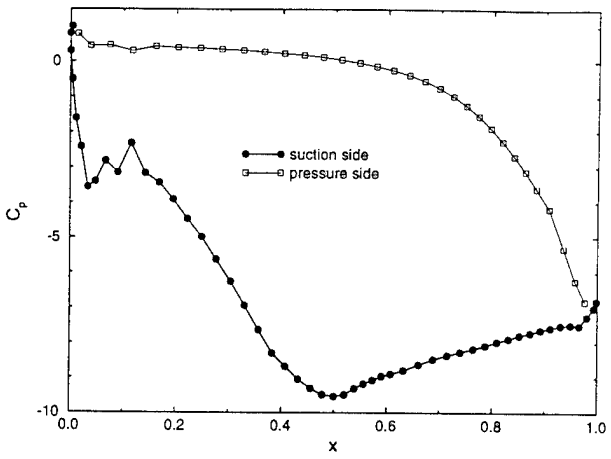

Figure 36: Pressure distribution on the upper (suction) and lower (pressure) surface of the UTRC first stator blade.

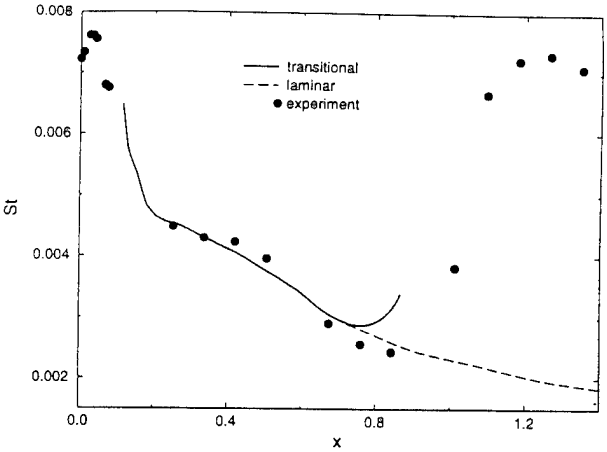

Figure 37: Variation of the Stanton number with the arclength s along the suction surface. Comparison of experiment, laminar flow, and PSE results.

affect slope and curvature of the surface. Otherwise, the pressure distribution agrees with the experimental data.

The boundary-layer computations were performed with a modification of the Kaups-Cebeci code to account for the heat flux at the wall. The code had already been modified to provide curvature and metric data. The agreement of the Stanton number for laminar flow with the experiment is marginal, one cause may be different choices of reference quantities in the two sets of data.

Before attempting a transition analysis, it is useful to gain insight into the stability characteristics by analyzing the pressure distribution and the boundary layer characteristics which both suggest significant differences of the stability on suction and pressure side. The short region of adverse pressure gradients near the leading edge on the upper surface together with Reynolds numbers in the range of $Re \approx 500$ causes instability to TS waves in this region followed by a stable region with favorable pressure gradient yet increasing Re. Strong instability will appear downstream of $x \approx 0.5$ once the stable boundary-layer profile has adapted to the adverse pressure gradient since $Re \approx 750$ in this region. The nondimensional frequencies F relevant to instability in this region are typically of the order $F \approx 80 \cdot 10^{-6}$ and higher for decelerated flows which translates to physical frequencies $f > 5$ KHz. The disturbance spectrum given by Dring et al. [85] provides no information in this frequency range. The strong fluctuation at the rotor passing frequency of 190 Hz and its significant harmonics are far outside the critical frequency range. A frequency of 8 KHz was chosen for the analysis. A linear PSE analysis confirmed a short region of weak TS growth near arclength $s = 0.2$ followed by a steep drop of the amplitude by more than seven orders of magnitude until instability resumed near $s = 0.6$ in reaction to the adverse pressure gradient.

The parameters for the nonlinear PSE run were chosen as before except for the frequency $\omega = 0.1573$. The turbulence level was assumed to be fixed at 0.5%. The result is shown in figure 37 together with the laminar flow and the experimental data. The run was continued through the transition location at $s = 0.764$ to amplitudes of about 10%. The transition location is slightly upstream of the experimental result, probably because of overestimated initial amplitudes. The distance between the neutral point and the transition location is about 16% of the axial chord length.

A similar study of the pressure side revealed a significant increase of the heat transfer in agreement with the experiments. As in the case of a concave plate, the heat transfer is enhanced by strong Görtler vortices without interaction with the TS wave.

Although applications of the PSE approach for transition prediction in engineering problems are just at the beginning, the results so far show that transition can be predicted with minimal empirical feedback for the formulation of input models to represent the disturbance environment. This capability allows reliable trade-off analysis between different formulations.

In addition, the PSE approach helps to close the gaps in our understanding of receptivity, stability, and transition to the benefit of future applications.

Acknowledgment

G. K. Stuckert developed major parts of the code for compressible flow in general curvilinear coordinates. Together with V. Esfahanian and N. Lin, he contributed to a realm of data which still await discussion and publication. The foundations of this work have been developed with support from the Air Force Office of Scientific Research under Contracts AFOSR-

91-02-62 and F49620-92-J-0271 and from the Office of Naval Research under Contract N00014-90-J-1520. Specific applications have been supported by NASA Lewis Research Center under SBIR Contract NAS3-26602, NASA Ames Research Center under SBIR Contract NAS2-13513, and by the Flight Dynamics Directorate, Wright Laboratory, under Contract F33615-90-C-3009.

References

[1] Squire, H. B. 1933 "On the stability for three-dimensional disturbances of viscous fluid flow between parallel walls," *Proc. Roy. Soc. A.*, Vol. 142, pp. 621-628.

[2] Arnal, D. 1984 "Description and prediction of transition in two-dimensional, incompressible flow," AGARD Report R-709, Paper No. 2.

[3] Arnal, D. 1993 "Prediction based on linear theory," AGARD Report R-793, Paper No. 2.

[4] Herbert, Th. 1988 "Secondary instability of boundary layers," *Ann. Rev. Fluid Mech.*, Vol. 20, pp. 487-526.

[5] Herbert, Th. and Crouch, J. D. 1990 "Threshold conditions for breakdown of laminar boundary layers," in: *Laminar Turbulent Transition*, Editors R. Michel, D. Arnal, pp. 93-99, Springer-Verlag.

[6] Cowley, S. 1993 "Asymptotic methods and weakly nonlinear analysis," AGARD Report R-793, Paper No. 3.

[7] Kleiser, L. and Zang, T. A. 1991 "Numerical simulation of transition in wall-bounded shear flows," *Ann. Rev. Fluid Mech.*, Vol. 23, pp. 495-537.

[8] Klebanoff, P. S., Tidstrom, K. D., and Sargent, L. M. 1962 "The three-dimensional nature of boundary-layer instability," *J. Fluid Mech.*, Vol. 12, pp. 1-34.

[9] Kovasznay, L. S. G., Komoda, H., and Vasudeva, B. R. 1962 "Detailed flow field in transition," in: Proc. 1962 Heat Transfer and Fluid Mech. Inst., Stanford Univ. Press, pp. 1-26.

[10] Kachanov, Yu. S. and Levchenko, V. Ya. 1984 "The resonant interaction of disturbances at laminar-turbulent transition in a boundary layer," *J. Fluid Mech.*, Vol. 138, pp. 209-247.

[11] Gaster, M. 1974 "On the effects of boundary-layer growth on flow stability," *J. Fluid Mech.*, Vol. 66, pp. 465-480.

[12] Huerre, P. and Monkewitz, P. A. 1990 "Local and global instabilities in spatially developing flows," *Ann. Rev. Fluid Mech.*, Vol. 22, pp. 473-537.

[13] Mack, L. M. 1984 "Boundary-layer linear stability theory," AGARD Report No. 709, Paper 3, pp. 1-81.

[14] Mack, L. M. 1977 "Transition prediction and linear stability theory," in: *Laminar-Turbulent Transition*, AGARD CP-224, Paper No. 1.

[15] Herbert, Th. and Bertolotti, F. P. 1987 "Stability analysis of nonparallel boundary layers," *Bull. Am. Phys. Soc.*, Vol. 32, p. 2079.

[16] Bouthier, M. 1972 "Stabilité linéaire des écoulements presque parallèles," *J. Mécanique*, Vol. 11, pp. 599-621.

[17] Bouthier, M. 1973 "Stabilité linéaire des écoulements presque parallèles: Partie II, la couche limite des Blasius" *J. Mécanique*, Vol. 12, pp. 75-95.

[18] Saric, W. S. and Nayfeh, A. H. 1977 "Nonparallel stability of boundary layers with pressure gradients and suction," in: *Laminar-Turbulent Transition*, AGARD CP-224, Paper 6, pp. 1-21

[19] Bertolotti, F. P. 1991 "Linear and nonlinear stability of boundary layers with streamwise varying properties," Ph. D. Thesis, The Ohio State University, Columbus, Ohio.

[20] Haj-Hariri, H. 1992 "Characteristics analysis of the parabolized stability equations," *Stud. Appl. Math.*, submitted for publication.

[21] Chang, C-L., Malik, M.R., Erlebacher, G., and Hussaini, M. Y. 1991 "Compressible stability of growing boundary layers using parabolized stability equations," AIAA 91-1636.

[22] Bertolotti, F. P., Herbert, Th., and Spalart, P. R. 1992 "Linear and nonlinear stability of the Blasius boundary layer." *J. Fluid Mech.*, Vol. 242, pp. 441-474.

[23] McAninch, G. L. 1986 "Higher order parabolic approximations for sound propagation in stratified moving media," *AIAA J.*, Vol. 24, pp. 253-260.

[24] Gustavsson, L. H. 1991 "Energy growth of three-dimensional disturbances in plane Poiseuille flow," *J. Fluid Mech.*, Vol. 224, pp. 241-260.

[25] Henningson, D. S. and Schmid, P. J. 1992 "Vector eigenfunction expansions for plane channel flows," *Stud. Appl. Math.*, to appear.

[26] Butler, K. M. and Farrel, B. F. 1992 "Three-dimensional optimal perturbations in viscous shear flow," *Phys. Fluids A*, Vol. 4, pp. 1637-1650.

[27] Trefethen, L. N., Trefethen, A. E., and Reddy, S. C. 1992 "Pseudospectra of the linear Navier-Stokes evolution operator and instability of plane Poiseuille and Couette flows," Techn. Report TR 92-1291, Dept. Computer Science, Cornell Univ.

[28] Hall, P. 1983 "The linear development of Görtler vortices in growing boundary layers," *J. Fluid Mech.*, Vol. 130, pp. 41-58.

[29] Dryden, H. L. 1936 NACA Report No. 562.

[30] Klebanoff, P. S. 1971 "Effect of free-stream turbulence on a laminar boundary layer," *Bull. Am. Phys. Soc.*, Vol. 16, and Personal Communication, 1985.

[31] Kendall, J. M. 1987 "Studies on Tollmien-Schlichting wave packets induced in a Blasius boundary layer by weak freestream turbulence," *Bull. Amer. Phys. Soc.*, Vol. 32, p. 2079, and Personal Communication, 1987.

[32] Kendall, J. M. 1992 "Boundary layer receptivity to weak freestream turbulence," Report presented at the T.S.G. Meeting, Big Sky, Montana, July 13, 1992.

[33] Nishioka, M., Iida, S., and Ichikawa, Y. 1975 "An experimental investigation of the stability of plane Poiseuille flow," *J. Fluid Mech.*, Vol. 72, pp. 731-751.

[34] Herbert, Th. 1991 "Exploring transition by computer," *J. Appl. Num. Math.*, Vol. 7, pp. 3-27.

[35] Kendall, J. M. 1985 "Experimental study of disturbances produced in a pre-transitional laminar boundary layer by weak freestream turbulence," AIAA 85-1695.

[36] Taylor, G. I. 1938 "Some recent developments in the study of turbulence," Proc. Int. Congr. Applied Mechanics, Cambridge, Massachusetts, pp.294-309.

[37] Tollmien, W. 1931 *"Grenzschichttheorie,"* in: Handbuch der Experimental Physik, Vol. IV, Part I, p. 238, Springer Verlag.

[38] Gaster, M. 1982 "The development of a two-dimensional wave packet in a growing boundary layer," *Proc. Roy. Soc.* A, Vol. 384, pp. 317-332.

[39] Mack, L. M. 1985 "Instability wave patterns from harmonic point and line sources in laminar boundary layers," in: *Laminar-Turbulent Transition*, Ed. V. V. Kozlov, pp. 125-132, Springer Verlag.

[40] Gaster, M. 1975 "A theoretical model of a wave packet in the boundary layer on a flat plate," *Proc. Roy. Soc.* A, Vol. 347, pp. 271-289.

[41] Wang, M. 1993 "Stability analysis of three-dimensional boundary layers with parabolized stability equations," forthcoming Ph.D. Thesis, The Ohio State University.

[42] Malik, M. R. and Balakumar, P. 1991 "Nonparallel stability of rotating disk flow using PSE," in: Proc. ICASE/NASA Transition Workshop, Springer Verlag.

[43] Malik, M. R., Balakumar, P., and Masad, J. "Linear stability of three-dimensional boundary layers: effects of curvature and non-parallelism," AIAA 93-0080.

[44] Schrauf, G. 1992 "Curvature effects for three-dimensional compressible boundary layer stability," *Z. Flugwiss. Weltraumf.*, Vol. 16, pp.119-127.

[45] Spalart, P. 1989 "Direct numerical study of cross-flow instability," in: *Laminar-Turbulent Transition,* eds. D. Arnal and R. Michel, pp. 622-630, Springer Verlag.

[46] Malik, M. R. and Li, F. 1992 "Three-dimensional boundary layer stability and transition," SAE Paper 921991.

[47] Malik, M. R. and Li, F. 1993 "Transition studies for swept wing flows using PSE," AIAA 93-0077.

[48] Fedorov, A. V. 1988 "Excitation of waves of instability of the secondary flow in the boundary layer on a swept wing," *Zh. PMTF*, No. 5, pp. 46-52.

[49] Radeztsky, R. H., Reibert, M. S., Saric, W. S., and Takagi, S. 1993 "Effect of micron-sized roughness on transition in swept-wing flows," AIAA 93-0076.

[50] Saric, W. S. 1993 "Physical description of boundary-layer transition: experimental evidence," AGARD Report R-793, Paper No. 3.

[51] Crouch, J. D. 1993 "Receptivity of three-dimensional boundary layers" AIAA 93-0074.

[52] Müller, B. and Bippes, H. 1988 "Experimental study of instability modes in a three-dimensional boundary layer," In: *Fluid Dynamics of Three-Dimensional Turbulent Shear Flows*, AGARD CP-438.

[53] Herbert, Th. 1974 "Über endliche Amplituden periodischer Störungen der Grenzschicht an der ebenen Platte," Dissertation, Universität Karlsruhe, Germany.

[54] Herbert, Th. 1975 "On finite amplitudes of periodic disturbances of the boundary layer along a flat plate," Proc. Fourth Int. Conf. on Numerical Methods in Fluid Dynamics, Boulder, Colorado, 1974. Lecture Notes in Physics, Vol. 35, p. 212. Springer-Verlag.

[55] Itoh, N. 1974 "Spatial growth of finite wave disturbances in parallel and nearly parallel flows," *Trans. Japan Soc. Aeron. Space Sci.* Vol. 17, Part 1: pp. 160-174, Part 2: pp. 175-186.

[56] Fasel, H. 1976 "Investigation of the stability of boundary layers by a finite-difference model of the Navier-Stokes equations," *J. Fluid Mech.* Vol. 78, pp. 355-383.

[57] Herbert, Th. 1991 "Boundary-layer transition - analysis and prediction revisited," AIAA Paper No. 91-0737.

[58] Bayliss, A., Maestrello, L., Parikh, P., and Turkel, E. 1986 "Numerical simulation of boundary layer excitation by surface heating/cooling," *AIAA J.* Vol. 24, pp.

[59] Goldstein, M. E. and Durbin, P. A. "Nonlinear critical layers eliminate the upper branch of spatially growing Tollmien-Schlichting waves," *Phys. Fluids*, Vol. 29, pp. 2344-2355.

[60] Herbert, Th. 1983 "On perturbation methods in nonlinear stability theory," *J. Fluid Mech.* Vol. 126, pp. 167-186.

[61] Crouch, J. D. 1992 "Non-localized receptivity of boundary layers," *J. Fluid Mech.* Vol. 224, pp. 567-581.

[62] Choudhari, M. and Street, C. L. 1992 "A finite Reynolds-number approach for the prediction of boundary-layer receptivity in localized regions," *Phys. Fluids A*, Vol. 4, pp. 2495-2514.

[63] Crouch, J. D. and Bertolotti, F. P. 1992 "Nonlocalized Receptivity of boundary layers to three-dimensional disturbances," AIAA 92-0740.

[64] Cornelius, K. C. 1985 "Three dimensional wave development during boundary layer transition," Lockheed Georgia Research Report LG85RR0004.

[65] Fasel, H. F., Rist, U., and Konzelman, U. 1990 "Numerical investigation of the three-dimensional development in boundary-layer transition," *AIAA J.*, Vol. 28, pp. 29-37.

[66] Bertolottii, F. P. and Herbert, Th. 1991 "Analysis of the Linear Stability of Compressible Boundary Layers using the PSE," *J. Theor. Comp. Fluid Dyn.*, Vol. 3, pp. 117-124.

[67] Bertolotti, F. P. 1991 "Compressible boundary layer stability analyzed with the PSE equations," AIAA 91-1637.

[68] Stuckert, G. K., Herbert, Th., and Esfahanian, V. 1993 "Stability and Transition on Swept Wings," AIAA 93-0078.

[69] Malik, M. R. 1990 "Numerical methods for hypersonic boundary layer stability," *J. Comp. Phys.*, Vol.86, pp. 376-423.

[70] Collatz, L. 1966 *The Numerical Treatment of Differential Equations*, Springer-Verlag.

[71] El-Hady, N. M. 1991 "Spatial three-dimensional secondary instability of compressible boundary-layer flows," *AIAA J.*, Vol. 29, pp. 688-696.

[72] Malik, M. R. 1982 "COSAL - A black box stability analysis code for transition prediction in three-dimensional boundary layers," NASA CR-165925.

[73] Kaups, K. and Cebeci, T. 1977 "Compressible laminar boundary layers on swept and tapered wings," *J. Aircraft*, Vol. 14, pp. 661-667.

[74] Stetson, K. F., Thompson, E. R., Donaldson, J. C. and Siler, L. G. 1984 "Laminar Boundary Layer Stability Experiments on a Cone at Mach 8, Part 1: Blunt Cone," AIAA-83-1761.

[75] Esfahanian, V. 1991 "Computation and stability analysis of laminar flow over a blunt cone in hypersonic flows," Ph.D. Thesis, The Ohio State University, Columbus, Ohio.

[76] Esfahanian, V., Herbert, Th. and Burggraf, O. R. 1992 "Computation of laminar flow over a long slender axisymmetric blunted cone in hypersonic flow," AIAA 92-0756.

[77] Herbert, Th. and Esfahanian, V. 1993 "Stability of Hypersonic Flow over a Blunt Body," In: *Theoretical and Experimental Methods in Hypersonic Flows*, AGARD CP 514, pp. 28/1-12.

[78] Ng, L. L. and Erlebacher, G. 1992 "Secondary instabilities in compressible boundary layers," *Phys. Fluids A*, Vol. 4, pp. 710-726.

[79] Adams, N. A. and Kleiser, L. 1993 "Numerical simulation of transition in a compressible flat plate boundary layer," In: Proc. *Symposium on Transitional and Turbulent Flows*, 1993 ASME Fluids Engineering Conference, Washington, D. C.

[80] Kleiser, L. 1993 "Direct Navier-Stokes simulation of transition: the temporal approach," AGARD Report R-793, Paper No. 5.

[81] Herbert, Th., Stuckert, G. K., and Esfahanian, V. 1993 "Effects of free-stream turbulence on boundary-layer transition," AIAA 93-0488.

[82] Sohn, K. H. and Reshotko, E. 1991 "Experimental study of boundary layer transition with elevated freestream turbulence on a heated flat plate," NASA TM 187068.

[83] Wang, T., Simon, T. W., and Buddhavarapu, J. 1985 "An experimental investigation of curvature and freestream turbulence effects on heat transfer and fluid mechanics in transitional boundary layer flows," Contractor Report, NAG 3-286.

[84] Kim, J. and Simon, T. W. 1991 "Free-stream turbulence and concave curvature effects on heated, transitional boundary layers," NASA Contractor Report 187150.

[85] Dring, R. P., Blair, M. F., Joslyn, H. D., Power, G. D., and Verdon, J. M. 1986 "The effects of inlet turbulence and rotor/stator interactions on the aerodynamics and heat transfer of a large-scale rotating turbine model," NASA Contractor Report 4079.

[86] Dring, R. P., Blair, M. F., and Joslyn, H. D. 1986 "The effects of inlet turbulence and rotor stator interactions on the aerodynamics and heat transfer of a large-scale rotating turbine model," NASA Contractor Report 179468.

[87] Rai, M. M. and Moin, P. 1991 "Direct numerical simulation of transition and turbulence in a spatially evolving boundary layer," AIAA-91-1607.